UCRL-18470

cy. 2

University of California

RECEIVED
LAWRENCE
RADIATION LABORATORY

JAN 7 1969

LIBRARY AND
DOCUMENTS SECTION

Ernest O. Lawrence Radiation Laboratory

THE (α, d) REACTION ON LIGHT AND MEDIUM MASS NUCLIDES

Chi Chang Lu

(Ph. D. Thesis)

August 1968

TWO-WEEK LOAN COPY

This is a Library Circulating Copy
which may be borrowed for two weeks.
For a personal retention copy, call
Tech. Info. Division, Ext. 5545

UCRL-18470
cy. 2

DISCLAIMER

This document was prepared as an account of work sponsored by the United States Government. While this document is believed to contain correct information, neither the United States Government nor any agency thereof, nor the Regents of the University of California, nor any of their employees, makes any warranty, express or implied, or assumes any legal responsibility for the accuracy, completeness, or usefulness of any information, apparatus, product, or process disclosed, or represents that its use would not infringe privately owned rights. Reference herein to any specific commercial product, process, or service by its trade name, trademark, manufacturer, or otherwise, does not necessarily constitute or imply its endorsement, recommendation, or favoring by the United States Government or any agency thereof, or the Regents of the University of California. The views and opinions of authors expressed herein do not necessarily state or reflect those of the United States Government or any agency thereof or the Regents of the University of California.

UCRL-18470

UNIVERSITY OF CALIFORNIA
Lawrence Radiation Laboratory
Berkeley, California

AEC Contract No. W-7405-eng-48

THE (α,d) REACTION ON LIGHT AND MEDIUM MASS NUCLIDES

Chi Chang Lu

(Ph.D. Thesis)

August 1968

Contents

ABSTRACT v

I. INTRODUCTION 1

II. EXPERIMENTAL PROCEDURE 5

A. Experiments 5

1. The 88-Inch Cyclotron and Beam Optics 5

2. The 36-Inch Scattering Chamber 5

3. Electronics 8

4. Targets 12

B. Data Reduction Methods 13

III. METHODS OF THEORETICAL CALCULATIONS 15

A. Shell Model Calculation 15

B. Interaction Energy between Particles in Non-Equivalent Orbits 22

IV. EXPERIMENTAL RESULTS 24

A. The (α,d) Reactions 24

1. $^{13}C(\alpha,d)^{15}N$ 24

2. $^{14}C(\alpha,d)^{16}N$ 24

3. $^{15}N(\alpha,d)^{17}O$ 31

4. $^{20}Ne(\alpha,d)^{22}Na$ 31

5. $^{52}Cr(\alpha,d)^{54}Mn$, $^{54,56}Fe(\alpha,d)^{56,58}Co$, $^{59}Co(\alpha,d)^{61}Ni$, $^{58,60,62}Ni(\alpha,d)^{60,62,64}Cu$, $^{63}Cu(\alpha,d)^{65}Zn$, and $^{64,66,68}Zn(\alpha,d)^{66,68,70}Ga$ 39

B. The (α,t) Reactions 43

V. DISCUSSION 79

A. Criteria to Identify the $(1d_{5/2})^2_{5+}$ and $(1g_{9/2})^2_{9+}$ Levels and Rationale for These Criteria 79

B. Residual Interaction Energies between Proton and Neutron in the Configuration of $(1d_{5/2})^2_{5+,0}$ or $(1f_{7/2})^2_{7+,0}$ or $(1g_{9/2})^2_{9+,0}$ 86

C. Calculation of Excitation Energies of States with the Configuration $(1d_{5/2})^2_{5+,0}$ 103

D. Shell Model Calculations 106

E. $-Q_f$ vs $A_{residual}$ Plot for States with Configuration $(1d_{5/2})^2_{5+,0}$ 118

F. Other Possible Two-Nucleon Excited States 120

VI. CONCLUSIONS 125

ACKNOWLEDGMENTS 127

REFERENCES 129

THE (α,d) REACTION ON LIGHT AND MEDIUM MASS NUCLIDES

Chi Chang Lu

Lawrence Radiation Laboratory
University of California
Berkeley, California

August 1968

ABSTRACT

The (α,d) reactions on targets of ^{13}C, ^{14}C, ^{15}N, and ^{20}Ne were studied using alpha particle beams of 40.1, 46.0, 45.4, and 44.5 MeV, respectively. Angular distributions were obtained. States with $(1d_{5/2})^2_{5+,0}$ configuration were located and possible spin assignments were suggested. These states are: ^{15}N 13.03 MeV(11/2-), 11.95 MeV(9/2-); ^{16}N 5.75 MeV(5+); ^{17}O 7.74 MeV(11/2-), 9.14 MeV(9/2-); ^{22}Na 1.528 MeV 5+.

Separated isotopes of ^{52}Cr, $^{54,56}Fe$, ^{59}Co, $^{58,60,62}Ni$, ^{63}Cu, and $^{64,66,68}Zn$ were used as targets to study the (α,d) reaction with a 50 MeV alpha particle beam. States with a probable configuration of $(1g_{9/2})^2_{9+,0}$ were located. These states are ^{54}Mn 9.47 MeV, ^{56}Co 8.92 Mev, ^{58}Co 6.79 MeV, ^{60}Cu 5.99 MeV, ^{62}Cu 4.75 MeV, ^{64}Cu 4.57 Mev, ^{66}Ga 2.99 Mev, ^{68}Ga 2.88 Mev, ^{70}Ga 2.88 Mev.

The residual interaction energies between the proton and neutron in the configurations $(1d_{5/2})^2_{5+,0}$ and $(1f_{7/2})^2_{7+,0}$, and $(1g_{9/2})^2_{9+,0}$ were extracted from the excitation energies determined in the present work and previous work on $(1d_{5/2})^2_{5+,0}$ and $(1f_{7/2})^2_{7+,0}$ states. For $T_z \neq 0$ nuclides, an "interaction model" method was proposed to extract the residual interaction energy. The mean values of the residual interaction energies are about -3.9, -3.0, -2.2 MeV respectively for the three mentioned configurations. These is a slight decrease of residual interaction energy with

increasing A. These results are reproduced excellently by conventional shell model calculations.

The results of (α,t) reactions studied simultaneously with the (α,d) reactions are also briefly reported.

I. INTRODUCTION

Pioneering spectroscopic studies of (α,d) reaction on nuclides with $A \leq 40$ using alpha particle beam energy from 42 MeV to 53 MeV[1,2,3] have suggested that the most strongly populated states are those in which the captured proton and neutron enter the same shell model state[1] and couple to the maximum angular momentum with zero isobaric spin.[2] The pair couples to the spin and isobaric spin of the target nuclide to give the total angular momentum and isobaric spin of the preferentially populated state. The situation can be represented by the following vector coupling relation:

$$\{\vec{J}_i, \vec{T}_i + [(\vec{j}_1,\vec{t}_1) + (\vec{j}_2, \vec{t}_2)]_{2j,0}\}\ J_f, T_f = T_i$$

where J_i, T_i are the total angular momentum and isobaric spin of the target nuclide; $j_1 = j_2$, $t_1 = t_2 = 1/2$ are those of the shell model states into which the proton and neutron are captured; and J_f, T_f are those of the final state. The allowed J_f values have the range:

$$|J_i - 2j| \leq J_f \leq |J_i + 2j|$$

Hence, levels with a multiplicity of $(2J_i+1)$ (if $2j>J_i$) or $[2(2j)+1]$ (if $2j<J_i$) will be strongly populated.

These studies of (α,d) reactions were carried out by Rivet et al.[3] on target nuclides ^{12}C, $^{14,15}N$, ^{16}O, ^{20}Ne, $^{24,26}Mg$, ^{28}Si, ^{32}S, ^{40}Ar, and ^{40}Ca. The following levels of the residual nuclides were strongly populated and were assigned to the configuration

$[J_i,T_i + (1d_{5/2})_{5+,0}]^2_{J_f,T_f} = T_i$:

^{14}N: 9.00 MeV(5+)

^{16}O: 14.33 MeV(4+), 14.74 MeV(6+), 16.16 MeV(5+)

^{17}O: 7.6 MeV(11/2-), 9.0 MeV(9/2-)

^{18}F: 1.119 MeV(5+) (Ref. 4)

^{22}Na: 1.53 MeV(5+)

^{26}Al: Ground state (5+).

Those of $[J_i,T_i + (1f_{7/2})^2_{7+}]_{J_f,T_f} = T_i$ are:

^{26}Al: 8.27 MeV(7+)

^{28}Al: 9.80 MeV(7+)

^{30}P : 7.03 MeV(7+)

^{34}Cl: 5.2 MeV (7+)

^{42}K : 1.87 MeV(7+)

^{42}Sc: 0.60 MeV(7+)

Since $2j > J_i$ in all these cases, we expect a multiplicity of $(2J_i + 1)$ levels for each nuclide. For even-even target nuclides with $J_i = 0$, there should be only one highly populated level. For target nuclides ^{14}N($J_i = 1$) and ^{15}N($J_i = 1/2$) we expect a multiplet of three and two levels, respectively, to occur. These predictions were borne out by the experiments.

The assignments of these high spin levels were based on three criteria:

a) Large cross section.

b) Similarity in the shape of the angular distributions (a more or less monotonically decreasing curve with little structure).

c) That a smooth decreasing curve be obtained when $-Q_f$ was plotted against $A_{residual}$, where $-Q_f$ is equal to the sum of -[Q value of the (α,d) reaction] and the excitation energy of the assigned state; and $A_{residual}$ is the mass number of the residual nucleus $(A_{target}+2)$. At the time when these assignments were made the only spins known from other work were a possible 5+ state at about 1 MeV in ^{18}F, the ^{26}Al g.s. with $J\pi$ = 5+, and ^{42}Sc 0.6 MeV 7+ or 6+. Recently, the 8.963 MeV level of ^{14}N was assigned spin 5+,[5,6] the 1.131 MeV level of ^{18}F was definitely established as having spin 5+,[7] and the 1.530 MeV level of ^{22}Na was assigned the spin 5+.[8] All these direct experimental assignments are in agreement with the predictions of the proposed model obtained from the systematics of the (α,d) reactions. These agreements strongly indicate the correctness and the reliability of the model.

In order to test further the validity of the model and to extend the study to the medium mass region $(52 \leq A \leq 70)$ in a search for the existence of $[J_i,T_i + (1g_{9/2})^2_{9+,0}]_{J_f,T_f = T_i}$ states, the target nuclei $^{13,14}C$, ^{15}N, ^{20}Ne, ^{52}Cr, $^{54,56}Fe$, $^{58,60,62}Ni$, ^{59}Co, ^{63}Cu and $^{64,66,68}Zn$ were used in the study of the (α,d) reaction with alpha-particle beam energies from 40 MeV to 50 MeV. The spectra from (α,t) reactions were simultaneously recorded. The multiplicities of the strongly populated levels were found to be in accord with the predictions. Levels with a probable $(1g_{9/2})^2_{9+,0}$ configuration were located.

The residual interaction energies between the captured proton and neutron in $(1d_{5/2})^2_{5+,0}$ or $(1f_{7/2})^2_{7+,0}$ or $(1g_{9/2})^2_{9+,0}$ configuration were extracted. They are in satisfactory agreement with the values calculated by a conventional shell model calculation.

II. EXPERIMENTAL PROCEDURE

A. Experiments

1. The 88-Inch Cyclotron and Beam Optics

The Berkeley 88-inch Sector-focused cyclotron was used to provide alpha particle beams from 40 MeV to 50 MeV. The beams were then transported to the scattering chamber as shown in Fig. 1. After extraction from the cyclotron, the beam passed through a radial collimator (X-collimator); a quadrupole doublet which brought the beam to a radial focus at the first radial focus position marked on the figure; a vertical collimator (Y-collimator); a uniform field circular pole magnet which bent the beam 57° and focused the beam at the position of analyzing slit (which has a typical width of 0.06"); and a second quadrupole focusing magnet which focused the beam on the target located in the center of the scattering chamber. Finally the beam was stopped by a Faraday cup connected to an integrating electrometer used to measure the beam current. The beam energy was determined by measuring its range in aluminum foils of known thickness and then converting the range into equivalent energy by using Williamson and Boujot's range and energy table.[9] The beam spot size on the target was 0.06" wide and 0.1" high in general. The beam intensity was 0.5-1 μA. Quartz plates were used at both analyzing slit and target position to reveal the beam image.

2. The 36-Inch Scattering Chamber

The arrangement of the equipment in the scattering chamber is shown in Fig. 2. The target frame in the center could be raised, lowered or rotated and could hold either a frame for solid targets or a gas target cell. The detector box was fastened both to a mounting ring

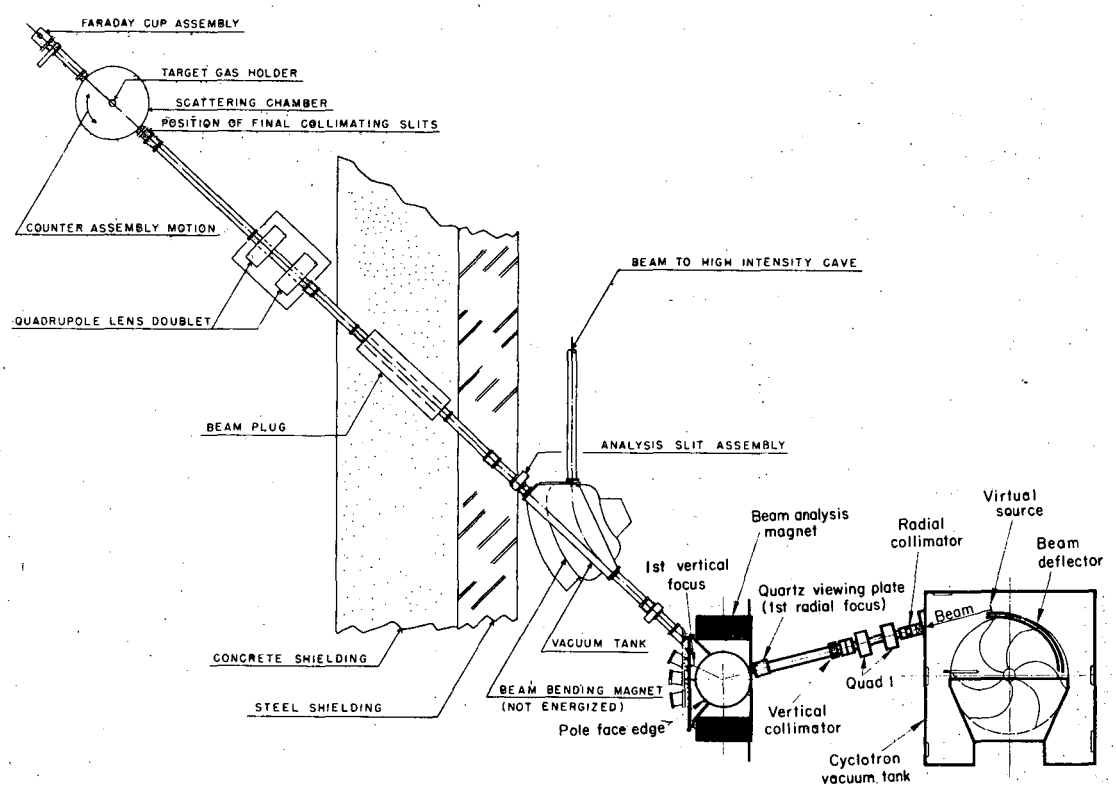

XBL 689-5958

Fig. 1 Beam optics system of 88-inch cyclotron, cave 1.

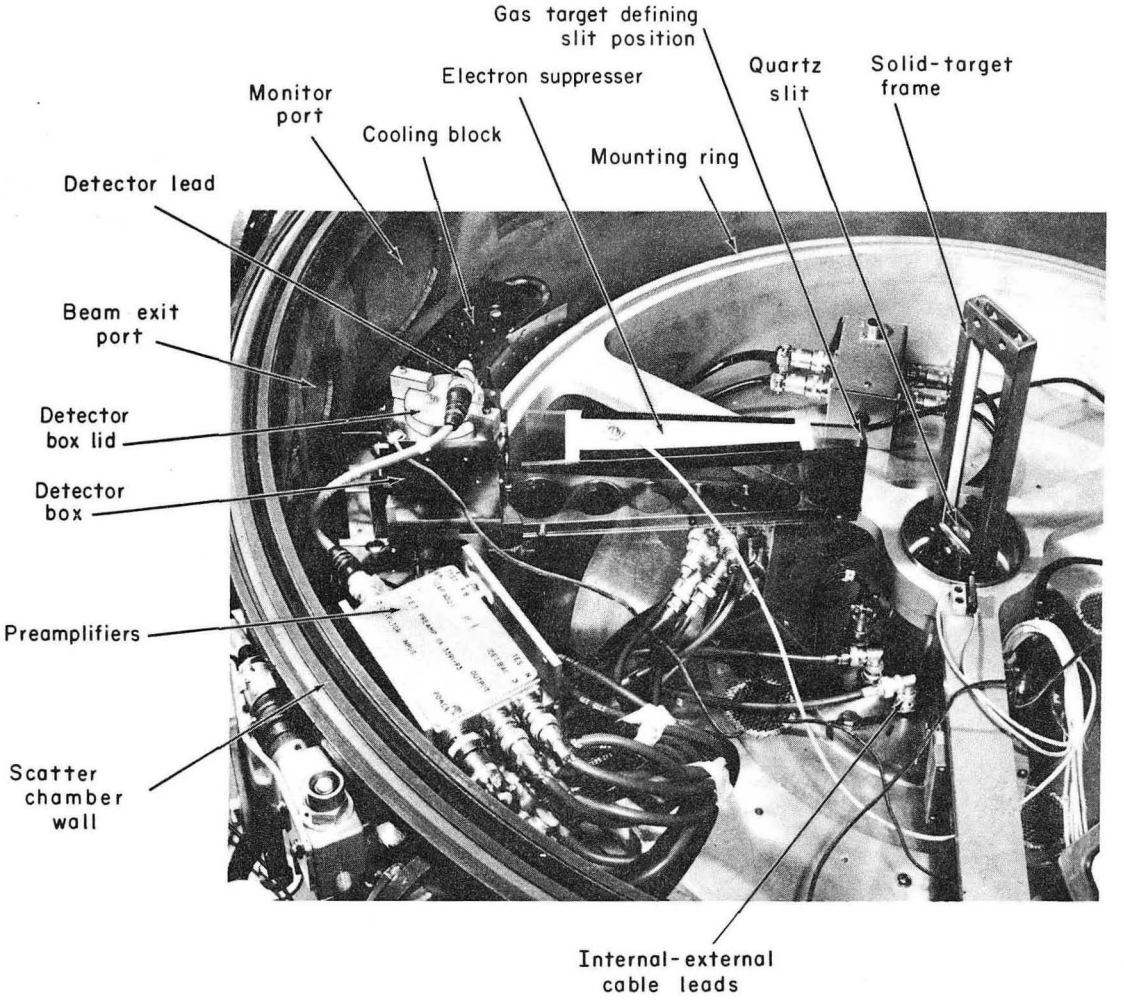

XBB 679-5089

Fig. 2. 36-inch scattering chamber.

which could be rotated and to a Freon-cooled copper block to permit operation of the Si(Li) detectors at about -25°C. Electronic noise generated by the detectors was much reduced by cooling. Both the mounting ring and the target assembly could be moved by remote control. An oil-diffusion pump and mechanical pump were used to evacuate the chamber and beam pipes.

3. Electronics

The electronics used are shown schematically in Fig. 3. Two counter telescopes each consisting of two lithium-drifted silicon semiconductor detectors (called ΔE and E detectors), were used to measure the energy as well as to identify the particles. ΔE detectors with a typical thickness of 0.020" or 0.060" and E detectors with a thickness 0.120" were used. The detector voltage applied depended on the thickness of the counter. Typically, 200 volts were used for 0.060" thick ΔE detector and 400 volts for 0.120" E detector.

Signals generated by the ΔE and E detectors were fed into a charge-sensitive preamplifier (P.A.) located in the scattering chamber and then connected to the linear amplifier system in the counting room where the incoming pulses were shaped, amplified, and stretched to 3-4 μsec wide. In pulse shaping, typically a time constant of 0.5 μsec (for ΔE amplifier) or 0.2 μsec (for E amplifier) was used for the integrator. Delay line was used for differentiation. A slow coincidence of 1 μsec was required between the ΔE and E signal to feed into the Goulding-Landis particle identifier.[11] This identifier is based on the property that the light charged particles follow the empirical range energy relation

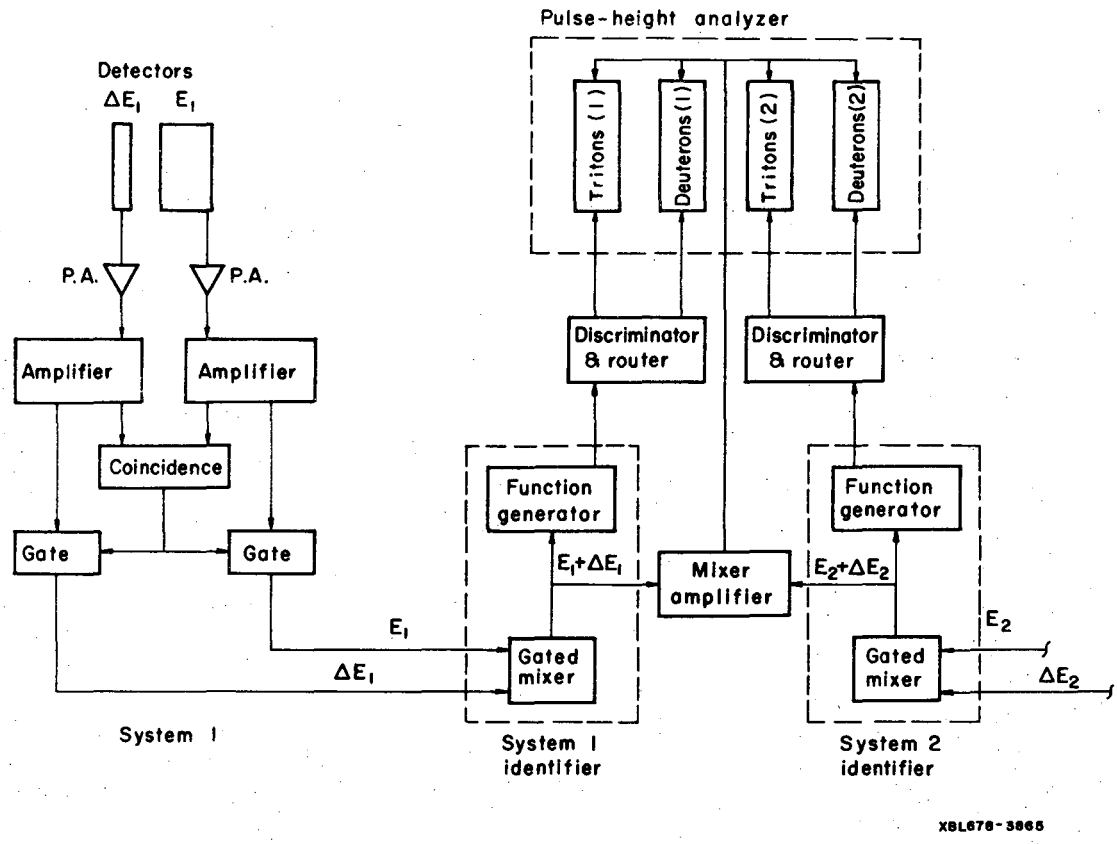

Fig. 3 Schematic diagram of electronics.

$R = A\,E^{1.73}$ between E = 10-100 MeV. A is a constant and is equal to 32.2, 19.1, 14.2, 3.54, 2.95 for p, d, t, ^{3}He, and ^{4}He respectively where R is the range in mg/cm^2 and E is the energy in MeV. If T is the thickness of the ΔE detector, and ΔE, E are the energy lost in the ΔE and E detectors, it follows:

$$T/A = (E + \Delta E)^{1.73} - E^{1.73}$$

Since T is a constant, different particles will have different T/A values. Since the voltage signals generated by ΔE, E detectors are directly proportional to the energy loss in each detector, a circuit that treats the signal voltages from ΔE, E detectors in a combination equivalent to the right side of the above equation will generate different size output signal (i.e., voltage) for different kinds of particles. This signal is called the identifier signal. Figure 4 shows the spectrum of identifier signals stored in a 400 channel pulse-height analyzer-RIDL. Discriminators in the router were set at the positions of the valleys in the identifier spectrum so that deuteron and triton energy spectra could be stored in different groups of a Nuclear Data pulse-height analyzer ND-160M which contains four groups each having 1024 channels. Two systems, i.e., two detector telescopes at about 20 degrees apart, were simultaneously used to take the data. After each run, the information stored in the ND-160M were transferred to a "micro" magnetic tape of an on-line PDP-5 computer.[12] While the ND was storing the data for the next run, the PDP-5 was used to plot out the spectra of previous runs or to calculate the differential cross sections for peaks of interest in the spectrum. This immediate data analysis is very valuable

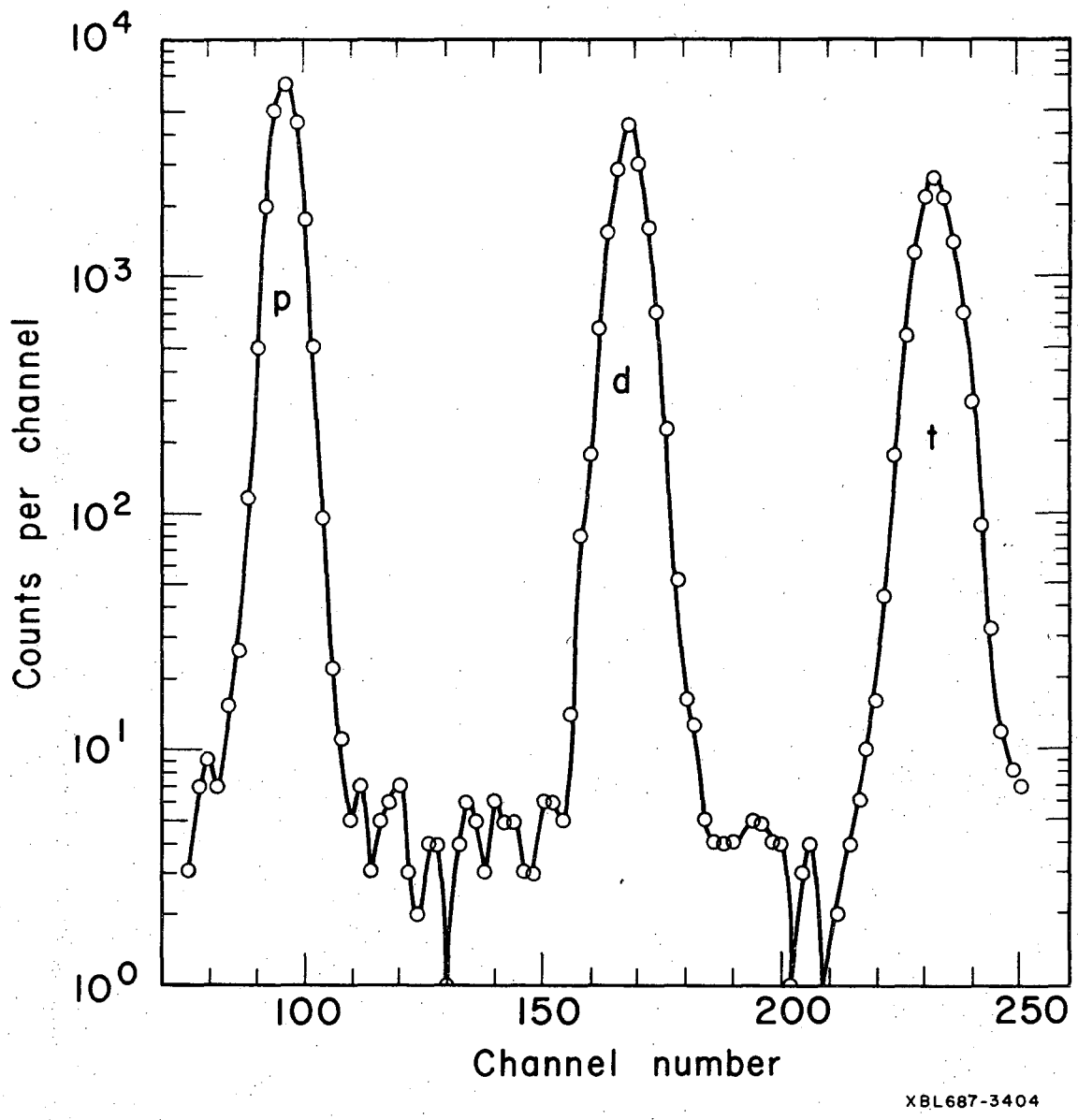

Fig. 4 Particle-identifier spectrum obtained from incidenting a 50 MeV alpha particle beam on ^{68}Zn target at 20 deg (lab) using a 0.06-0.12 inch thick ΔE-E counter telescope.

because it allows one to check that all the systems are working correctly and that the aims of the experiment are being fulfilled at a rather early stage of the experiment. After the conclusion of the experiment, the information stored in the "micro" tape were transferred to an IBM magnetic tape which was used for further data analysis on the CDC-6600 computer.

A monitor counter located in the scattering chamber at 19 deg to the incident beam was used to monitor the target thickness as well as beam energy.

4. Targets

A cylindrical chamber of approximately 3" in diameter and 1" in height was used as gas target. The windows for entry and exit of beam particles and for the escape of secondary particles were 0.0001" thick Havar foil manufactured by Hamilton Watch Company.[13] A typical pressure of about 20 cm Hg was used in the gas cell.

The ^{13}C target was a CH_4 gas which contained 93.7% ^{13}CH.[14] The ^{15}N target gas had an isotropic purity of 99.71%[15] and the ^{20}Ne target gas had an isotropic purity of 98.1%.[16]

The solid targets of medium mass nuclides were prepared by vacuum evaporation of the metal onto a glass or metal plate coated with a thin layer of NaCl or Teepol[17] as parting agent to permit separation of the foil from the plate. The self-supporting foils were then mounted on aluminum rectangular plates with 3/4 inch holes in the center. The target materials were obtained from Union Carbide Nuclear Company.[18] The purity of the ^{52}Cr, ^{54}Fe, ^{56}Fe, ^{58}Ni, ^{60}Ni, ^{62}Ni, ^{59}Co, ^{63}Cu, ^{64}Zn, ^{66}Zn, and ^{68}Zn targets were 99.9%, 90-98%, 98-99.9%, 98-99.9%, 95-99.8%, 95-99%, 99.9%, 99.9%, 99%, 90-99%, and 95-99% respectively.

The ^{14}C target was borrowed from Bookhaven.[19] Gold backing of thickness 2 mg/cm^2 were used. This target contained large amounts of ^{12}C and ^{16}O impurity.

B. Data Reduction Methods

The excitation energies of the levels were determined by using the computer program Lorna[20] which uses as input known excitation energies of states to establish an energy scale and then uses this scale to determine the unknown excitation energies. Differential cross sections were also calculated by using this program according to the following formulas:

For Solid Target:

$$\left(\frac{d\sigma}{d\Omega}\right)_{c.m.} = 2.660 \times 10^{-7} \left(\frac{M_t}{N_t \cdot t_t}\right) \left(\frac{R^2}{W_2 \cdot H_2}\right) \left(\frac{ZC}{B}\right) J \quad \text{mb/sr}$$

where N_t, M_t, t_t are the number of nuclei/molecule, molecular weight in g/mole, and thickness in mg/cm^2 of the target respectively; R is the distance from the center of the target to the back of the detector slits in inches; W_2, H_2 are the width, the height of the detector slit in inches respectively; Z is the atomic number of the incident particle; C is the total counts in the peak of interest; B is the total μc(micro Coulomb) of the incident beam used for taking the spectrum; J is the Jacobian for the transformation of the differential cross section in laboratory coordinates to center-of-mass coordinates.

For Gas Target:

$$\left(\frac{d\sigma}{d\Omega}\right)_{c.m.} = 6.530 \times 10^{-7} \left(\frac{1}{N_t} \cdot \frac{\sin \theta_L}{W_1(1+R_1/R_2)} \cdot \frac{(T + 273)}{P}\right) \cdot \left(\frac{R^2}{W_2 \cdot H_2}\right) \left(\frac{ZC}{B}\right) J \quad \text{mb/sr}$$

where θ_L is the laboratory angle between outgoing light particle and incident beam; T, P are the temperature in °C, and pressure in cm of Hg of the gas target respectively; R_1 and R_2 are the distance from the center of the gas target to the back of the gas target defining slit (see Fig. 2), to the back of the detector slits in inches respectively; W_1 is the width of the gas target defining slit; and N_t, R, W_2, H_2, Z, C, B, J have the same definition mentioned before.

The relation between total cross section and differential cross section is as follows:

$$\sigma_T = 2\pi \int_0^{\pi} \left(\frac{d\sigma}{d\Omega}\right)_{c.m.} \sin\theta \, d\theta = 2\pi \int_{-1}^{1} \left(\frac{d\sigma}{d\Omega}\right)_{c.m.} d(\cos\theta)$$

where θ is the center-of-mass scattering angle. σ_T is only integrated over the range of angles studied in each experiment. The trapezoidal method is used for the integration.

III. METHODS OF THEORETICAL CALCULATIONS

A. Shell Model Calculation

Conventional shell model calculations were used to calculate matrix element of the residual interaction between the two nucleons outside the core-nucleus. This method was described in detail in Moshinsky and Brody's "Table of Transformation Brackets."[21] Following is a brief outline of the general principle of this table and its application to calculate the diagonal matrix elements of the interaction.

Harmonic oscillator (HO) wave functions were used for single particle wave functions. The general form is:

$$|n_1 \ell_1 m_1\rangle = \psi_{n_1 \ell_1 m_1}(r_1,\theta,\phi) = R_{n_1 \ell_1}(r_1)\, Y_{\ell_1 m_1}(\theta,\phi) \qquad (3\text{-}1)$$

where $Y_{\ell_1 m_1}$ are spherical harmonics normalized over the unit sphere and $R_{n_1 \ell_1}(r_1)$ are the radial wave functions which are defined as:

$$R_{n_1 \ell_1}(r_1) = \left[\frac{2(n_1!)}{\Gamma(n_1+\ell_1+3/2)}\right]^{1/2} r_1^{\ell_1} e^{-r_1^2/2} L_{n_1}^{\ell_1+1/2}(r_1^2)$$

$$= \left[\frac{2(n_1!)}{\Gamma(n_1+\ell_1+3/2)}\right]^{1/2} r_1^{\ell_1} e^{-r_1^2/2} \left[\sum_{k=0}^{n_1} \binom{n_1+\ell_1+1/2}{n_1-k} \frac{(-1)^k}{k!} r_1^{2k}\right]$$

$$= r_1^{\ell_1} e^{-r_1^2/2} \sum_{k=0}^{n_1} \left\{\left[\frac{2(n_1!)}{\Gamma(n_1+\ell_1+3/2)}\right]^{1/2} \binom{n_1+\ell_1+1/2}{n_1-k} \frac{(-1)^k}{k!}\right\} r_1^{2k}$$

$$= r_1^{\ell_1} e^{-r_1^2/2} \sum_{k=0}^{n_1} a_{n_1 \ell_1 k}\, r_1^{2k} \qquad (3\text{-}2)$$

and

$$\int_0^\infty \left[R_{n_1 \ell_1}(r_1) \right]^2 r_1^2 \, dr_1 = 1 \tag{3-3}$$

Here, r is in units of the size parameter $1/\sqrt{\nu}$, so that r is written instead of the usual $\sqrt{\nu r}$, where ν is the HO parameter.

The radial quantum number n_1 used had value one less than the usual definition for shell model states. Hence, a $1d_{5/2}$ state was denoted by HO wave function $|n_1 = 0, \ell_1 = 2\rangle$.

The motion of the two particles in a HO well can be described by the radius vectors $\vec{r}_1$, $\vec{r}_2$; radial quantum numbers n_1, n_2; and orbital angular momentum quantum numbers ℓ_1, ℓ_2. This motion can equally well be described as consisting of the motion of the center-of-mass and the relative motion of the two particles around their mass-center. The radius vector, radial and orbital quantum numbers were then designated by R, N, L and r, n, ℓ for the two parts respectively. The relation between these two coordinate systems was defined as:

$$\vec{r} = (\vec{r}_1 - \vec{r}_2)/\sqrt{2} \qquad \vec{R} = (\vec{r}_1 + \vec{r}_2)/\sqrt{2} \tag{3-4}$$

$$2n_1 + \ell_1 + 2n_2 + \ell_2 = 2n + \ell + 2N + L \equiv \rho \tag{3-5}$$

The quantities defined in Eq. (3-4) are more convenient than those given by the more usual definitions:

$$\vec{r} = \vec{r}_1 - \vec{r}_2 \qquad \vec{R} = (\vec{r}_1 + \vec{r}_2)/2$$

They have the advantage that the HO wave functions have the same form in both coordinate systems. Equation (3-5) was obtained from energy conservation considerations. The quantity ρ is called "the energy index of the two particle system." It is the energy above the zeroth order energy of two non-interacting particles in a HO well, since the single particle energy $E_{n_1\ell_1}$, in units of $\hbar\omega$, is equal to $2n_1+\ell_1+3/2$. The total wave functions for a two-particle system can be written in the two schemes as:

$$|n_1\ell_1,\ n_2\ell_2,\ \lambda\mu\rangle = \sum_{m_1m_2} \langle \ell_1\ell_2m_1m_2|\lambda\mu\rangle\ R_{n_1\ell_1}(r_1)\ R_{n_2\ell_2}(r_2)\ \cdot$$

$$Y_{\ell_1m_1}(\theta_1,\phi_1)\ Y_{\ell_2m_2}(\theta_2,\phi_2) \qquad (3\text{-}6)$$

or

$$|n\ell,\ NL,\ \lambda\mu\rangle = \sum_{mM} \langle \ell LmM|\lambda\mu\rangle\ R_{n\ell}(r)\ R_{NL}(R)\ \cdot\ Y_{\ell m}(\theta,\phi)\ Y_{LM}(\Theta,\Phi) \qquad (3\text{-}7)$$

where λ is the total orbital angular momentum, μ is its magnetic quantum number, and m_1, m_2, m, M are the magnetic quantum numbers. The wave function of Eq. (3-6) can be expanded as a linear combination of wave functions of the type (3-7) as follows:

$$|n_1\ell_1,n_2\ell_2,\lambda\mu\rangle = \sum_{n\ell N\ell} |n\ell,NL,\lambda\mu\rangle\ \langle n\ell,NL,\lambda|n_1\ell_1,n_2\ell_2,\lambda\rangle \qquad (3\text{-}8)$$

The expansion coefficients, $\langle n\ell,NL,\lambda|n_1\ell_1,n_2\ell_2,\lambda\rangle$ (which were tabulated by Moshinsky and Brody),[21] are called the "transformation brackets." They transform the wave function from HO well coordinates to relative center-of-mass coordinates. This transformation is independent of the magnetic quantum number μ.

If V(r) is the interaction potential between the two particles, then using Eq. (3-2), one has:

$$\int_0^\infty R_{n\ell}(r)\, V(r)\, R_{n'\ell'}(r)\, r^2\, dr$$

$$= \sum_{k=0}^{n} a_{n\ell k} \sum_{k'=0}^{n'} a_{n'\ell'k'} \int^\infty r^{\ell+\ell'+2k+2k'}\, e^{-r^2} V(r)\, r^2\, dr$$

$$= \sum_{p=1/2(\ell+\ell')}^{1/2(\ell+\ell')+n+n'} \left[\left(\sum_{k=\alpha}^{\beta} a_{n\ell k}\, a_{n'\ell' p-1/2(\ell+\ell')-k}\right) \cdot \frac{\Gamma(p+3/2)}{2}\right]$$

$$\cdot \left[\frac{2}{\Gamma(p+3/2)} \int_0^\infty r^{2p}\, e^{-r^2}\, V(r)\, r^2\, dr\right]$$

$$= \sum_{p=1/2(\ell+\ell')}^{1/2(\ell+\ell')+n+n'} B(n\ell, n'\ell', p) \cdot I_p \tag{3-9}$$

here the summation over the index k,k' has been changed to p,k and hence the summation limits should be changed. Therefore, p has the limit

$$1/2(\ell + \ell') \leq p \leq 1/2(\ell + \ell') + n + n' \tag{3-10}$$

If $n > n'$ then

$$\begin{cases} \alpha = 0 \\ \beta = p - 1/2(\ell+\ell') \end{cases} \quad \text{for } 1/2(\ell+\ell') \leq p \leq 1/2(\ell+\ell')+n'$$

$$\begin{cases} \alpha = p - 1/2(\ell+\ell')-n' \\ \beta = p - 1/2(\ell+\ell') \end{cases} \quad \text{for } 1/2(\ell+\ell')+n' + 1 \leq p \leq 1/2(\ell+\ell')+n$$

$$\begin{cases} \alpha = p - 1/2(\ell+\ell')-n' \\ \beta = n \end{cases} \quad \text{for } 1/2(\ell+\ell')+n + 1 \leq p \leq 1/2(\ell+\ell')+n+n' \tag{3-11}$$

The B coefficient, i.e., $B(n\ell,n'\ell',p)$, the summation index p, and Talmi integral I_p are defined as:

$$B(n\ell,n'\ell',p) = \frac{\Gamma(p+3/2)}{2} \sum_{k=\alpha}^{B} a_{n\ell k} \; a_{n'\ell' p-1/2(\ell+\ell')-k} \quad (3\text{-}12)$$

$$p = k + k' + (\ell + \ell')/2 \quad (3\text{-}13)$$

$$I_p = \frac{2}{\Gamma(p+3/2)} \int_0^\infty r^{2p} \, e^{-r^2} \, V(r) \, r^2 \, dr \quad (3\text{-}14)$$

Here, $\Gamma(x+1) = x\Gamma(x)$ for $x > 3/2$, and $\Gamma(3/2) = \sqrt{\pi}/2$. The definition of I_p is a special example of the general definition with ν set equal to 1. The transformation brackets, the B coefficients, and possible values of p for definite values of the energy index and the total orbital angular momentum λ were tabulated by Moshinsky and Brody. To calculate the diagonal matrix element of the interaction energy between two particles, the following equation can be applied.

$$\langle n_1\ell_1, n_2\ell_2, \lambda\mu | V(r) | n_1\ell_1, n_2\ell_2, \lambda\mu \rangle$$

$$= \sum_{n\ell NL} [\langle n\ell NL\lambda | n_1\ell_1 n_2\ell_2\lambda \rangle]^2 \int_0^\infty R_{n\ell}(r) \, V(r) \, R_{n\ell}(r) \, r^2 \, dr$$

$$= \sum_{n\ell NL} [\langle n\ell NL\lambda | n_1\ell_1 n_2\ell_2\lambda \rangle]^2 [\sum_p B(n\ell,n\ell,p) \cdot I_p] \quad (3\text{-}15)$$

For states with total angular momentum J:

$$\langle n_1\ell_1 1/2 j_1;\ n_2\ell_2 1/2 j_2;\ J|V(r)|n_1\ell_1 1/2 j_1;\ n_2\ell_2 1/2 j_2;\ J\rangle$$

$$= \sum_{\lambda S}\left[(2\lambda+1)(2S+1)(2j_1+1)(2j_2+1)\begin{Bmatrix}\ell_1 & 1/2 & j_1\\ \ell_2 & 1/2 & j_2\\ \lambda & S & J\end{Bmatrix}^2\right]\langle n_1\ell_1,n_2\ell_2,\lambda\mu|V(r)|n_1\ell_1,n_2\ell_2,\lambda\mu\rangle$$

$$= \sum_{\lambda S}\ \sum_{n\ell NL}\left\{\left[(2\lambda+1)(2S+1)(2j_1+1)(2j_2+1)\begin{Bmatrix}\ell_1 & 1/2 & j_1\\ \ell_2 & 1/2 & j_2\\ \lambda & S & J\end{Bmatrix}^2\right]\cdot\right.$$

$$\left.\langle n\ell NL\lambda|n_1\ell_1 n_2\ell_2\lambda\rangle^2\left[\sum_p B(n\ell,n\ell,p)\cdot I_p\right]\right\} \qquad (3\text{-}16)$$

There are no space symmetries in the ket($|>$) and bra ($<|$) wavefunction unless $(n_1\ell_1) = (n_2\ell_2)$. The brackets which contain a 9-j symbol are the squares of the coefficients for transforming from jj to LS coupling.

According to the Pauli principle, the total wavefunction must be antisymmetric. For two particles in states j_1, j_2 which couple to J and good isobaric spin quantum number T, the following antisymmetrization consideration should be followed. The total wave function of the two particles must be antisymmetric. It can be broken into three parts- T, S, ℓ - each havings its own symmetry. For T = 0 states, in using Eq. (3-16) if S = 1, ℓ can only take even values and only the triplet-even potential $V_{TE}(r)$ leads to non-zero matrix elements while for S = 0, ℓ can only take odd values and the singlet-odd potential $V_{SO}(r)$ leads to non-zero matrix elements. Similarily for T = 1 states, if S = 1 then only $V_{TO}(r)$, and if S = 0 then only $V_{SE}(r)$ contribute. Note here it is only the "ℓ" - the relative orbital angular momentum - and not "L" that determines the symmetry of the orbital part of the wave function. If the two particles have different n,ℓ values, i.e., $(n_1\ell_1) \neq (n_2\ell_2)$, then the right side of

Eq. (3-16) must be multiplied by a factor of 2. This factor arises from the normalization of the antisymmetrized wave function of two particles.

If the central interaction is assumed to have a Gaussian radial dependence, i.e.,:

$$V(r) = -V_o e^{-\beta_o r^2}$$

then the Talmi integral reduces to a simple form

$$I_p = \frac{-2V_o}{\Gamma(p+3/2)} \int_0^\infty r^{2p+2} e^{-(1+\beta_o)r^2} dr$$

$$= \frac{-V_o}{(1+\beta_o)^{p+3/2}} \qquad (3\text{-}17)$$

where r is in units of the size parameter b where $b = (\hbar/M\omega)^{1/2} = (1/\nu)^{1/2}$ and so ν is in units of $1/b^2$. Here ν is the HO parameter. Since the jj-LS expansion coefficients are easily available and the transformation brackets, B coefficients, and the allowed p values are tabulated, the calculation of diagonal matrix elements is very simple for a Gaussian interaction.

The potential used in the calculation was:

$$V_{TE} = -52\, e^{-0.2922\, F^{-2} \cdot r_a^{\,2}} \quad \text{MeV}$$

$$V_{TE}/V_{SE} = 1.6 \qquad V_{SO} = 0$$

$$V_{TO}/V_{TE} = -1/2.$$

This was the potential used by True[22] in calculating the ^{14}N spectrum except for V_{TO} which is the strongest repulsive potential estimated by Redlich.[23] Since r_a was the internucleon distance i.e., $\vec{r}_a = \vec{r}_1 - \vec{r}_2$, but $\vec{r}$ defined by Moshinsky was $\vec{r} = (\vec{r}_1 - \vec{r}_2)/\sqrt{2}$, it follows that:

$$I_p = \frac{-52}{(1 + \frac{0.2922}{\nu} \times 2)^{p + 3/2}} \text{ MeV} \tag{3-18}$$

for the triplet-even potential. For the other three potentials, only the V_o value should be changed. The HO parameter was estimated from $\nu = (2n_1+\ell_1+3/2)/R^2$ where n_1 has the Moshinsky definition given above and R^2 is the expectation value of r_1^2 of the state $|n_1\ell_1\rangle$.[24]

B. Interaction Energy between Particles in Non-Equivalent Orbits

Let there be n_1 particles of j_1 which couple to T_1J_1 and n_2 particles of j_2 which couple to T_2J_2. T_1J_1 and T_2J_2 couple to form the state TJ. The interaction energy between the n_1 particles and the n_2 particles can be expressed in terms of two body interaction energy matrix elements $V(j_1j_2,T'J')$ as follows:[25]

$$\langle j_1^{n_1}(\alpha_1T_1J_1)j_2^{n_2}(\alpha_2T_2J_2)TJ \left| \sum_{i=1}^{n_1} \sum_{k=n_1+1}^{n_1+n_2} V_{ik} \right| j_1^{n_1}(\alpha_1'T_1'J_1')j_2^{n_2}(\alpha_2'T_2'J_2')TJ\rangle$$

$$= n_1n_2 \sum_{\alpha_{11}T_{11}J_{11}\alpha_{22}T_{22}J_{22}} \left[j_1^{n_1} \alpha_1T_1J_1 \left\{ \left| j_1^{n_1-1} (\alpha_{11}T_{11}J_{11})j_1T_1J_1 \right] \right.\right.$$

$$\left.\left. \left[j_1^{n_1-1}(\alpha_{11}T_{11}J_{11})j_1T_1'J_1' \right| \right\} j_1^{n_1} \alpha_1'T_1'J_1' \right] \left[j_2^{n_2} \alpha_2T_2J_2 \left\{ \left| j_2^{n_2-1} (\alpha_{22}T_{22}J_{22})j_2T_2J_2 \right] \right.\right.$$

$$\times \left[j_2^{n_2-1} (\alpha_{22} T_{22} J_{22}) j_2 T_2' J_2' \middle| \right\} j_2^{n_2} \alpha_2' T_2' J_2' \Big] \times \Big[(2T_1+1)(2T_1'+1)(2T_2+1)(2T_+'+1)$$

$$\times \quad (2J_1+1)(2J_1'+1)(2J_2+1)(2J_2'+1) \Big]^{1/2} \times \sum_{T'J'} (2T'+1)(2J'+1) V(j_1 J_2 T' J')$$

$$\times \sum_{T_{12}} (2T_{12}+1) \begin{Bmatrix} T_{11} & 1/2 & T_1 \\ T_{22} & 1/2 & T_2 \\ T_{12} & T' & T \end{Bmatrix} \begin{Bmatrix} T_{11} & 1/2 & T_1' \\ T_{22} & 1/2 & T_2' \\ T_{12} & T' & T \end{Bmatrix}$$

$$\times \sum_{J_{12}} (2J_{12}+1) \begin{Bmatrix} J_{11} & j_1 J_1 \\ J_{22} & j_2 J_2 \\ J_{12} & J' \; J \end{Bmatrix} \begin{Bmatrix} J_{11} & j_1 & J_1' \\ J_{22} & j_2 & J_2' \\ J_{12} & J' & J \end{Bmatrix} \tag{3-19}$$

where the brackets $[\{|]$ and $[|\}]$ are the coefficients of fractional parentage (cfp), the V_{ik} are the interaction potentials between nucleons, and

$$V(j_1 j_2, T'J') = \langle j_1\ 1/2,\ j_2\ 1/2,\ T'J' | V_{12} | j_1\ 1/2,\ j_2\ 1/2,\ T'J' \rangle$$

The above equation was used to calculate the residual interaction energy between the proton and neutron both in the $1d_{5/2}$ shell model state for the 11/2- levels of ^{15}N and ^{17}O, the 5+ level of ^{16}N, and the 6+ level of ^{16}O, as well as $(1f_{7/2})^2_{7+}$, and $(1g_{9/2})^2_{9+}$ shell model states. It was also used in predicting the excitation energies by following the Talmi method of shell model calculation.[26]

IV. EXPERIMENTAL RESULTS

A. The (α,d) Reactions

1. $^{13}C(\alpha,d)^{15}N$

This reaction was studied with a methane gas target which contained 93.7% ^{13}C, at an alpha particle beam energy of 40.1 MeV. A typical spectrum taken at θ(lab) = 12.0° is shown in Fig. 5. The methane gas was found to decompose at a constant rate under irradiation of the incident beam. This effect was corrected by using the monitor counter results. Angular distributions for θ(lab) = 10.0°-75.0° are shown in Fig. 6. The resolution (FWHM) was about 130 keV. The excitation energies determined here, together with the total cross sections and previously known level information, are listed in Table I.

As shown in the spectrum, only a few levels were populated strongly. The 13.028 MeV and 11.950 MeV levels were assigned as the doublet state with configuration:

$$[(^{13}C\ g.s.)_{1/2-,1/2}\ (1d_{5/2})^2_{5+,0}]\ \begin{matrix}11/2-,1/2\\ 9/2-,1/2\end{matrix}$$

These assignments will be discussed in detail in Chapter V.

2. $^{14}C(\alpha,d)^{16}N$

Solid ^{14}C on a gold backing was used as the target. This reaction was studied with an alpha particle beam energy of 46.0 MeV. A typical spectrum taken at θ(lab) = 15.6° is shown in Fig. 7. Angular distributions for θ(lab) = 11.7°-80.2° are shown in Fig. 8. The resolution was about 160 keV.

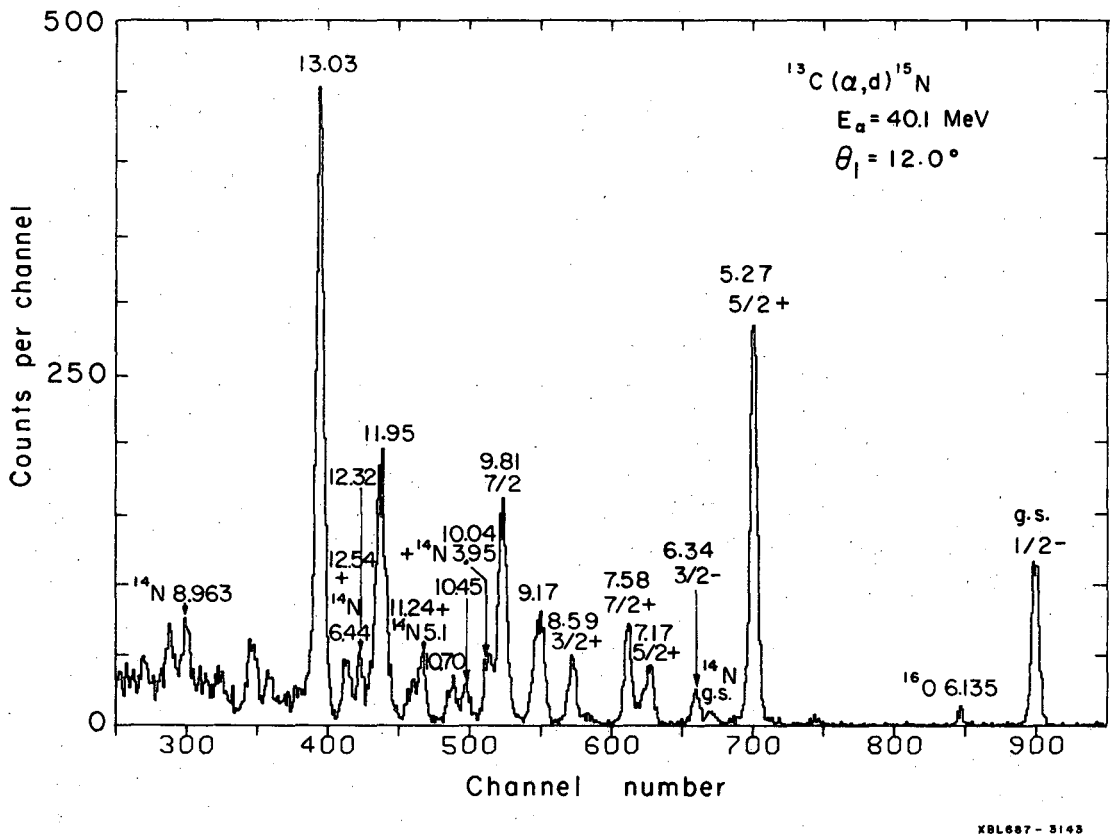

Fig. 5 Deuteron energy spectrum for the reaction $^{13}C(\alpha,d)^{15}N$ at θ(lab) = 12.0 deg with E(α) = 40.1 MeV.

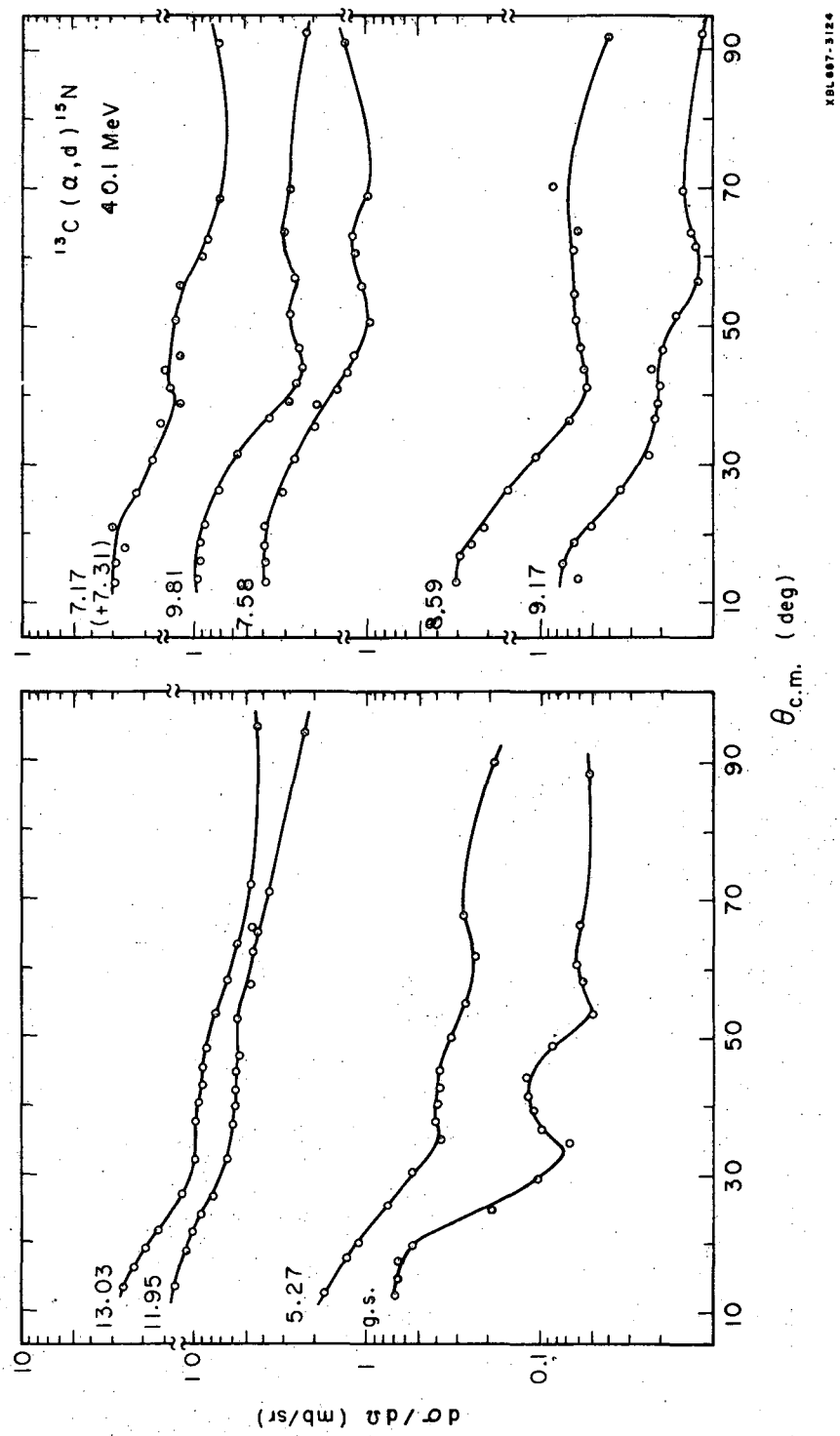

Fig. 6 Deuteron angular distributions for the reaction $^{13}C(\alpha,d)^{15}N$ at $E(\alpha)$ = 40.1 MeV.

Table I. ^{15}N levels observed in $^{13}C(\alpha,d)^{15}N$ reaction at 40.1 MeV.

Levels observed (MeV)	Previously reported levels[a,b,c] Energy (MeV)	J_π	Intensity[d] (mb)	Dominant[e] configuration
0	0	1/2-	0.61	$(p_{1/2})^{-1}$
5.266±0.020	5.270	5/2+	2.25	$(p_{1/2})^2_0\ d_{5/2}$
	5.299	1/2+		$(p_{1/2})^2_0\ 2s_{1/2}$
6.336±0.030	6.323	3/2-		$(p_{3/2})^{-1}_{3/2}$ [f]
7.170±0.020	7.154	5/2+	0.70	$(p_{1/2})^2_1\ d_{5/2}$
	7.300	3/2+		$(p_{1/2})^2_1\ 2s_{1/2}$
7.581±0.020	7.563	7/2+	0.94	$(p_{1/2})^2_1\ d_{5/2}$
	8.312	1/2+(3/2+)		$(p_{1/2})^2_1\ 2s_{1/2}$
8.587±0.020	8.570	3/2+	0.50	$(p_{1/2})^2_1\ d_{5/2}$
	9.052	1/2+,3/2+		
9.169±0.030	9.155	3/2-(5/2)	1.19	
	9.233	≤5/2		
	9.762	5/2-		
9.808±0.020	9.832	7/2(-)	2.15	
	9.929	1/2+,3/2+		
	10.074	3/2+		
10.451±0.020	10.458	3/2,5/2,7/2		
	10.548	5/2		

Table I. (continued)

Levels observed (MeV)	Previously reported levels Energy (MeV)	J_π	Intensity (mb)	Dominant configuration
10.698±0.020	10.710	3/2+		
	10.815	3/2		
	11.243	>1/2-		
	11.299	1/2-		
	11.438	1/2+		
	11.616	1/2+(T=3/2)		
	11.773	3/2+		
	11.885	3/2-		
11.950±0.020	11.950	(9/2-)[g]	3.20	$(d_{5/2})^2_5\ p_{1/2}$[g]
		>1/2		
	11.972	1/2-		
	12.103	5/2		
	12.152	3/2		
12.318±0.030	12.333	5/2		
	12.502	5/2+(T=3/2)		
	12.928	3/2+		
	12.93	7/2-		
13.028±0.020		(11/2-)[g]	4.82	$(d_{5/2})^2_{5,}p_{1/2}$[g]
	13.15			
	13.18			

[a]Ref. 27, [b]Ref. 28, [c]Ref. 29, [d]Range of integration: 10.0 to 75.0 deg (lab), [e]Ref. 30, [f]Ref. 31, [g]Assigned by this work.

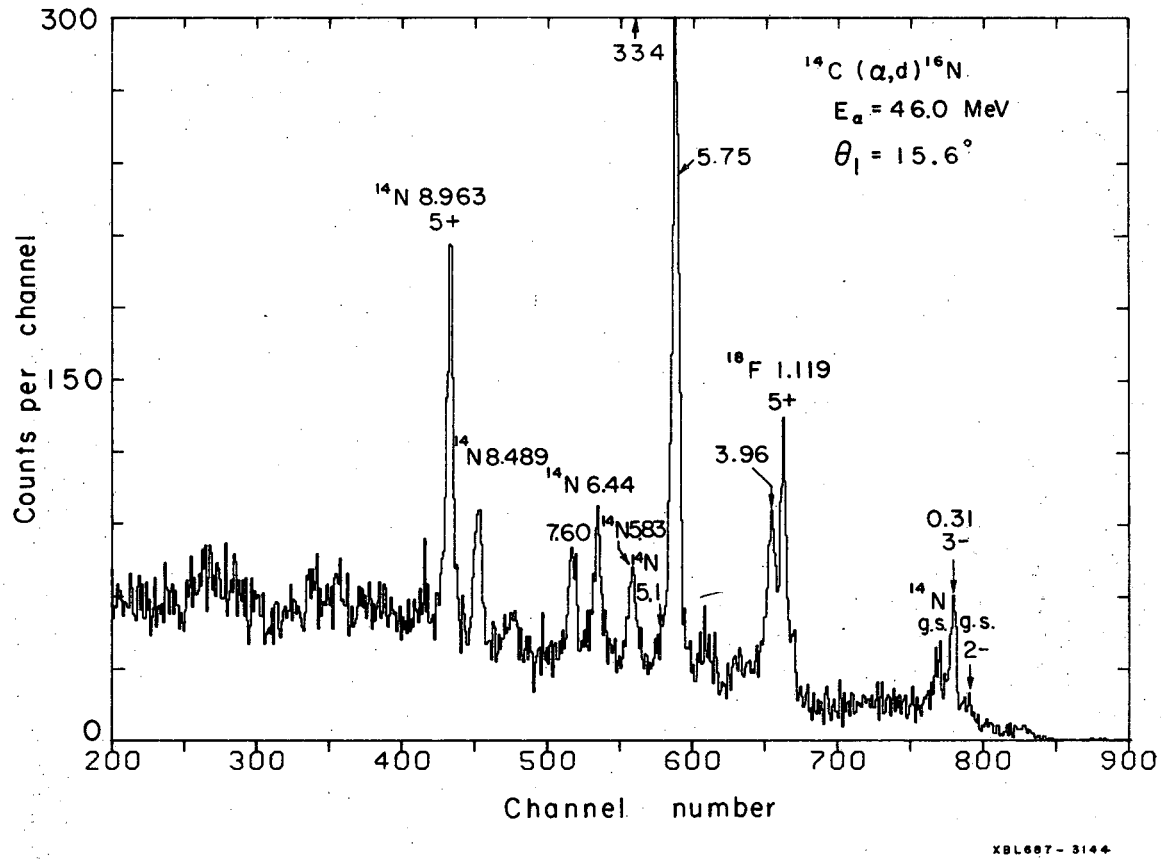

Fig. 7 Deuteron energy spectrum for the reaction $^{14}C(\alpha,d)^{16}N$ at θ(lab) = 15.6 deg with E(α) = 46.0 MeV.

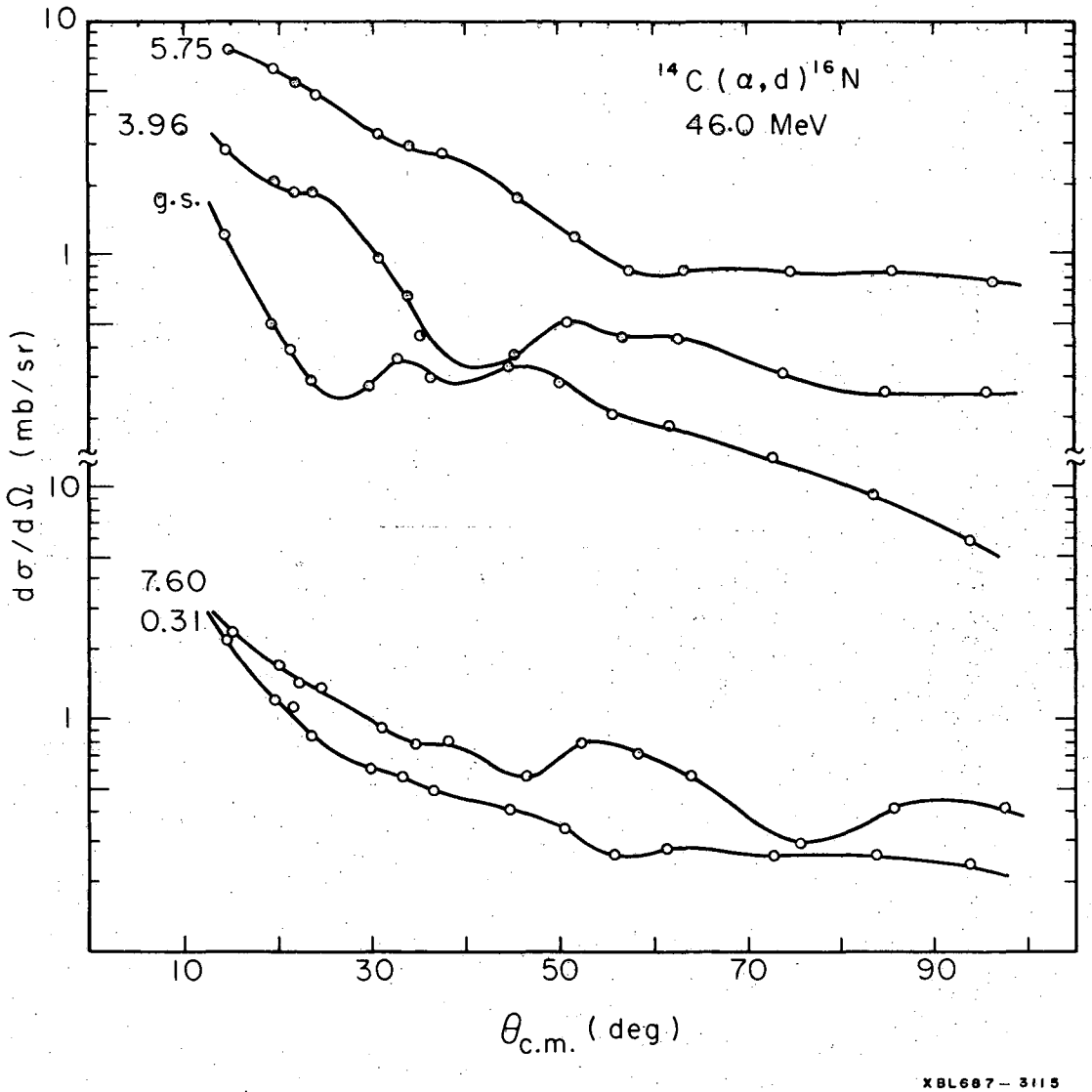

Fig. 8 Deuteron angular distributions for the reaction $^{14}C(\alpha,d)^{16}N$ at $E(\alpha)$ = 46.0 MeV.

The only highly populated level (at excitation 5.745 MeV) was assigned to have the dominant configuration:

$$[(^{14}C\ g.s.)_{0+,1}\ (1d_{5/2})^2_{5+,0}]_{5+,1}$$

The measured excitation energies and total cross sections together with recent energy level information of ^{16}N are listed in Table II.

3. $^{15}N(\alpha,d)^{17}O$

Gaseous ^{15}N with 99.71% purity was used as the target. The reaction was studied with an alpha particle beam energy of 45.4 MeV. A spectrum taken at θ(lab) = 13.2° is shown in Fig. 9. Angular distributions for θ(lab) = 11.2°-70.8° are shown in Fig. 10. The resolution was about 150 keV. The measured excitation energies and total cross sections together with energy level information of ^{17}O are listed in Table III.

Two strong levels at 7.742 and 9.137 MeV were assigned to have the dominant configuration:

$$[(^{15}N\ g.s.)_{1/2-,1/2}\ (1d_{5/2})^2_{5+,0}]_{\substack{11/2-,1/2\\9/2-,1/2}}$$

This result is in agreement with the previous (α,d) study at 47 MeV.[2] Better resolution was obtained in this work.

4. $^{20}Ne(\alpha,d)^{22}Na$

This reaction was studied with an alpha particle beam energy of 44.5 MeV with a gaseous ^{20}Ne target with purity 98.1%. Figure 11 is the spectrum taken at θ(lab) = 11.2°. Angular distributions for

Table II. ^{16}N levels observed in $^{14}C(\alpha,d)^{16}N$ reaction at 40.6 MeV.

Levels observed (MeV)	Previously reported levels[a] Energy (MeV)	J_π	Intensity[b] (mb)	Dominant[a] configuration
0	0	2-	1.35	$(p_{1/2})^{-1}\ d_{5/2}$
	0.120	0-		$(p_{1/2})^{-1}\ 2s_{1/2}$
0.307±0.02	0.300	3-	2.52	$(p_{1/2})^{-1}\ d_{5/2}$
	0.399	1-		$(p_{1/2})^{-1}\ 2s_{1/2}$
	3.359	1+		
	3.519	(0-)		
3.961±0.02	3.957	(1,2,3)+	3.43	
	4.318	1+		
	4.391			
	4.725	1-		$(p_{1/2})^{-1}\ d_{3/2}$
	4.774	(1,2,3)+		
	5.053			
	5.130			
	5.150			
	5.226			
	5.305	2-		$(p_{1/2})^{-1}\ d_{3/2}$
	5.520			
5.745±0.02	5.730	(5+)[c]	10.07	$(d_{5/2})^2_{5+}(p_{1/2})^2_{0+}$ [c]
	6.009	(3-)		$(p_{3/2})^{-1}\ d_{5/2}$
	6.167			

Table II. (Continued)

Levels observed (MeV)	Previously reported levels Energy (MeV)	J_π	Intensity (mb)	Dominant configuration
	6.371			
	6.422	(2-)		$(p_{3/2})^{-1}\ d_{5/2}$
	6.512			
	6.613			
	6.854			
	7.006			
	7.133			
	7.250			
7.599±0.03	7.573		4.30	
	7.640			

[a]Ref. 32; [b]Range of integration: 11.7 to 80.2 deg (lab); [c]This work.

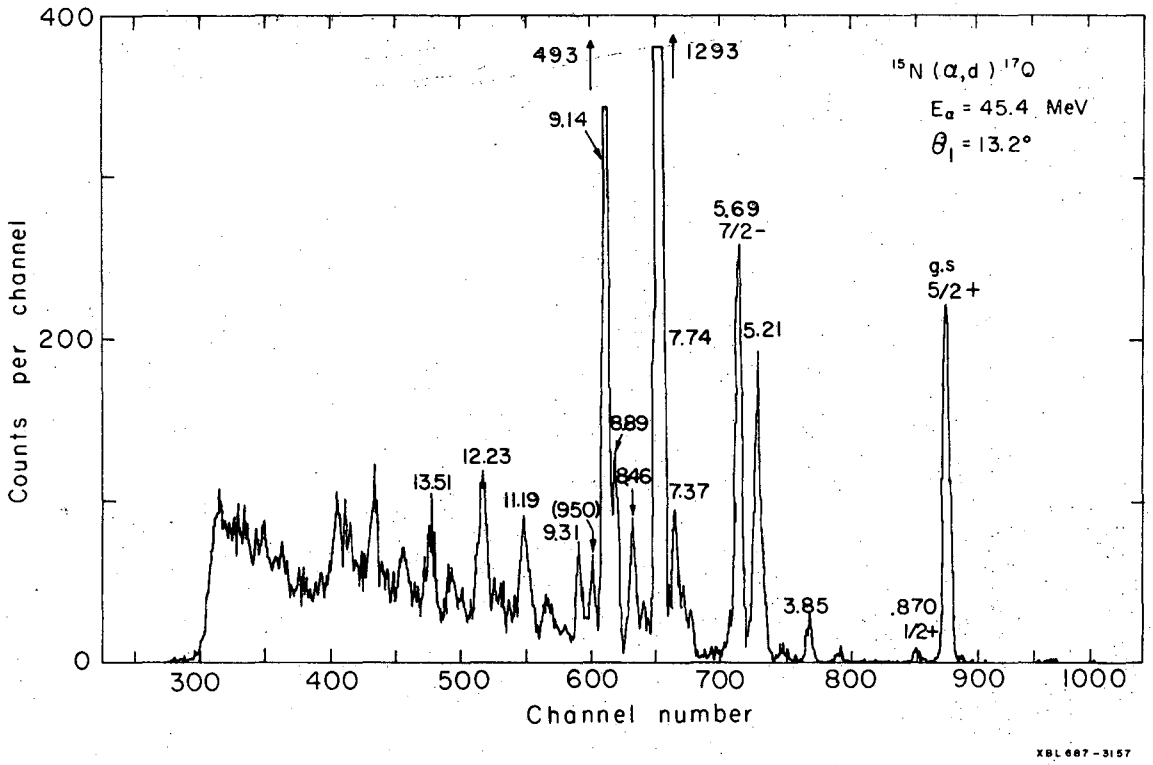

Fig. 9 Deuteron energy spectrum for the reaction $^{15}N(\alpha,d)^{17}O$ at θ(lab) = 13.2 deg with E(α) = 45.4 MeV.

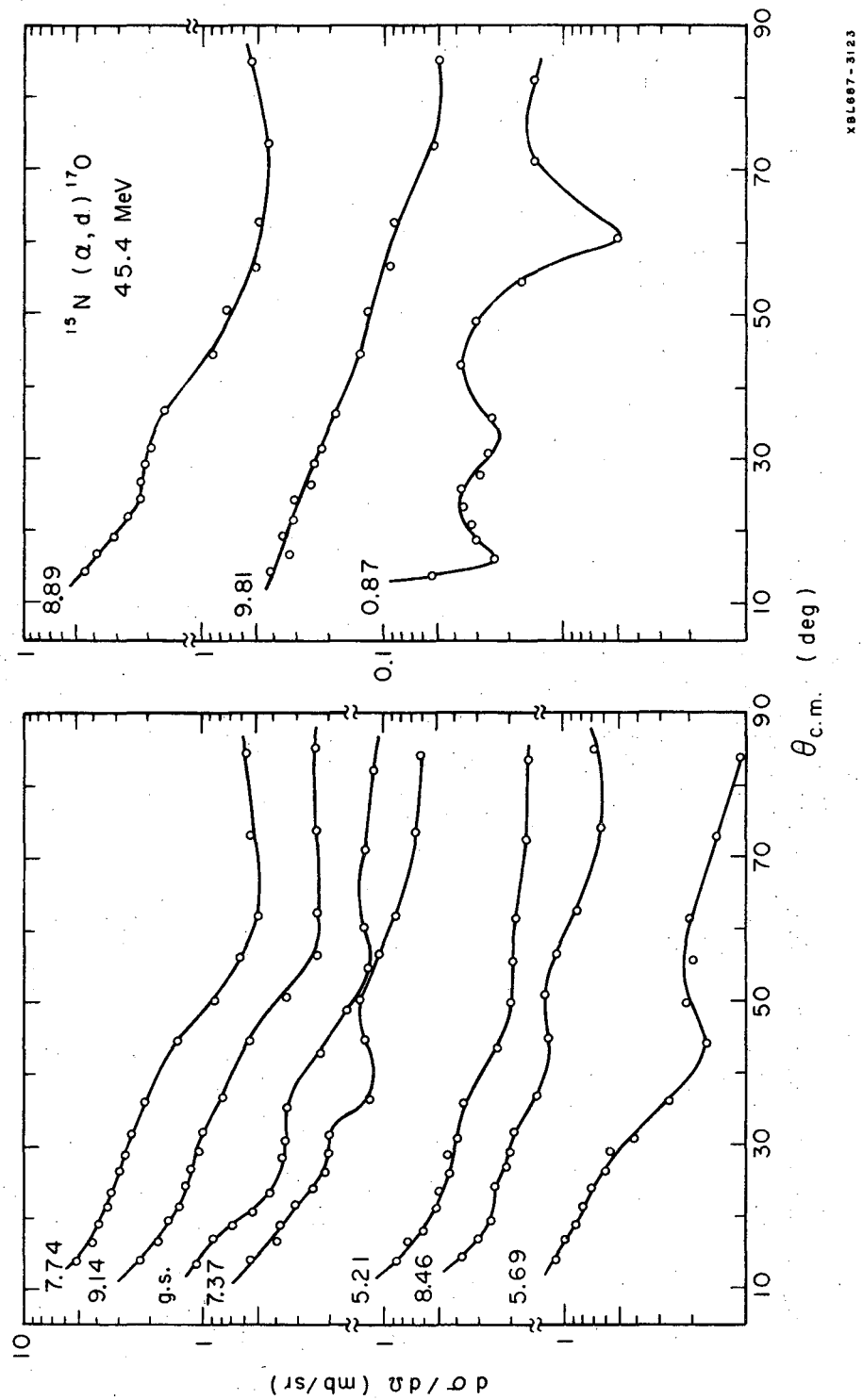

Fig. 10 Deuteron angular distributions for the reaction $^{15}N(\alpha,d)^{17}O$ at $E(\alpha)$ = 45.4 MeV.

Table III. ^{17}O levels observed in $^{15}N(\alpha,d)^{17}O$ reaction at 45.4 MeV.

Levels observed (MeV)	Previously reported levels[a,b] Energy (MeV)	J_π	Intensity[c] (mb)	Dominant configuration
0	0	5/2-	1.15	$d_{5/2}$ s.p.
0.870±0.050	0.871	1/2+	0.11	$2s_{1/2}$ s.p.
	3.058	(1/2-)		
3.850±0.050	3.846	5/2-	0.18	
4.566±0.050	4.555	3/2-	0.09	
	5.083	3/2+		$d_{3/2}$ s.p.
5.208±0.030	5.217		1.35	
	5.378	3/2-		
5.690±0.030	5.697	7/2-	1.37	
	5.729			
	5.866	≥3/2		
	5.940	1/2-		
	6.24			
	6.38	1/2+		
	6.87			
	7.161	5/2		
	7.28	3/2+		
7.367±0.030	7.373	5/2		0.67
	7.560	≥7/2		
	7.676	3/2		
	7.691	7/2		
	7.694	3/2		
7.742±0.020		(11/2-)[d,e]	6.58	$(d_{5/2})^2_5 p^{-1}_{1/2}$ [d,e]
	7.91	1/2		
	8.08	3/2		
8.147±0.030	8.20	3/2	0.30	
	8.27			

Table III. (Continued)

Levels observed (MeV)	Previously reported levels Energy (MeV)	J_{π}	Intensity (mb)	Dominant configuration
	8.340	1/2		
	8.390	5/2		
8.459±0.030	8.460	7/2	0.68	
	8.493	3/2		
	(8.59)			
	8.70	3/2		
8.890±0.030	8.89	3/2	0.53	
	8.96	7/2		
	9.06			
9.137±0.030	9.15	(9/2)[d,e]	2.70	$(d_{5/2})^2_5 p^{-1}_{1/2}$ [d,e]
	9.20	5/2		
	9.50	7/2		
	9.73	7/2		
9.814±0.030	9.78		0.69	
	9.89	9/2		

[a]Ref. 29; [b]Ref. 33; [c]Range of integration: 11.2 to 70.8 deg (lab); [d]Ref. 2; [e]Assigned by this work.

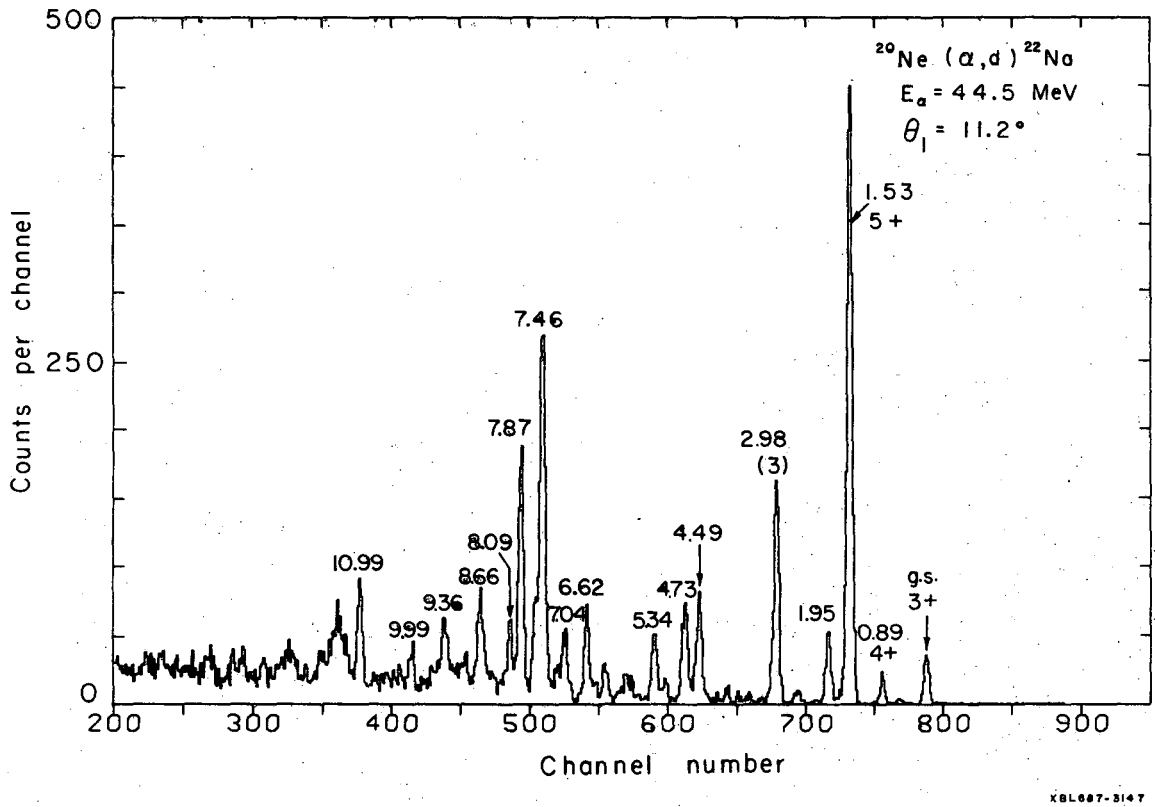

Fig. 11 Deuteron energy spectrum for the reaction $^{20}Ne(\alpha,d)^{22}Na$ at θ(lab) = 11.2 deg with E(α) = 44.5 MeV.

θ(lab) = 9.0°-50.0° are shown in Fig. 12. The resolution was about 110 keV. The measured excitation energies and total cross sections together with energy level information of ^{22}Na are listed in Table IV.

In general, the levels populated were the same as a previous study of this reaction.[3] However, a better resolution was obtained, and the excitation energy studied was extended to about 15 MeV. Three levels (1.528, 7.460 and 7.874 MeV) were strongly populated. The level at 1.528 MeV was assigned to have the dominant configuration:

$$[(^{20}\text{Ne g.s.})_{0+,0}\ (1d_{5/2})^2_{5+,0}]_{5+,0}$$

The level at 7.460 MeV was assigned to have:

$$[(^{20}\text{Ne g.s.})_{0+,0}\ (1d_{5/2},\ 1f_{7/2})_{6-,0}]_{6-,0}$$

configuration. A brief discussion of the configuration of the 7.460 and 7.874 MeV levels is made in Chapter V section F.

5. <u>^{52}Cr(α,d)^{54}Mn, ^{54,56}Fe(α,d)^{56,58}Co, ^{59}Co(α,d)^{61}Ni, ^{58,60,62}Ni(α,d) ^{60,62,64}Cu, ^{63}Cu(α,d)^{65}Zn, and ^{64,66,68}Zn(α,d)^{66,68,70}Ga</u>

These reactions were studied with an alpha particle beam energy of 50.0 MeV at four angles - 14,20,34 (or 35), 40 (or 41), except the reaction on ^{60}Ni for which data at 15 different angles were taken. Separated isotope targets with purity ranging from 90% to 99.9% were used. The target thicknesses were from 153 μg/cm^2 to 630 μg/cm^2. In order to stop the deuterons, a counter telescope with a ΔE counter 0.06" thick and an E counter 0.12" thick was used. The dead layer of

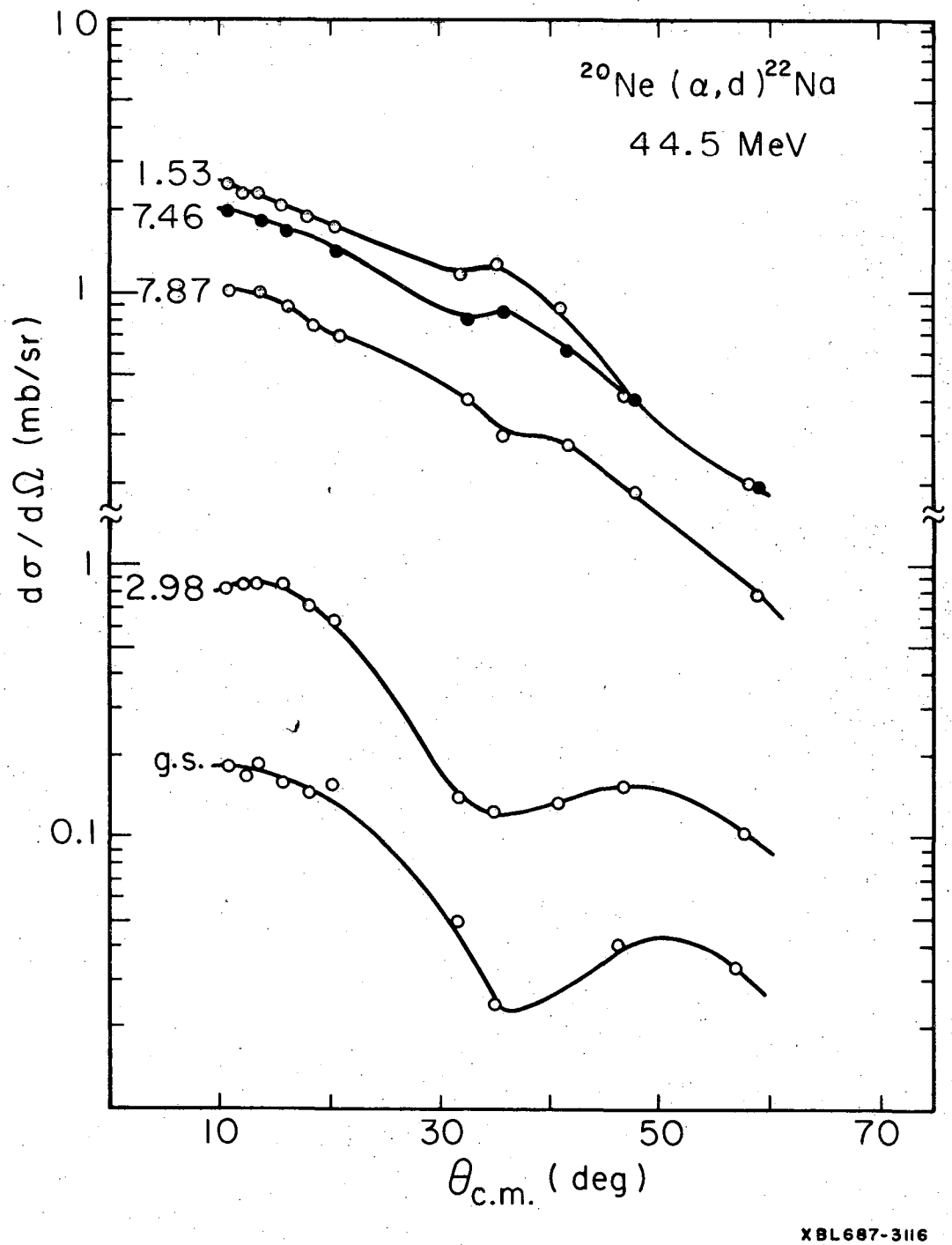

Fig. 12 Deuteron angular distributions for the reaction $^{20}Ne(\alpha,d)^{22}Na$ at $E(\alpha)$ = 44.5 MeV.

Table IV. ^{22}Na levels observed in $^{20}Ne(\alpha,d)^{22}Na$ reaction at 44.5 MeV.

Levels observed (MeV)	Previously reported levels[a,b] Energy (MeV)	Jπ	T	Intensity[d] (mb)	Dominant configuration
0	0	3+	0	0.17	
	0.58305	1+	0		
	0.656	0+	1		
	0.8909	4+	0		
1.528±0.020	1.5281	5+	0	2.49	$(d_{5/2})^2_{5+}$ [e,f]
1.946±0.030	1.9359	1+		0.35	
	1.9518	(2+)	1		
	1.9835	2+,3+			
	2.2104	1-			
2.558±0.040	2.5715	1(+),2		0.07	
2.976±0.020	2.9686	(3)		0.70	
	3.0594	(2)			
	3.526	≥2			
	3.712	≥2			
	3.949	1			
	4.077		(1)		
	4.325				
	4.363	1,2			
4.488±0.030				0.34	
4.733±0.020	High level density			0.50	
5.339±0.030	Spin and parity unknown			0.28	
6.274±0.020				0.22	
6.617±0.030				0.63	
7.042±0.030				0.42	
7.460±0.030	7.48[c]			2.05	$(d_{5/2},f_{7/2})_{6-}$ [e]
7.874±0.030	7.89[c]			0.97	
8.091±0.040				0.42	
8.659±0.040				0.72	

Table IV. (continued)

Levels observed (MeV)	Previously reported levels Energy (MeV)	Jπ	T	Intensity (mb)	Dominant configuration
9.356±0.040	High level density			0.59	
9.990±0.040				0.45	
10.990±0.040	Spin and parity unknown			0.69	

[a]Ref. 34; [b]Ref. 8; [c]Ref. 35; [d]Range of integration: 9.0 to 50.0 deg (lab); [e]Ref. 3; [f]Assigned by this work.

this thick ΔE detector was the main cause of the loss of resolution to a value of 170 keV. Spectra of deutrons from these reactions are shown in Figs. 13-23. The high selectivity in populating states by (α,d) reaction again prevailed in this mass region. States where the captured proton-neutron pair were probably both in $1g_{9/2}$ state and coupled to 9+ were assigned for these nuclides. These states are listed in Table VI in Chapter V section A. The differential cross sections for formation of these states at forward angles were about 1 mb/sr. Previously known level information for the product nuclei can be found in refs. 36-47.

B. The (α,t) Reactions

Very few (α,t) reactions have been previously studied.[48,49] In the present work, the (α,t) reaction was studied to locate previously unknown $1g_{9/2}$ single particle states. In the light elements, the (α,t) reaction was studied mainly because it could be observed simultaneously with the (α,d) reactions.

Since the Q-values of (α,d) and (α,t) reactions were close, the triton and deuteron spectra were recorded simultaneously in the different groups of the Nuclear Data pulse height analyzer. The triton spectra from (α,t) reactions on targets of $^{12,13,14}C$, ^{15}N, ^{20}Ne, ^{52}Cr, $^{54,56}Fe$, ^{59}Co, $^{58,60,62}Ni$, ^{63}Cu, $^{64,66,68}Zn$, together with angular distributions from $^{13,14}C$, ^{15}N, ^{20}Ne and ^{60}Ni targets are shown from Figs. 24-44. The measured excitation energies are marked on the spectra.

A comparison of the high cross section peaks populated by the (α,t) reaction with the known shell model configurations for the corresponding levels helps to elucidate the general characteristics of this

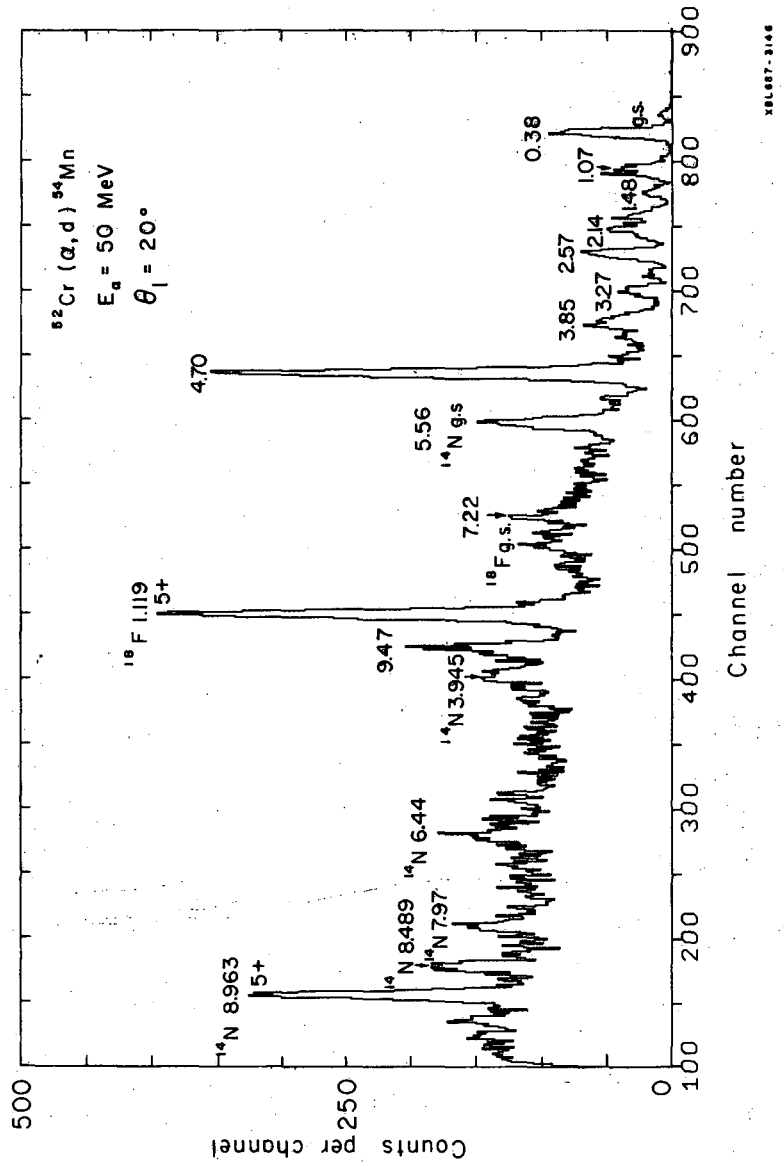

Fig. 13 Deuteron energy spectrum for the reaction $^{52}Cr(\alpha,d)^{54}Mn$ at θ(lab) = 20 deg with E(α) = 50.0 MeV. The ^{18}F peak in the spectrum is from the ^{16}O impurity in the target.

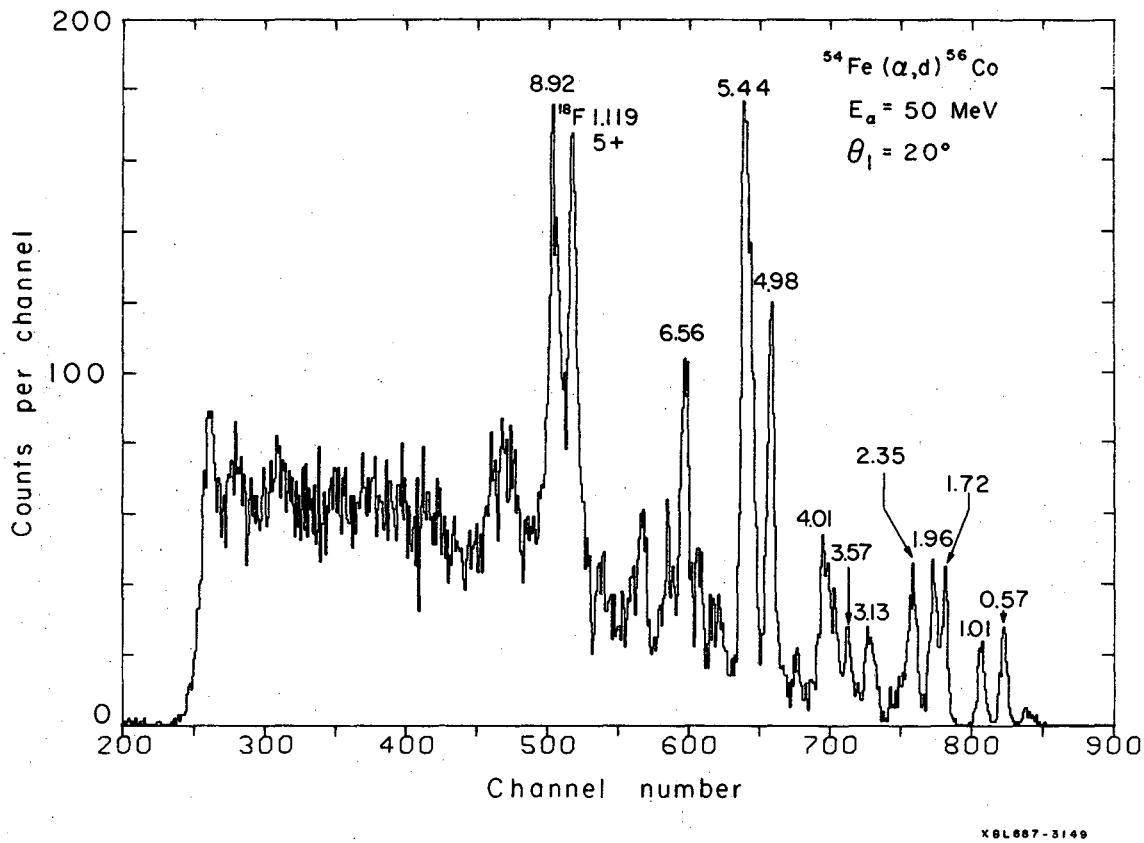

Fig. 14 Deuteron energy spectrum for the reaction $^{54}Fe(\alpha,d)^{56}Co$ at θ(lab) = 20 deg with E(α) = 50.0 MeV.

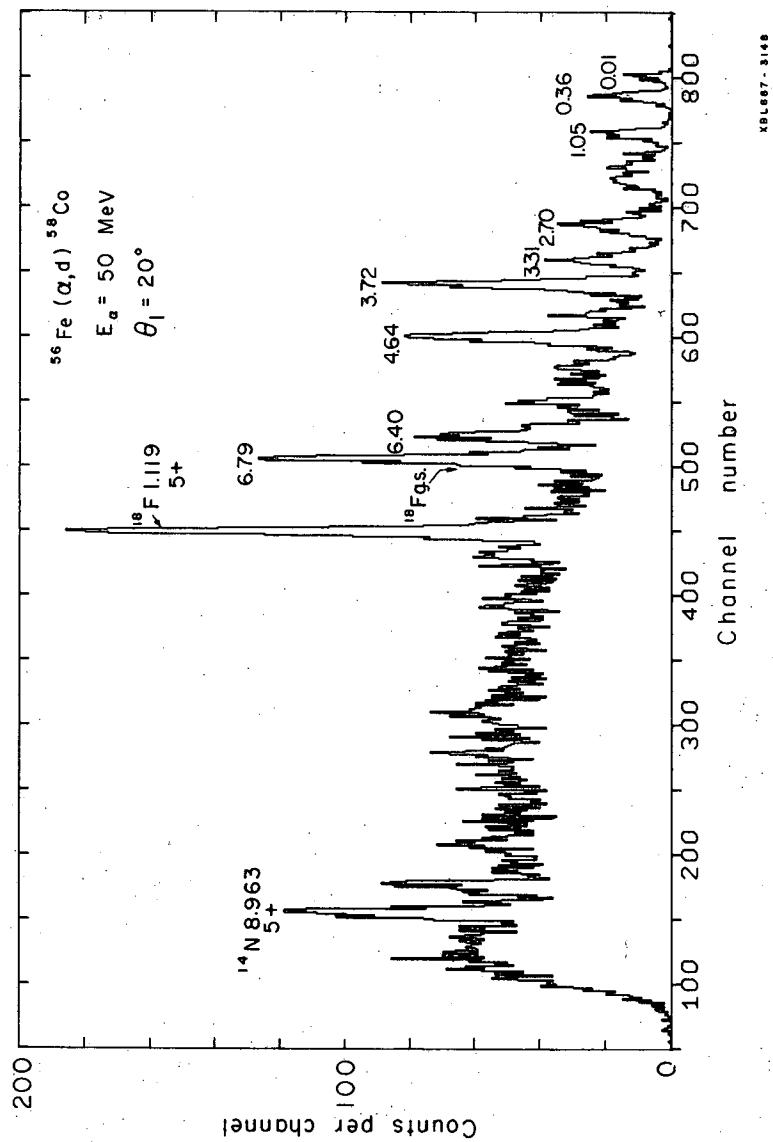

Fig. 15 Deuteron energy spectrum for the reaction $^{56}Fe(\alpha,d)^{58}Co$ at θ(lab) = 20 deg with E(α) = 50.0 MeV.

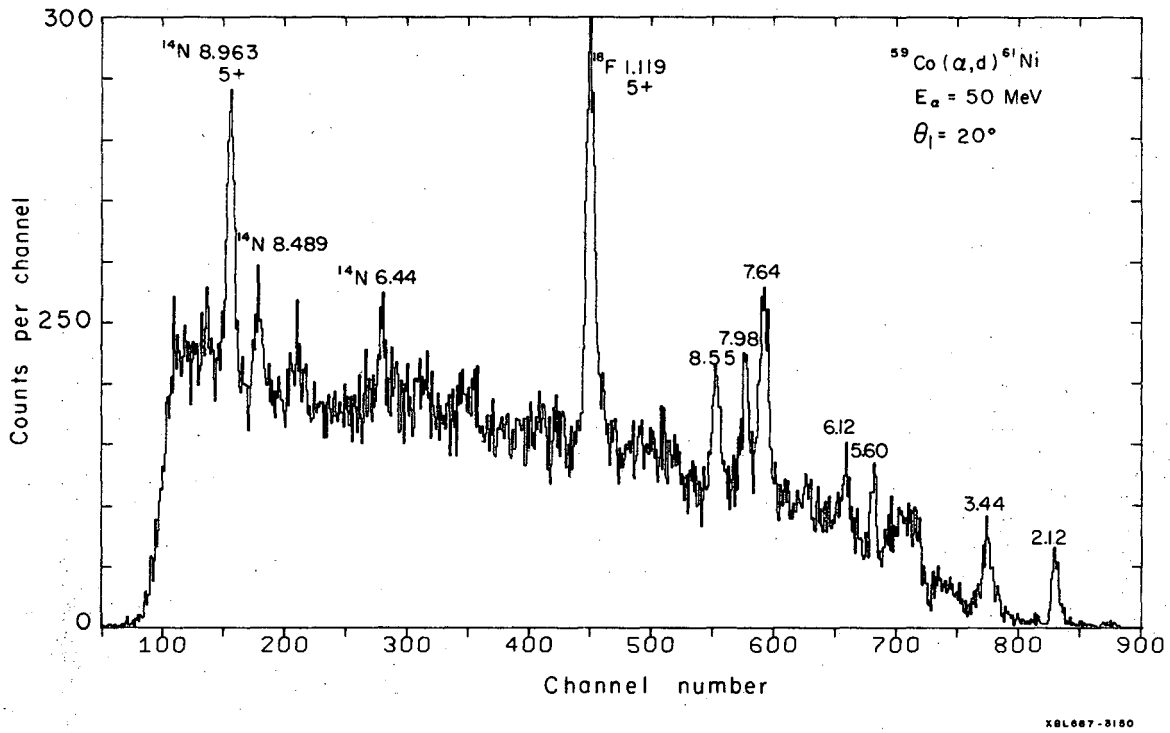

Fig. 16 Deuteron energy spectrum for the reaction $^{59}Co(\alpha,d)^{61}Ni$ at θ(lab) = 20 deg with E(α) = 50.0 MeV.

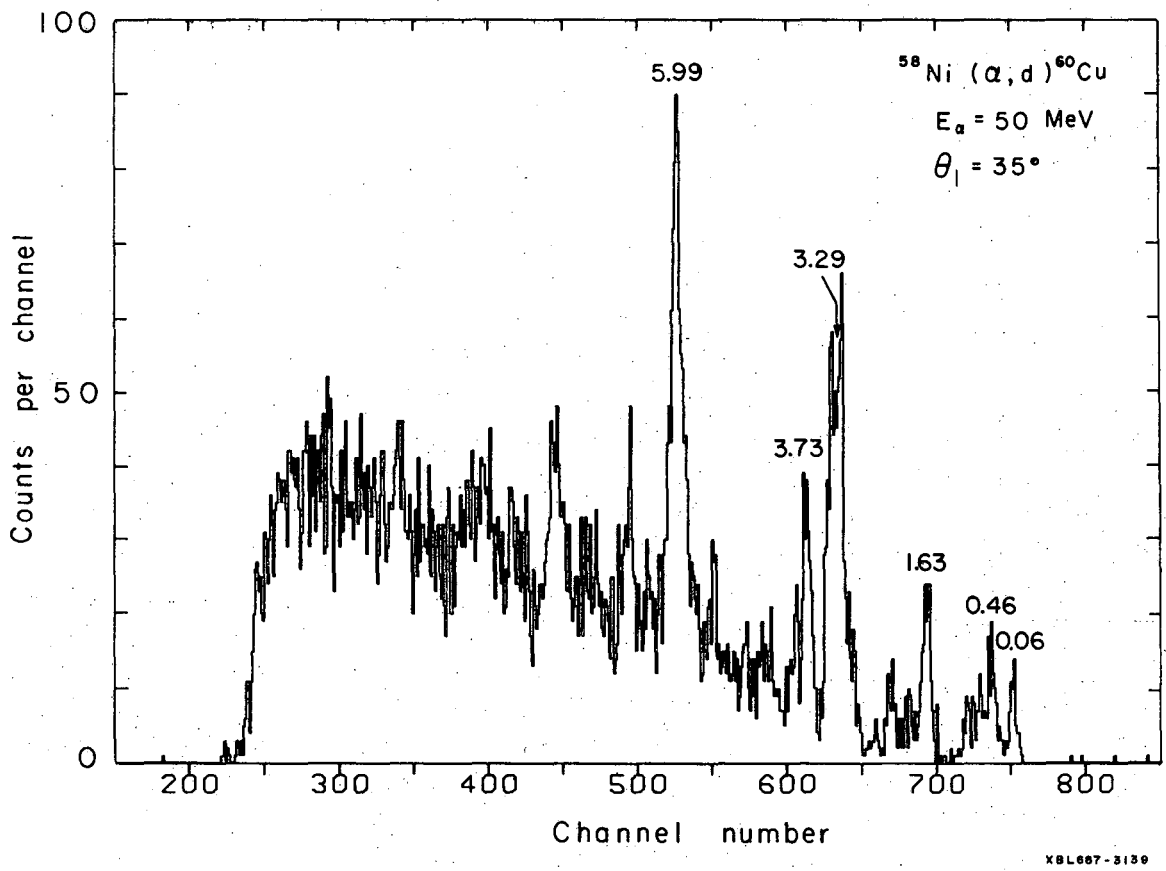

Fig. 17 Deuteron energy spectrum for the reaction $^{58}Ni(\alpha,d)^{60}Cu$ at θ(lab) = 35 deg with E(α) = 50.0 MeV.

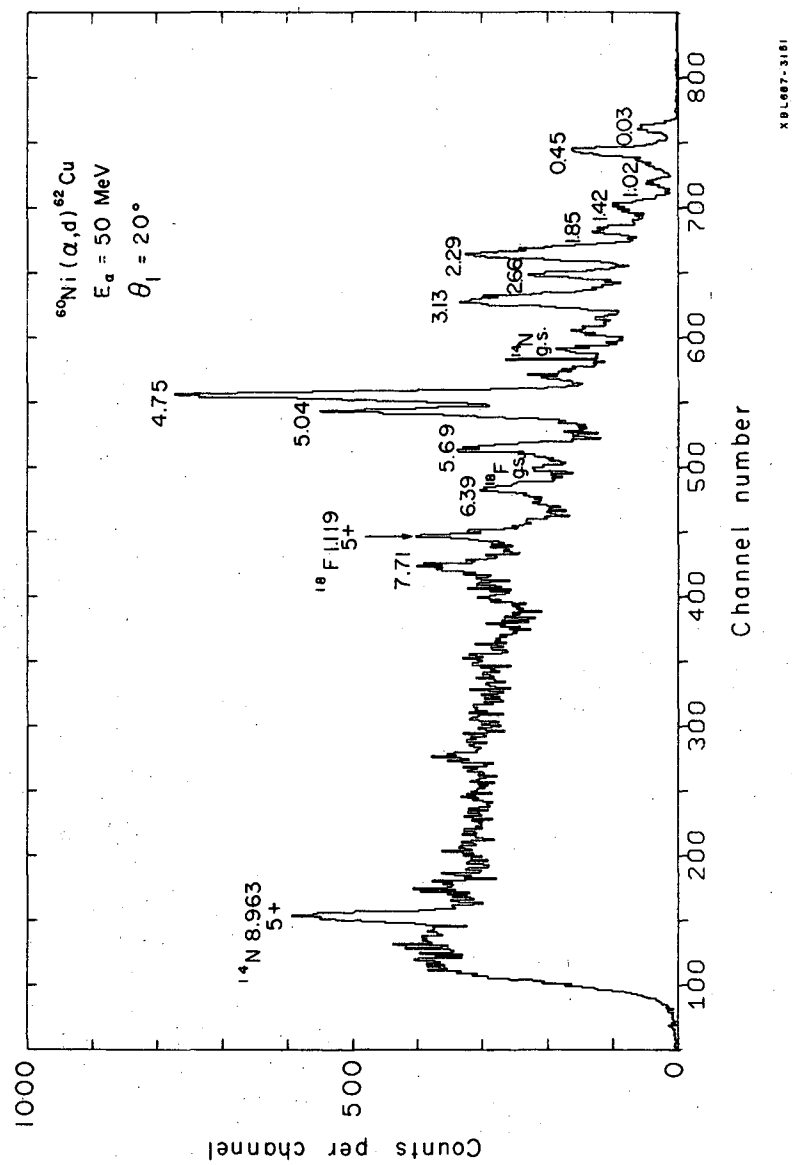

Fig. 18 Deuteron energy spectrum for the reaction $^{60}Ni(\alpha,d)^{62}Cu$ at θ(lab) = 20 deg with E(α) = 50.0 MeV.

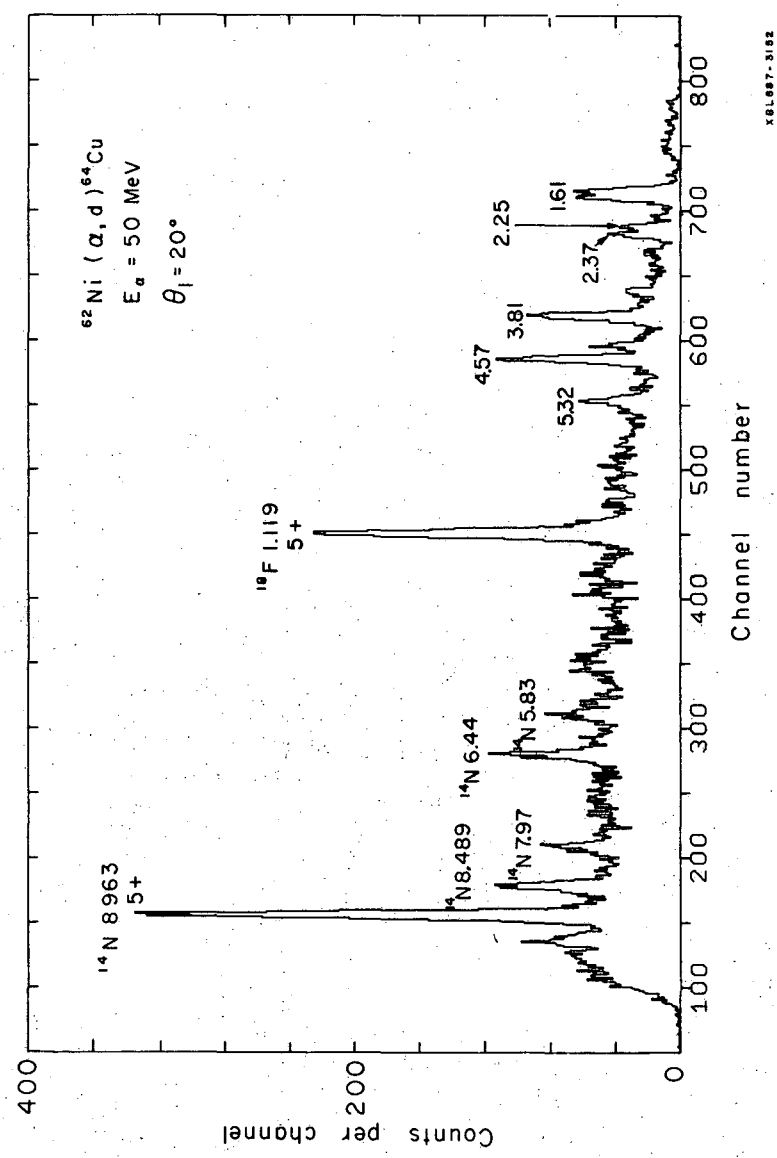

Fig. 19 Deuteron energy spectrum for the reaction $^{62}Ni(\alpha,d)^{64}Cu$ at θ(lab) = 20 deg with E(α) = 50.0 MeV.

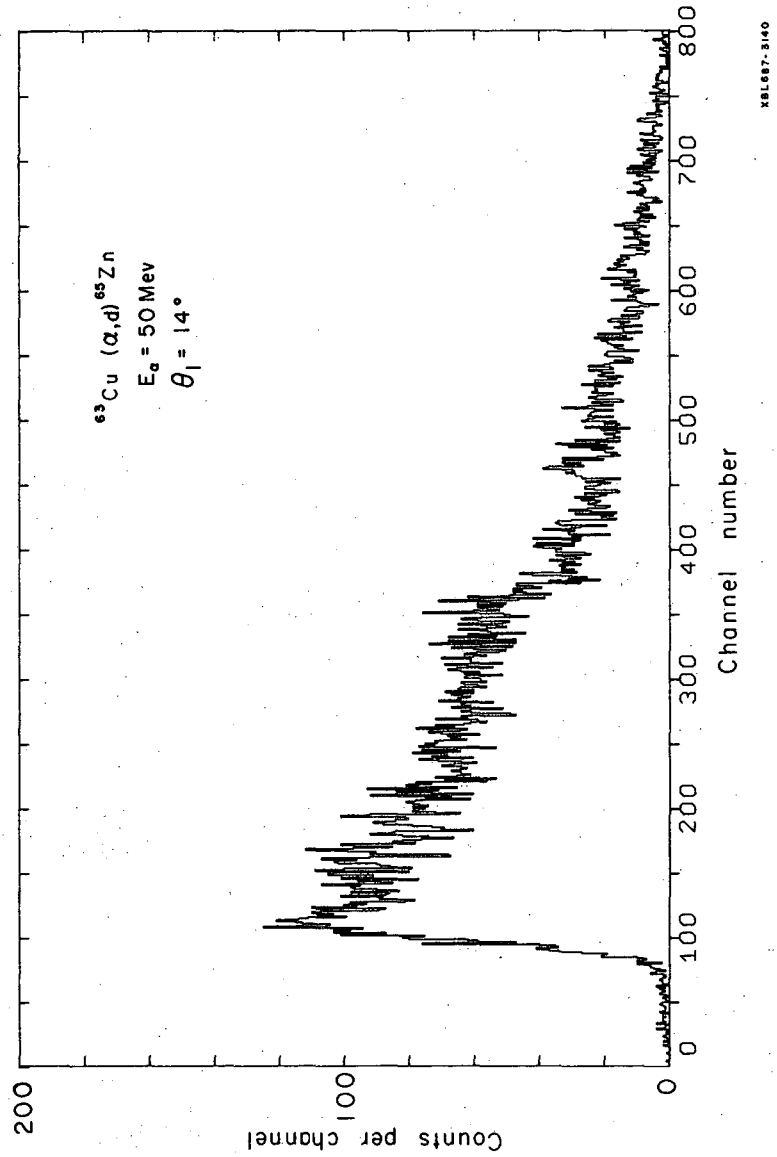

Fig. 20 Deuteron energy spectrum for the reaction $^{63}Cu(\alpha,d)^{65}Zn$ at θ(lab) = 14 deg with E(α) = 50.0 MeV.

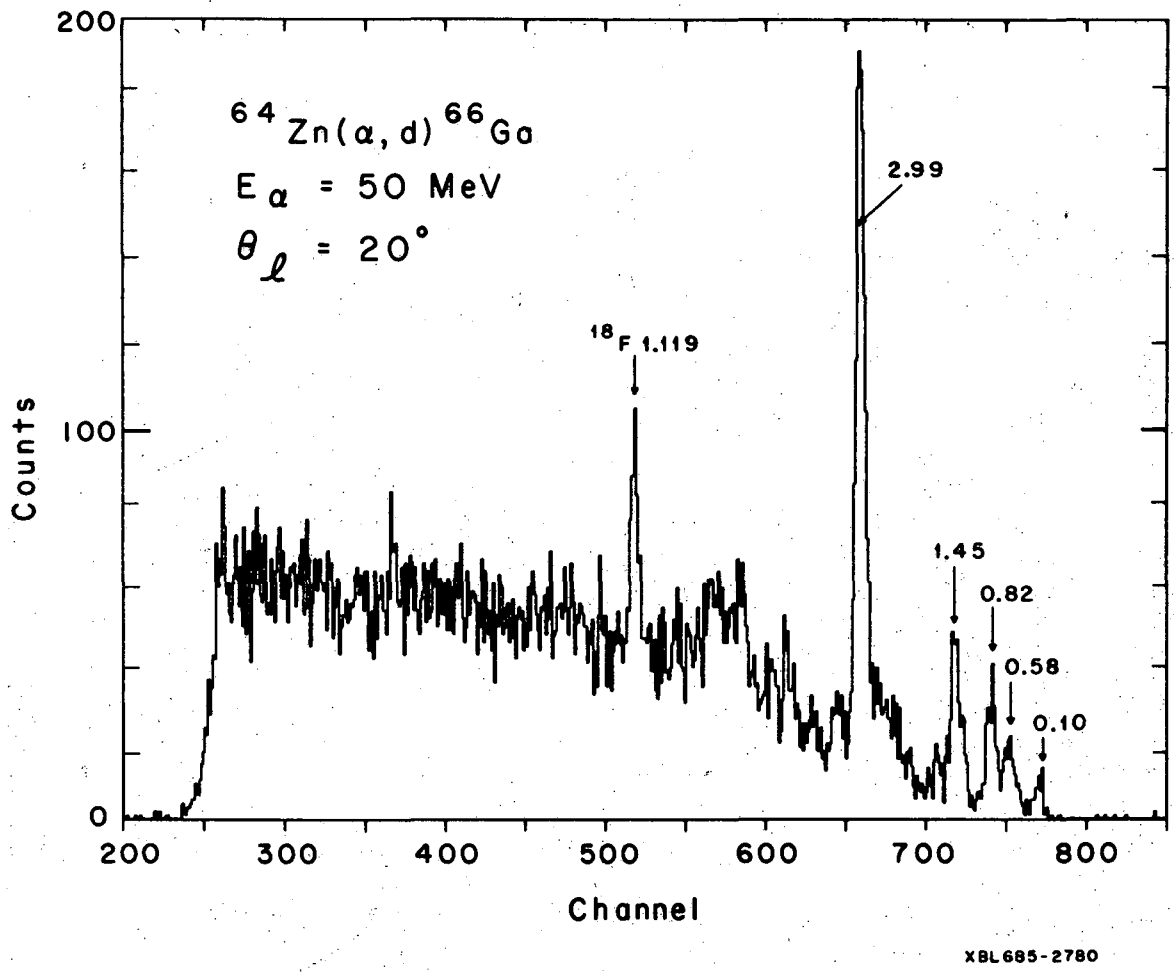

Fig. 21 Deuteron energy spectrum for the reaction $^{64}Zn(\alpha,d)^{66}Ga$ at θ(lab) = 20 deg with E(α) = 50.0 MeV.

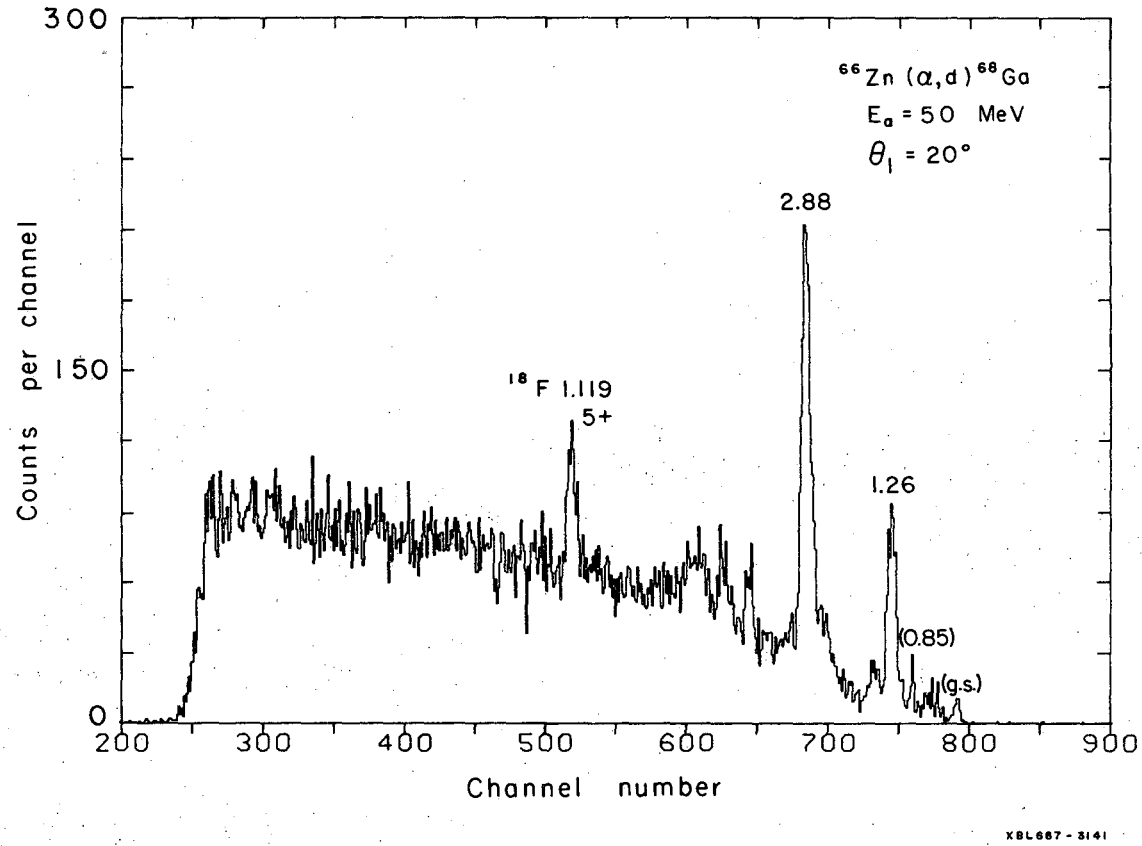

Fig. 22 Deuteron energy spectrum for the reaction $^{66}Zn(\alpha,d)^{68}Ga$ at θ(lab) = 20 deg with E(α) = 50.0 MeV.

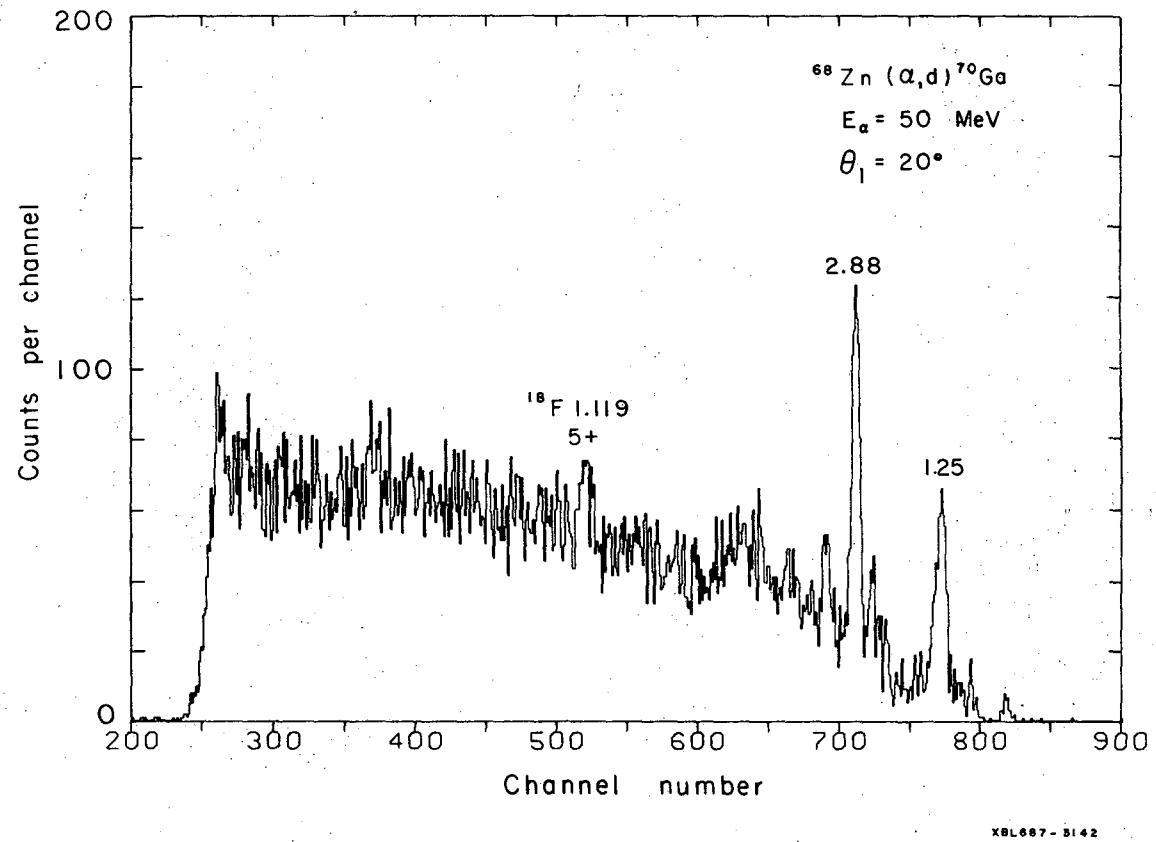

Fig. 23 Deuteron energy spectrum for the reaction $^{68}Zn(\alpha,d)^{70}Ga$ at θ(lab) = 20 deg with E(α) = 50.0 MeV.

reaction. Figure 24 is the spectrum from the $^{12}C(\alpha,t)^{13}N$ reaction. The single particle $1p_{1/2}$ and $1d_{5/2}$ level of ^{13}N (g.s. 1/2-, and 3.56 MeV 5/2+)[22] are strongly populated. The spectrum from the $^{13}C\ (\alpha,t)^{14}N$ reaction is shown in Fig. 25. The g.s. and the 5.104 and 5.832 MeV levels of ^{14}N are known to have the dominant configurations of $(1p_{1/2})^2_{1+,0}$, $(1d_{5/2},1p_{1/2})_{2-,0}$ and $(1d_{5/2},1p_{1/2})_{3-,0}$ respectively[22] and they are strongly populated. The stripped proton prefers to be captured in the $1p_{1/2}$ or $1d_{5/2}$ shell model state. The triton angular distributions are shown in Fig. 26. In the ^{15}N spectrum, shown in Fig. 27, two large peaks at 0 and 5.266 MeV excitation correspond to levels with dominant configurations $(1p_{1/2})^3_{1/2-,1/2}$ and $[1d_{5/2}(^{14}c\ g.s.)]_{5/2+,1/2}$ respectively.[30] In the ^{16}O spectrum shown in Fig. 29, three strong peaks at 0, 6.135 and 8.875 MeV are known to have the dominant configurations $(1p_{1/2})^4_{0+,0}$, $(1d_{5/2},1p_{1/2}^{-1})_{3-,0}$ and $(1d_{5/2},1p_{1/2}^{-1})_{2-,0}$ respectively.[50] The triton angular distributions for ^{15}N and ^{16}O are shown in Figs. 28 and 30 respectively. The spectrum of tritons from the $^{20}Ne(\alpha,t)^{21}Na$ reaction is shown in Fig. 31. The 0.32 MeV (the known value is 0.335 MeV) 5/2+ and 5.11 MeV levels are strongly populated. The 0.335 MeV level was described by several calculations to be the second member of the K = 3/2+ ground state rotational band.[51] Since the (d,n) reaction shows that this level has $\ell_p = 2$ and in (α,t) reaction it is populated much stronger than all the other members of the K = 3/2+ rotational band-g.s. 3/2+, 1.171 7/2+, and 2.81 (9/2), the evidence indicates that the 0.335 MeV level may have a strong parentage of the configuration $[(\pi 1d_{5/2})(^{20}Ne\ core)]$. Whether the collective description and the single particle description of the 0.335 MeV state

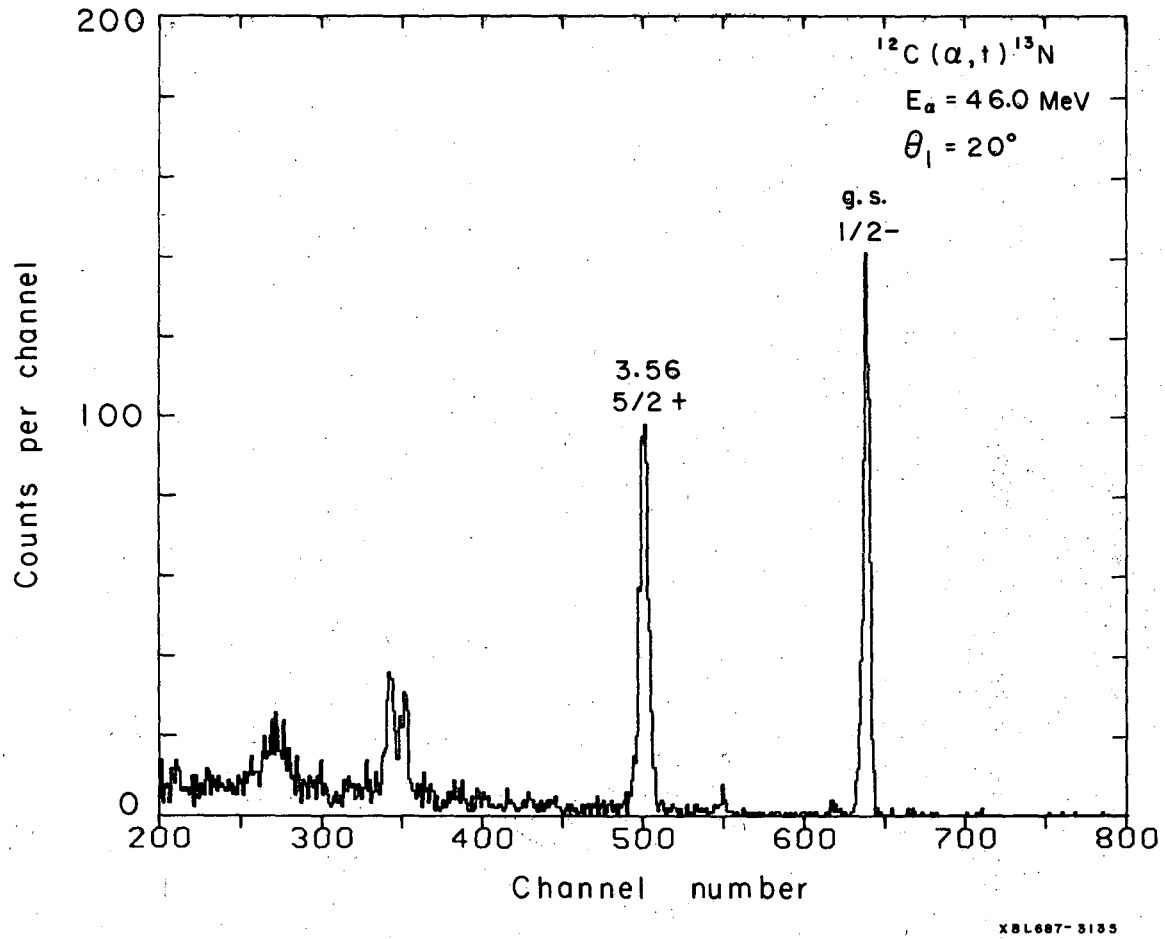

Fig. 24 Triton energy spectrum for the reaction $^{12}C(\alpha,t)^{13}N$ at θ(lab) = 20.0 deg with E(α) = 46.0 MeV.

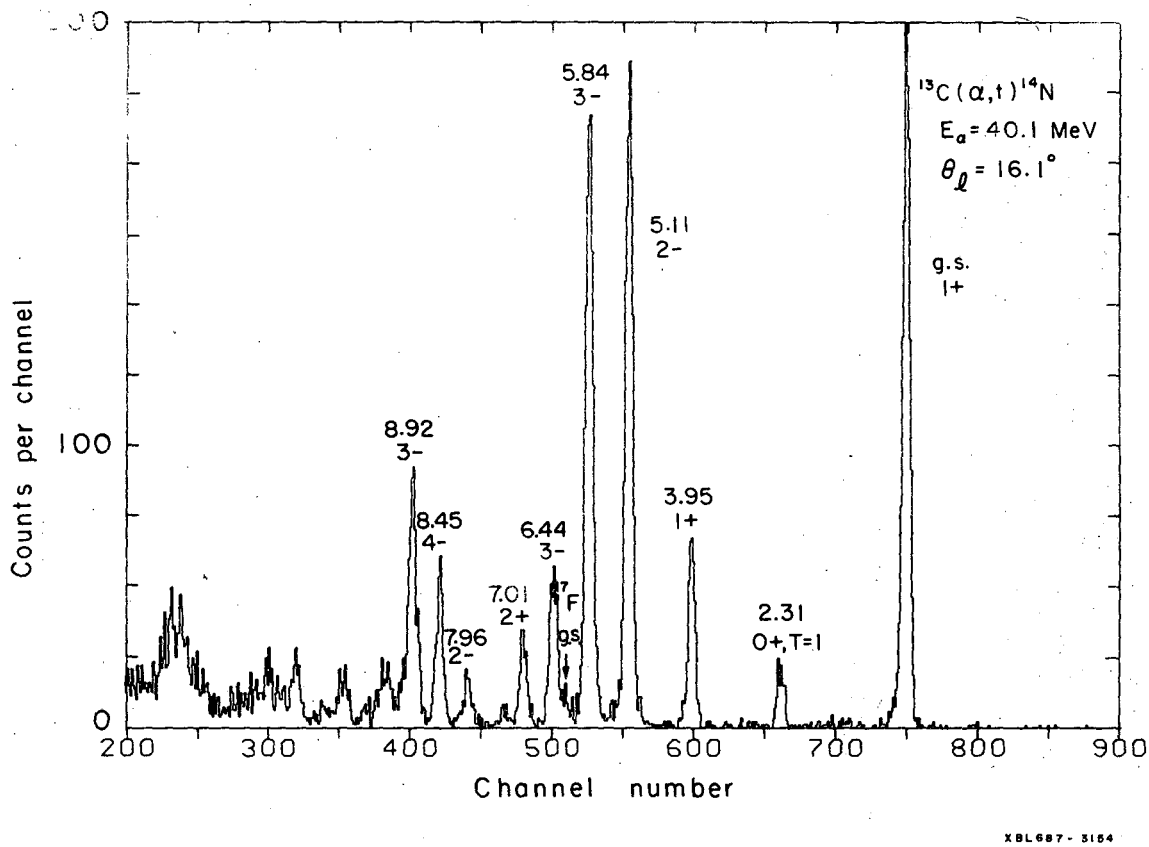

Fig. 25 Triton energy spectrum for the reaction $^{13}C(\alpha,t)^{14}N$ at θ(lab) = 16.1 deg with E(α) = 40.1 MeV.

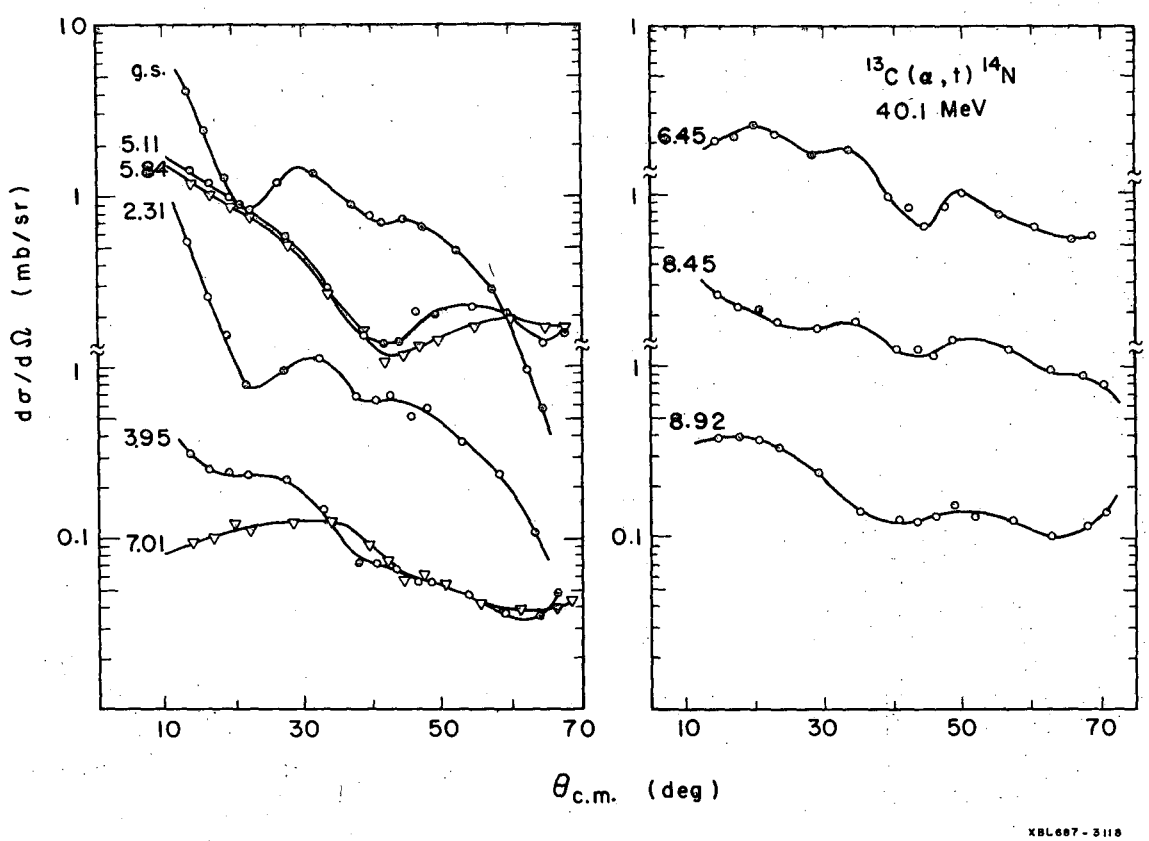

Fig. 26 Triton angular distributions for the reaction $^{13}C(\alpha,t)^{14}N$ at $E(\alpha)$ = 40.1 MeV.

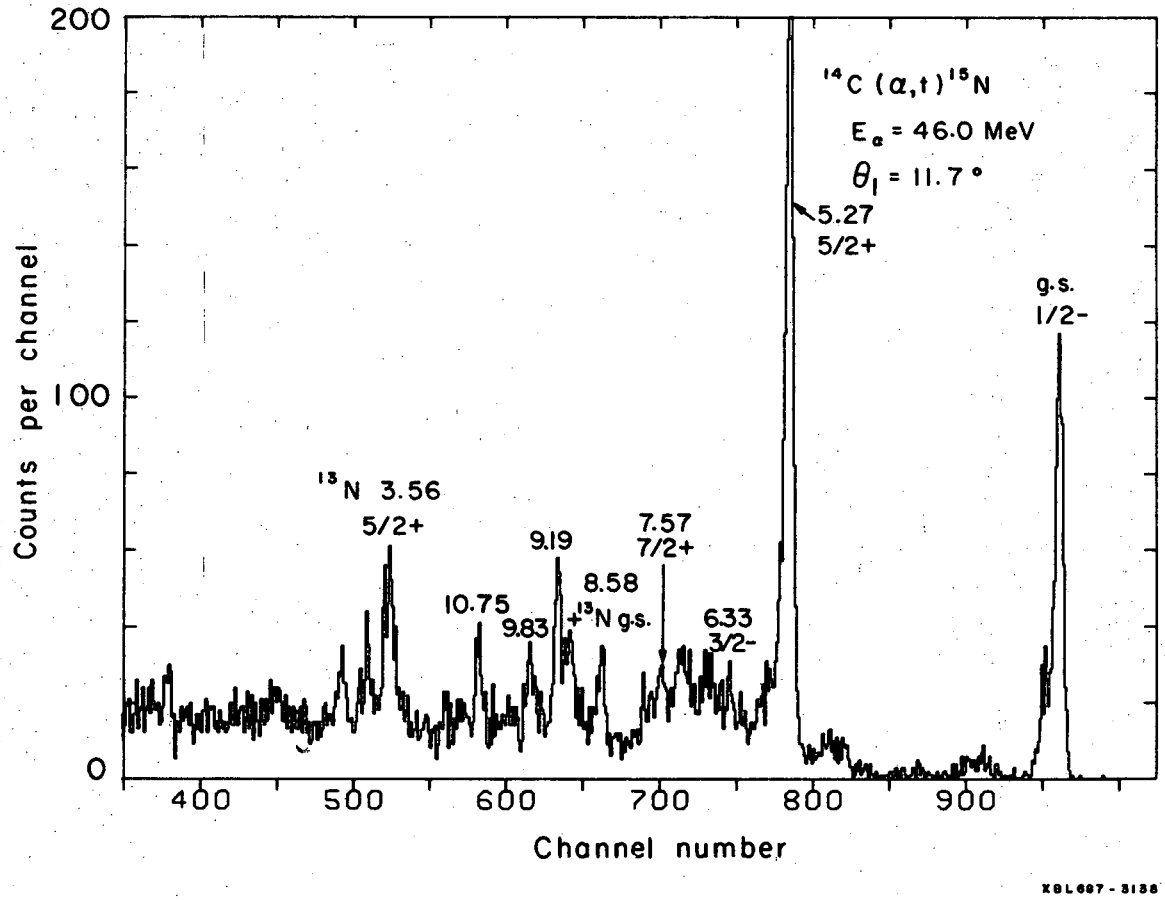

Fig. 27 Triton energy spectrum for the reaction $^{14}C(\alpha,t)^{15}N$ at θ(lab) = 11.7 deg with E(α) = 46.0 MeV.

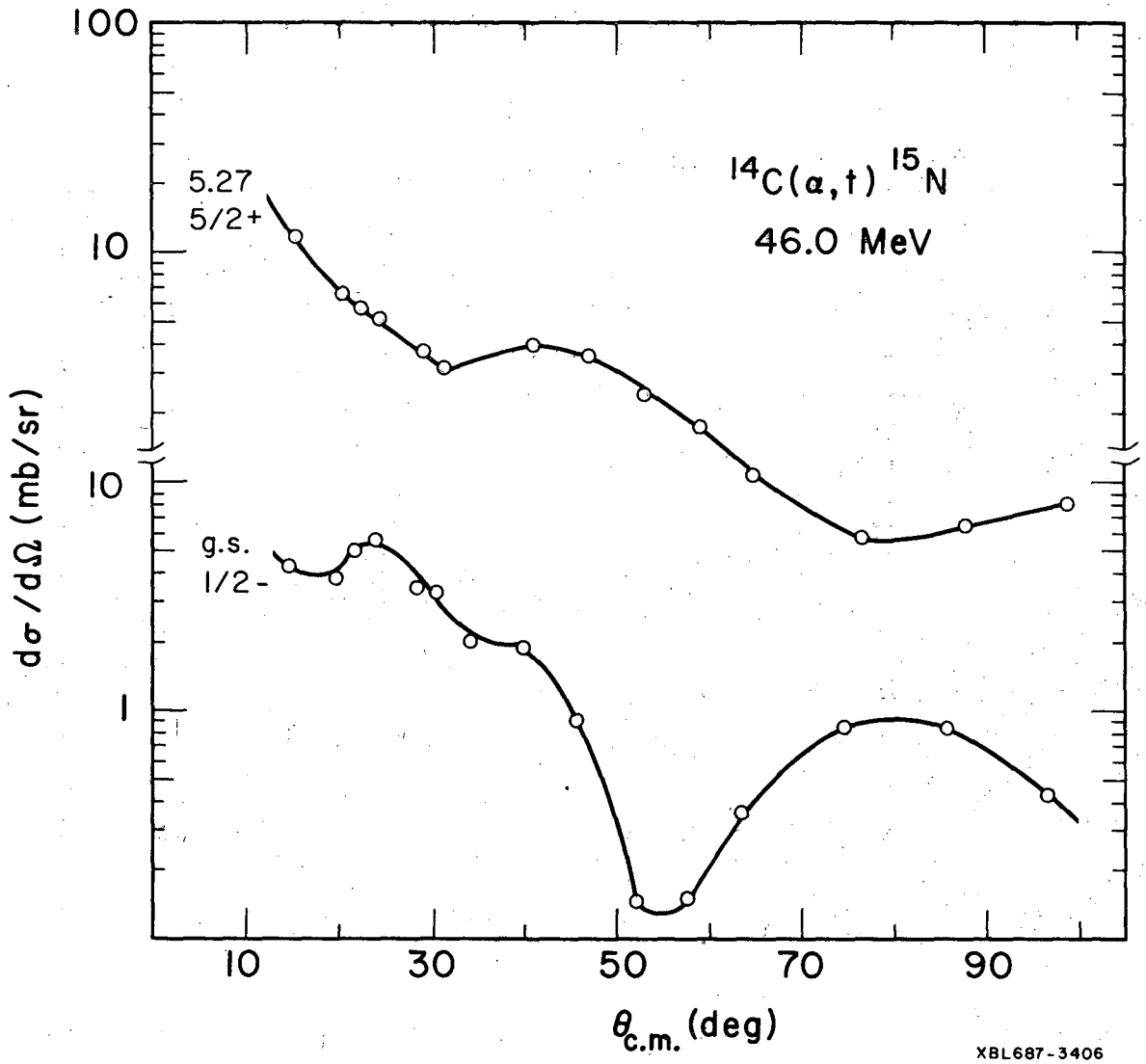

Fig. 28 Triton angular distributions for the reaction $^{14}C(\alpha,t)^{15}N$ at $E(\alpha) = 46.0$ MeV.

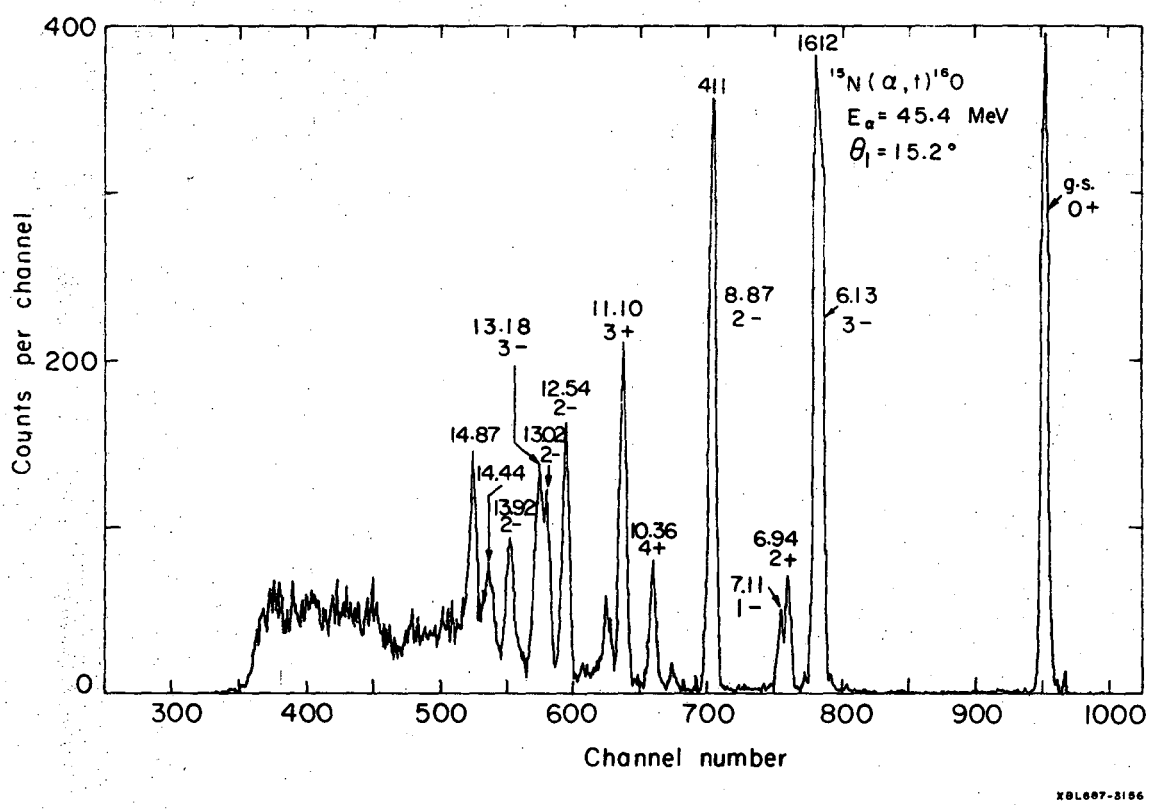

Fig. 29 Triton energy spectrum for the reaction $^{15}N(\alpha,t)^{16}O$ at θ(lab) = 15.2 deg with E(α) = 45.4 MeV.

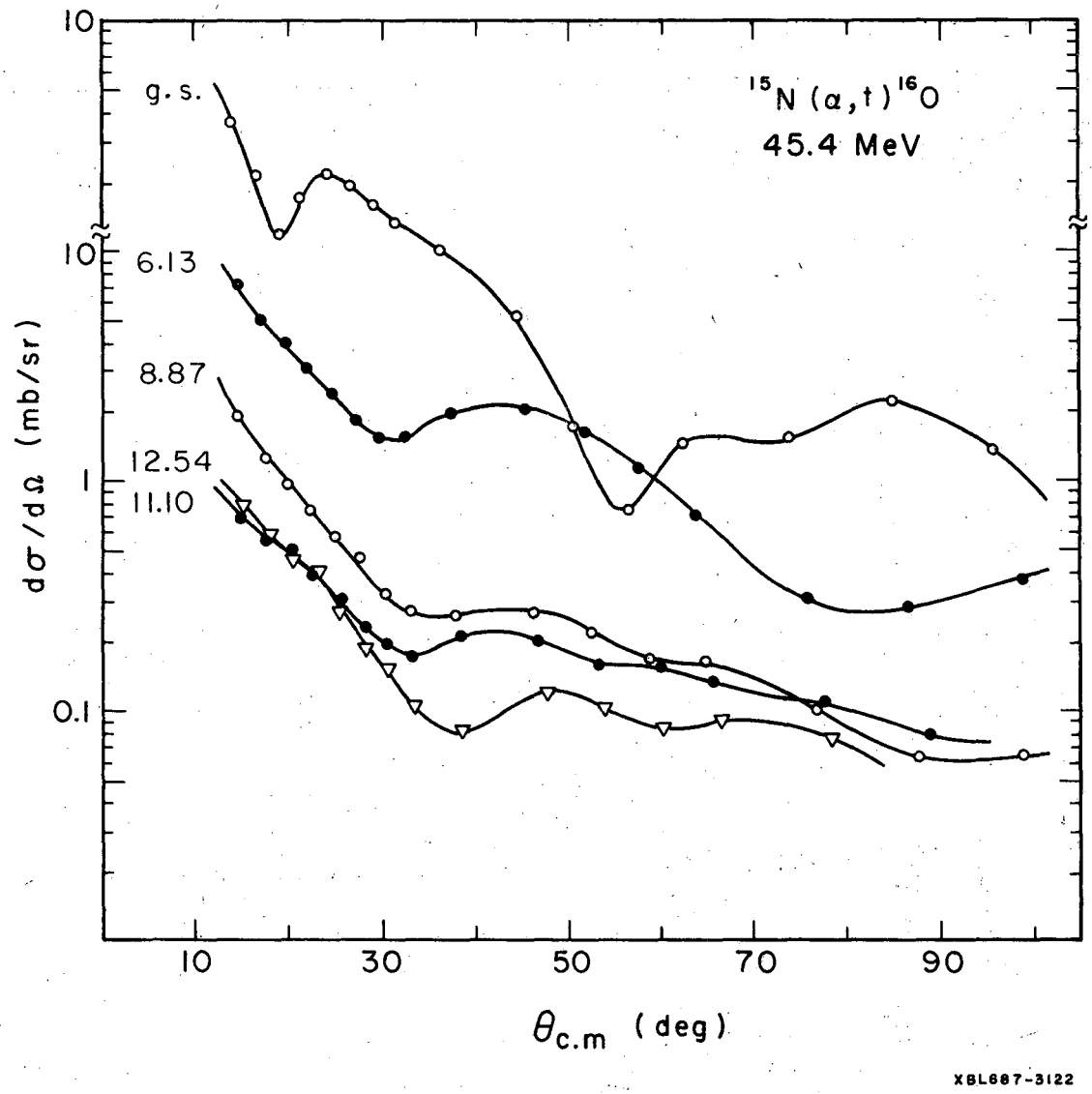

Fig. 30 Triton angular distributions for the reaction $^{15}N(\alpha,t)^{16}O$ at $E(\alpha) = 45.4$ MeV.

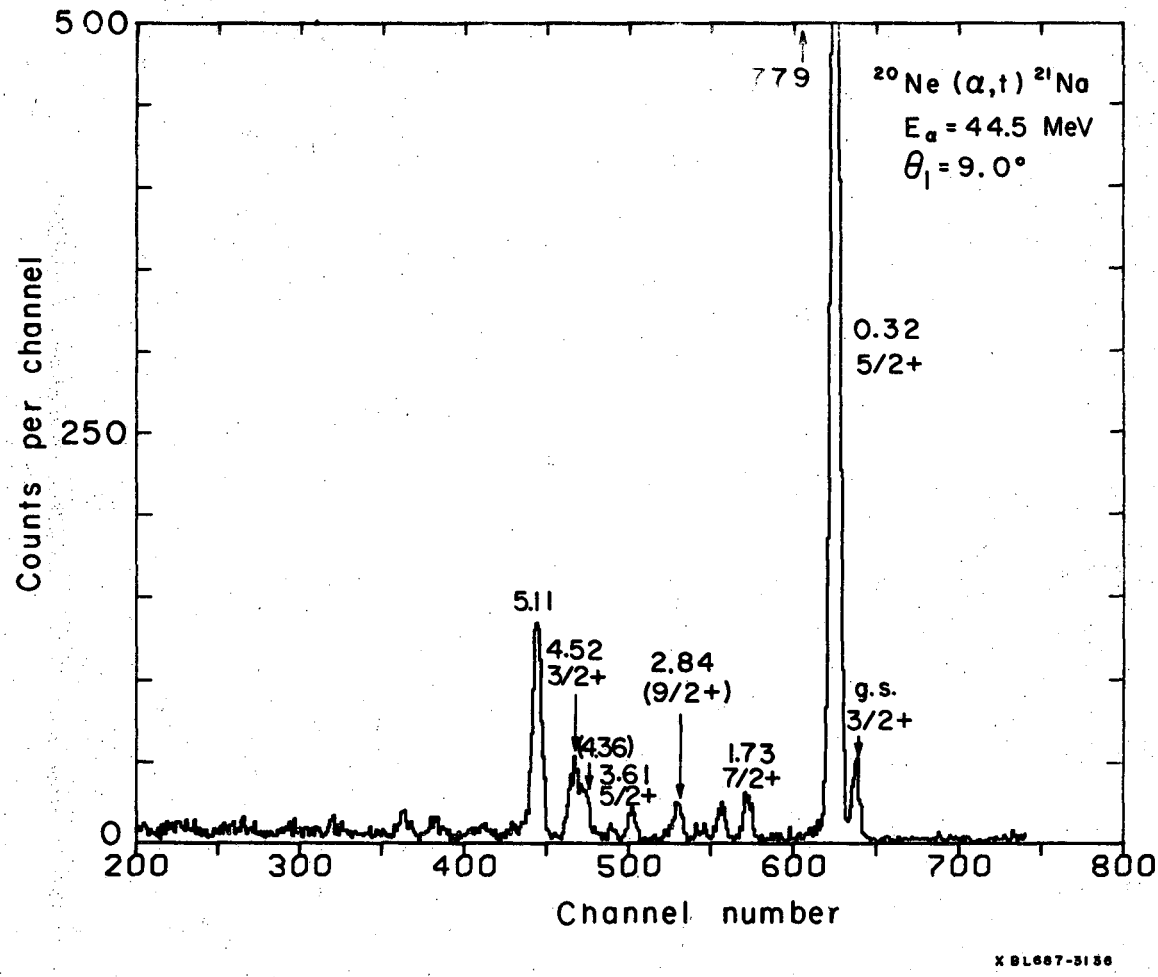

Fig. 31 Triton energy spectrum for the reaction $^{20}Ne(\alpha,t)^{21}Na$ at θ(lab) = 9.0 deg with E(α) = 44.5 MeV.

are the same is a problem remaining to be verified. The nature of the 5.106 MeV level is unknown. In ^{21}Ne, the mirror nucleus of ^{21}Na, there are three states (4.53, 5.434 and 5.632 MeV) in the vicinity of 5 MeV with $\ell_n = 2$ determined by the (d,p) reaction. In ^{17}O the $1d_{5/2}$-$1d_{3/2}$ splitting is 5.083 MeV. From this evidence, it is possible that the 5.11 MeV level may have the configuration $[(\pi 1d_{3/2})(^{20}\text{Ne core})]$. Experimental determination of the ℓ_p value from (^{3}He, d) or (d,n) reactions and the spin value from particle-gamma work are needed in order to establish the above postulation. The structureless angular distribution from the (α,t) reaction populating this state is shown in Fig. 32. Obviously it will not allow a unique determination of ℓ_p.

The spectra from (α,t) reactions on medium mass targets are shown from Figs. 33-44. The known single particle configurations are also shown on the spectra. Comparing to the known level information,[52-56] the $1f_{7/2}$, $1f_{5/2}$, and $1g_{9/2}$ single particle states are populated strongly. Following this trend, the following speculations are made:

a) The ^{53}Mn 6.31 or 6.54 MeV, ^{67}Ga 2.10 MeV and ^{69}Ga 0.58 MeV levels are $1g_{9/2}$ single particle levels.

b) The ^{63}Cu 0.97 MeV, ^{67}Ga 0.38 MeV, and ^{69}Ga 0.58 MeV levles are $1f_{5/2}$ single particle levels.

c) In ^{60}Ni the multiplets at about 6.5 MeV may have the configuration $(1g_{9/2}, 1f_{7/2}^{-1})_{8,7,6-}$. The broad peak at about 5 MeV obviously consists of several levels. These levels and the one at about 4.37 MeV may have the configuration $(1f_{7/2}, 1f_{5/2})$.

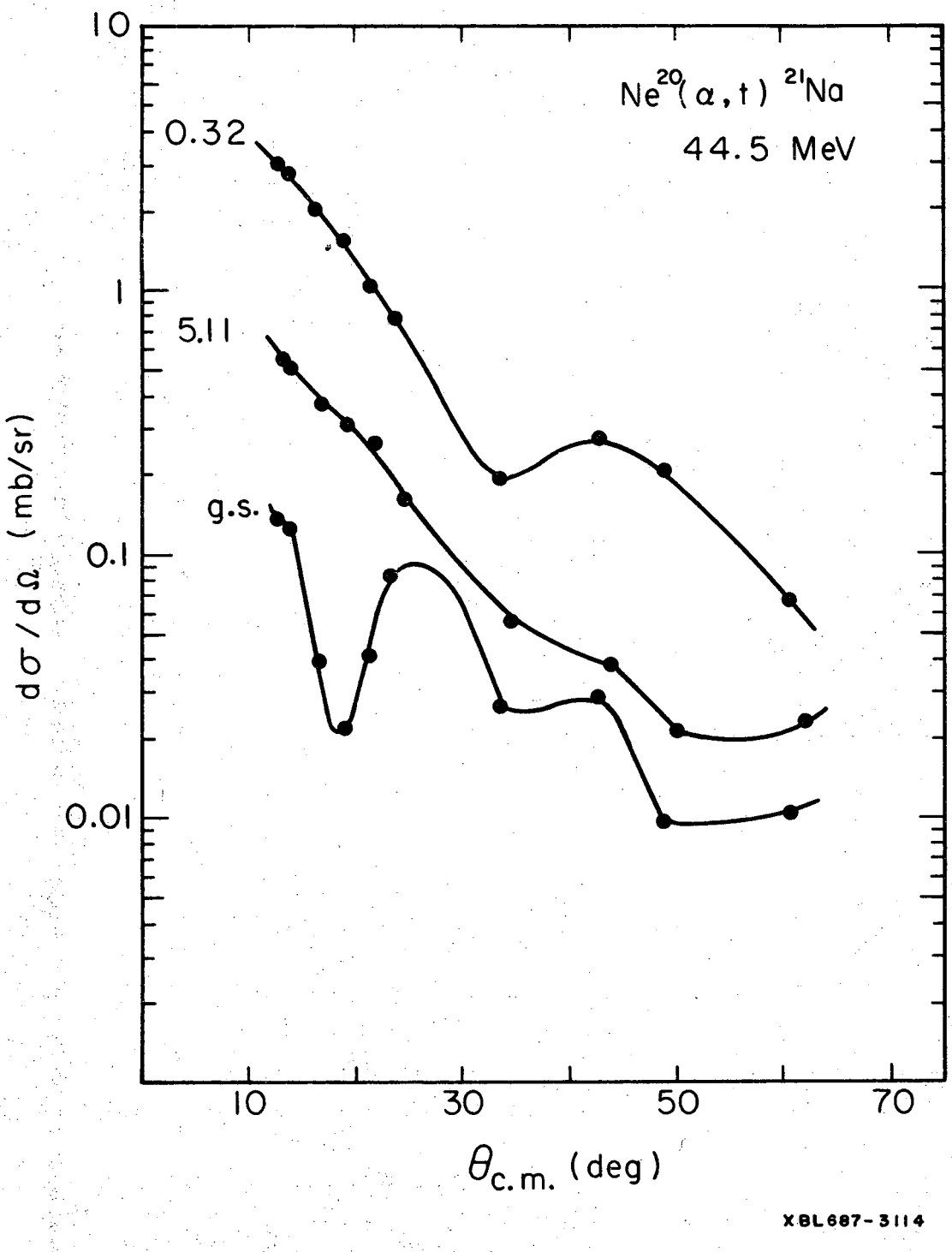

Fig. 32 Triton angular distributions for the reaction $^{20}Ne(\alpha,t)^{21}Na$ at $E(\alpha)$ = 44.5 MeV.

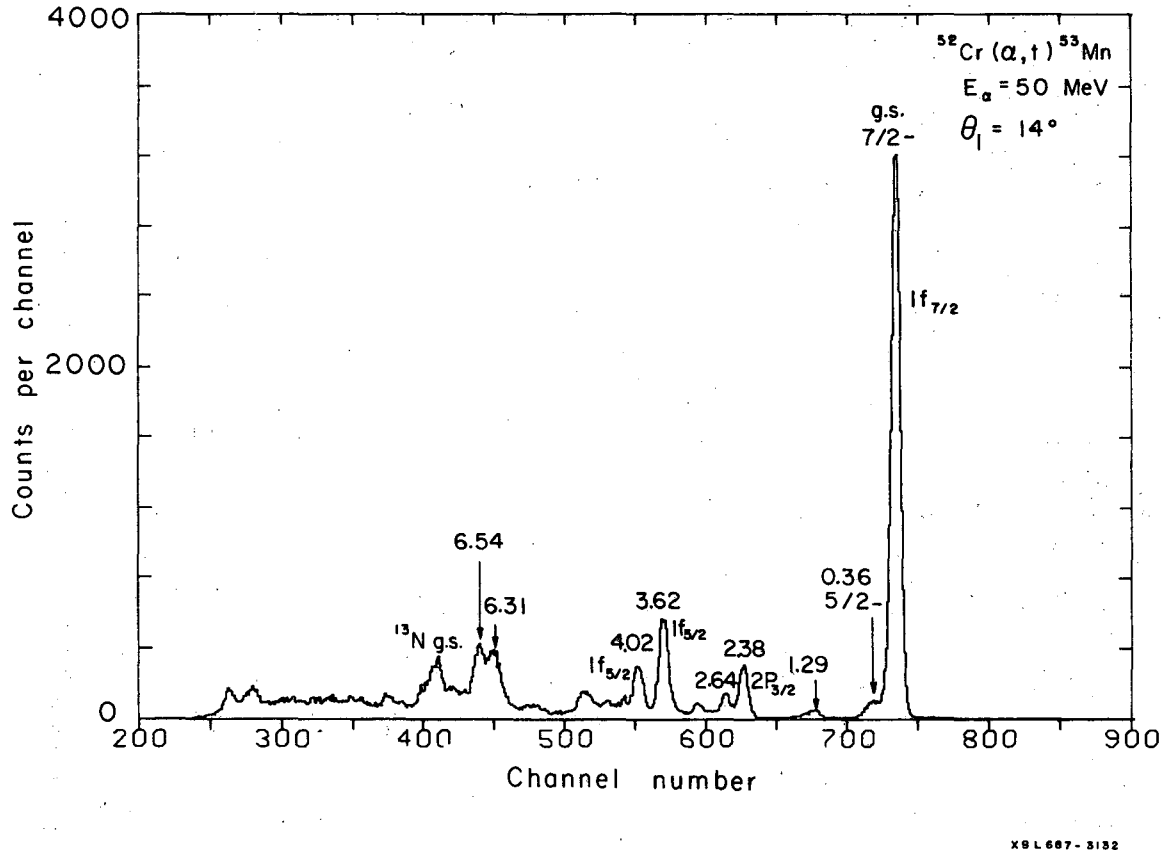

Fig. 33 Triton energy spectrum for the reaction $^{52}Cr(\alpha,t)^{53}Mn$ at θ(lab) = 14 deg with E(α) = 50.0 MeV.

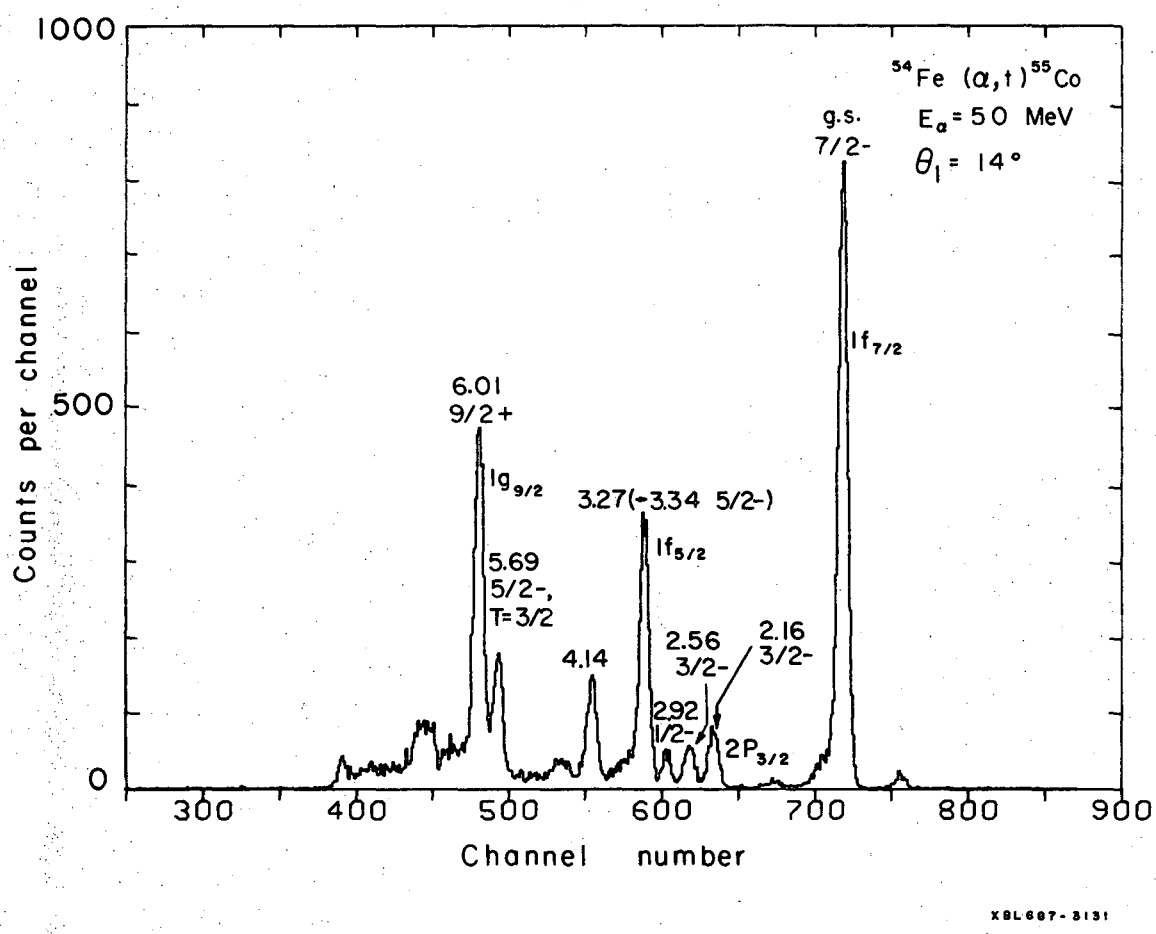

Fig. 34 Triton energy spectrum for the reaction $^{54}Fe(\alpha,t)^{55}Co$ at θ(lab) = 14 deg with E(α) = 50.0 MeV.

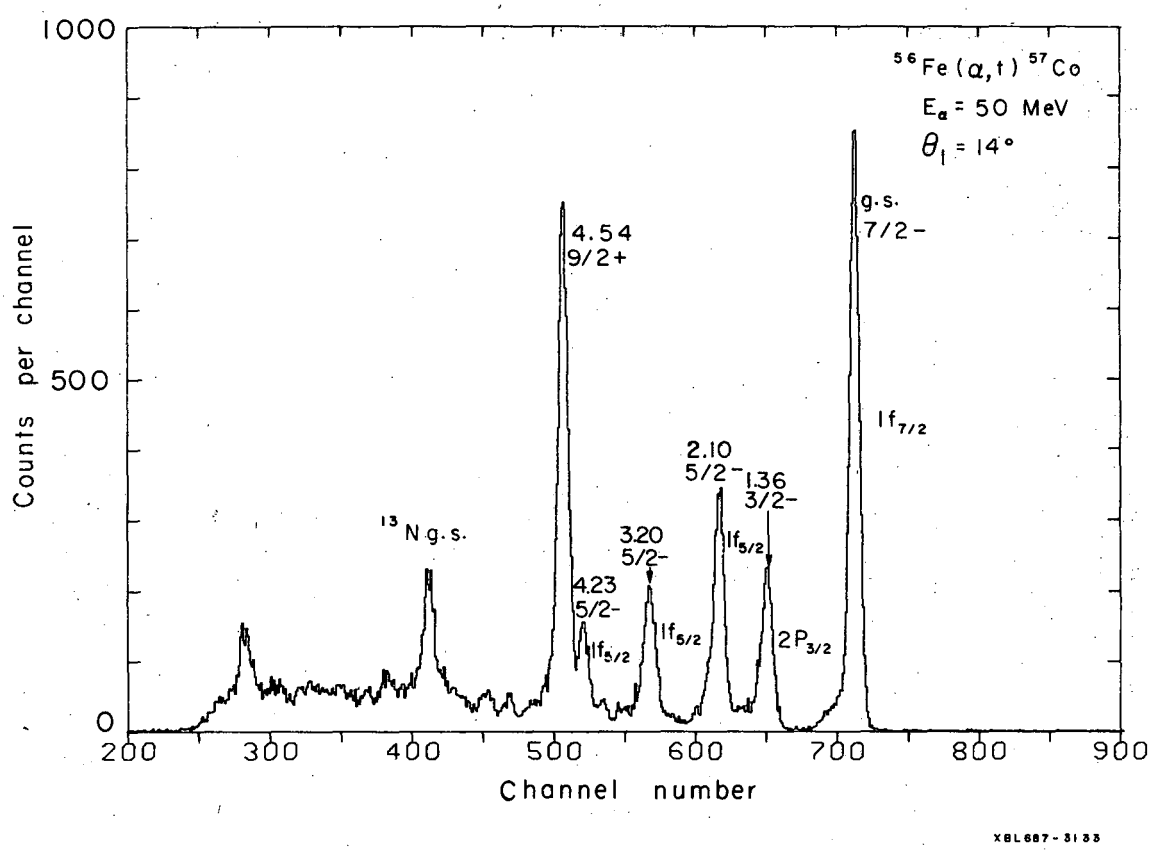

Fig. 35 Triton energy spectrum for the reaction $^{56}Fe(\alpha,t)^{57}Co$ at θ(lab) = 14 deg with E(α) = 50.0 MeV.

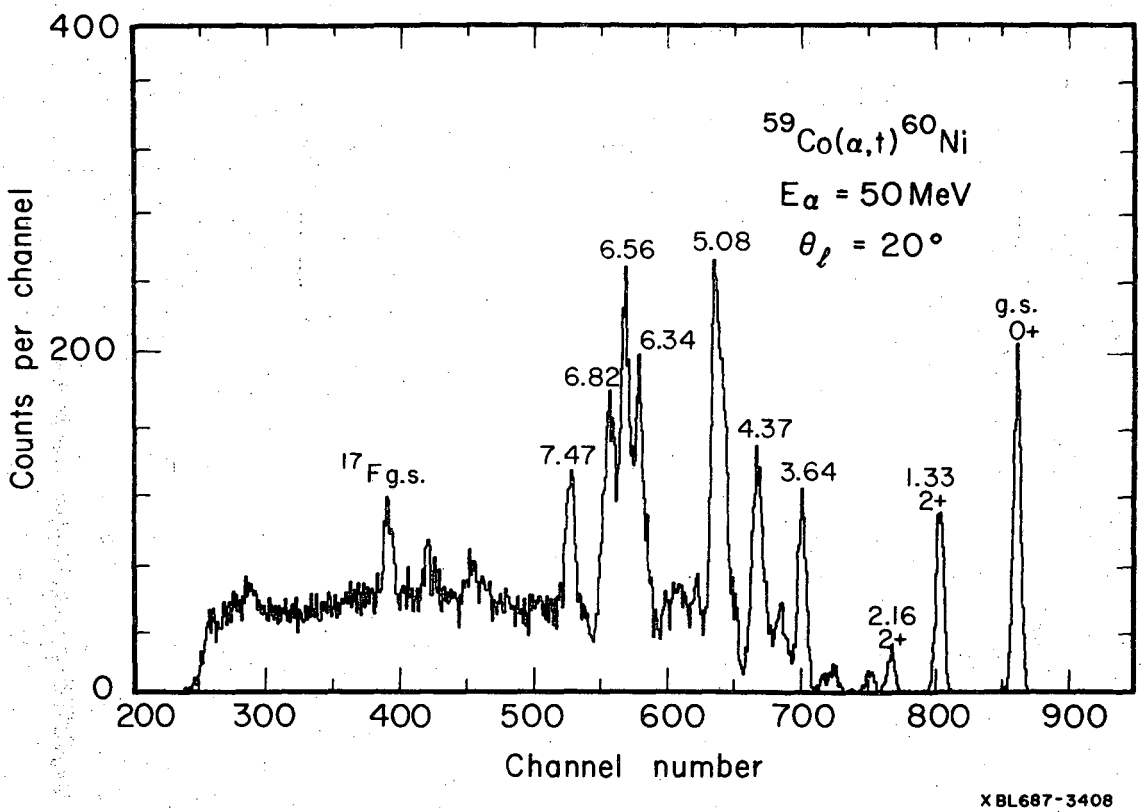

Fig. 36 Triton energy spectrum for the reaction ^{59}Co(α,t)^{60}Ni at θ(lab) = 20 deg with E(α) = 50.0 MeV.

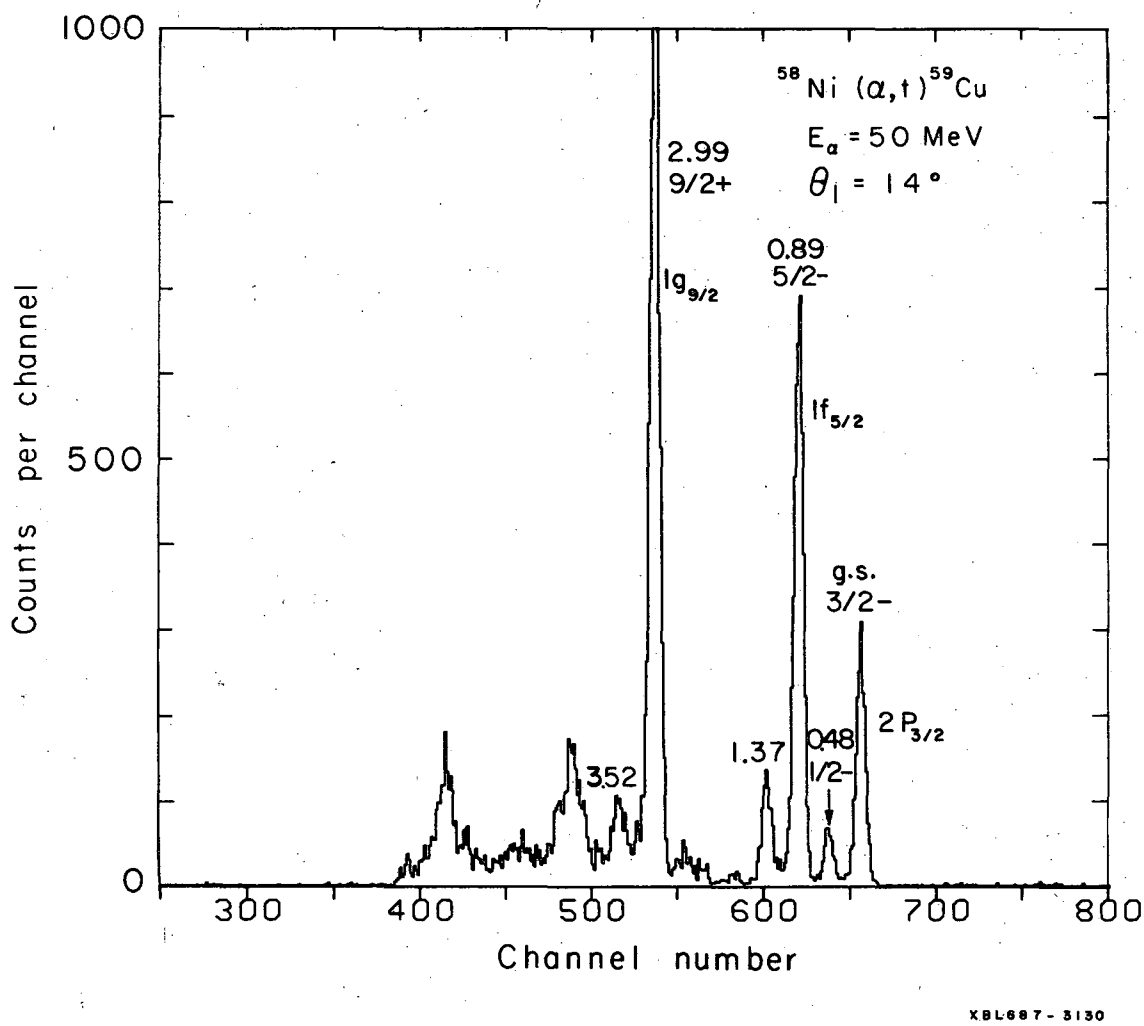

Fig. 37 Triton energy spectrum for the reaction $^{58}Ni(\alpha,t)^{59}Cu$ at θ(lab) = 14 deg with E(α) = 50.0 MeV.

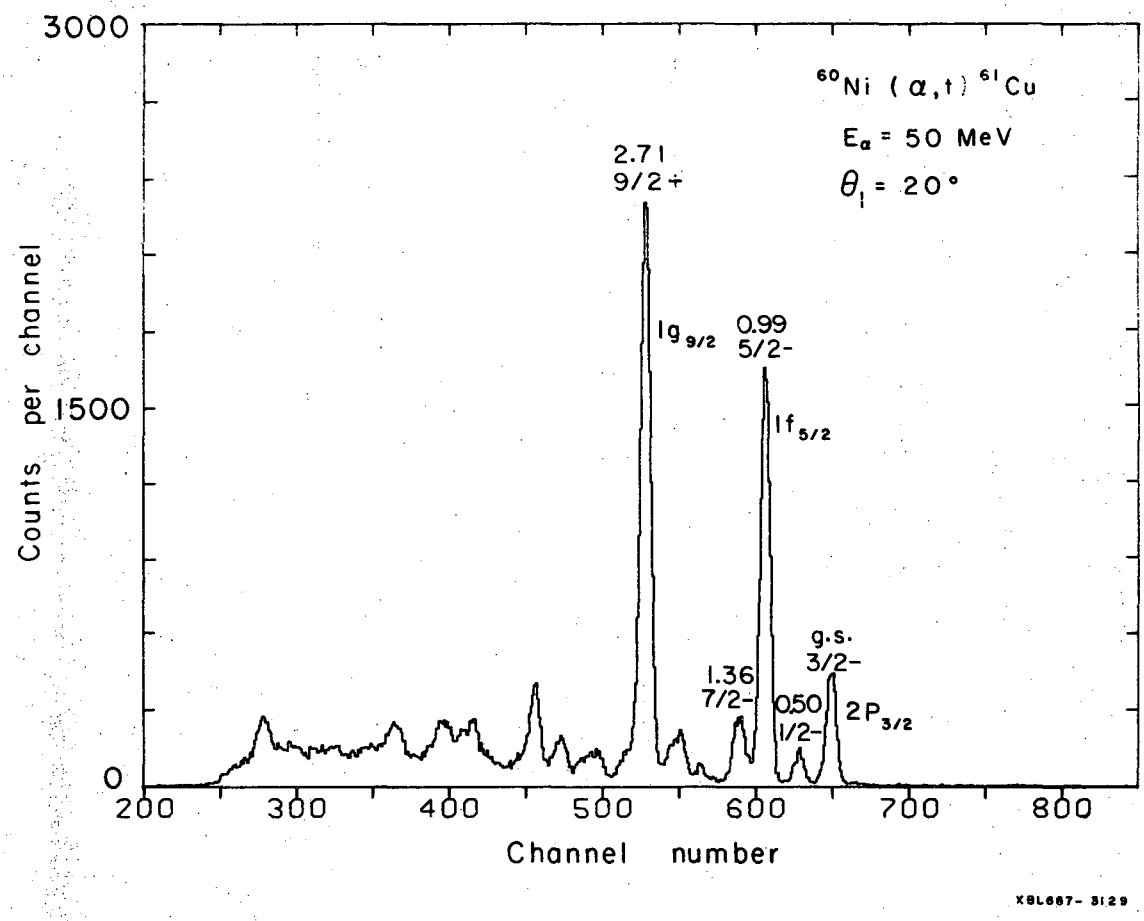

Fig. 38 Triton energy spectrum for the reaction $^{60}Ni(\alpha,t)^{61}Cu$ at θ(lab) = 20 deg with E(α) = 50.0 MeV.

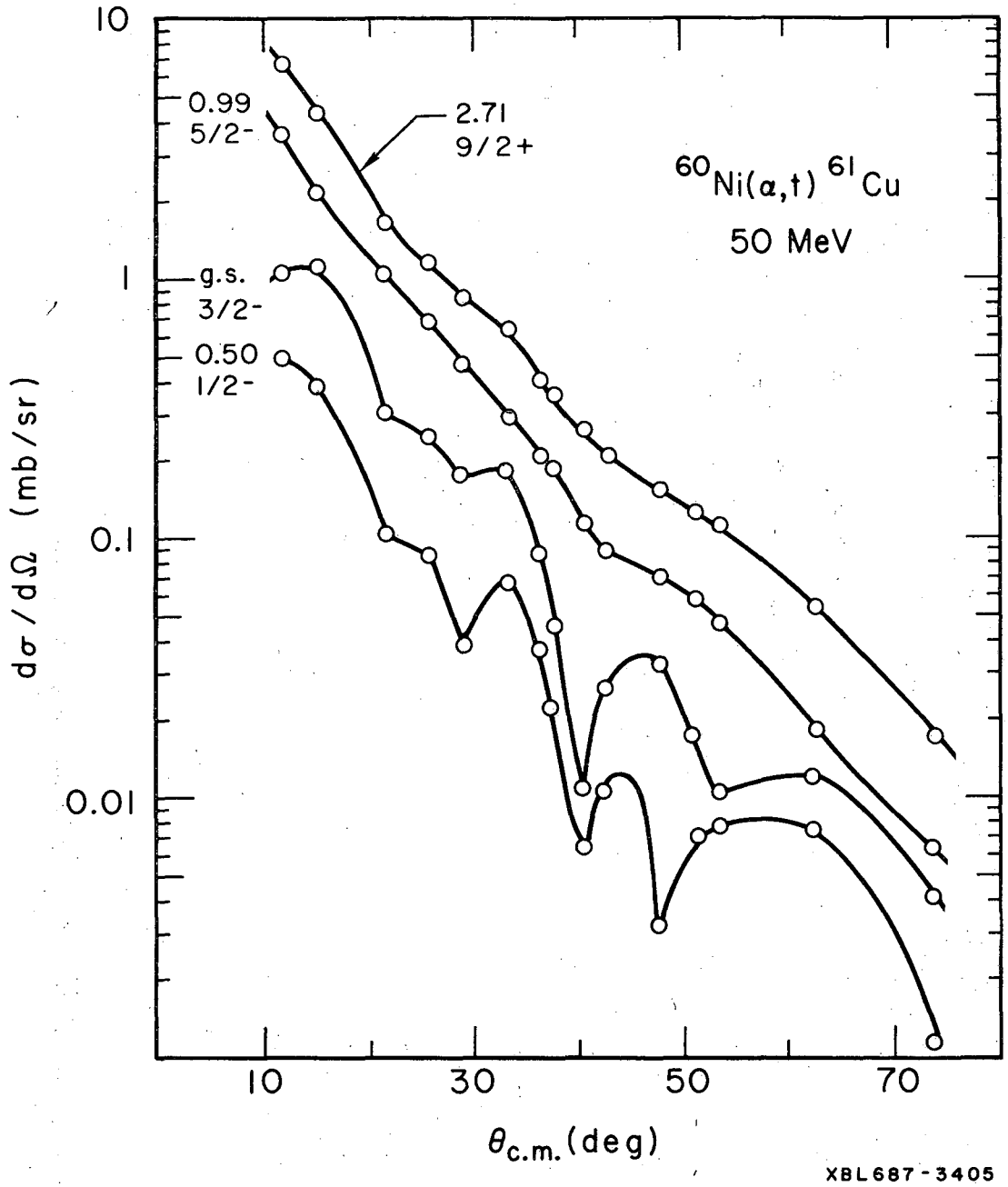

Fig. 39 Triton angular distributions for the reaction $^{60}Ni(\alpha,t)^{61}Cu$ at $E(\alpha) = 50.0$ MeV.

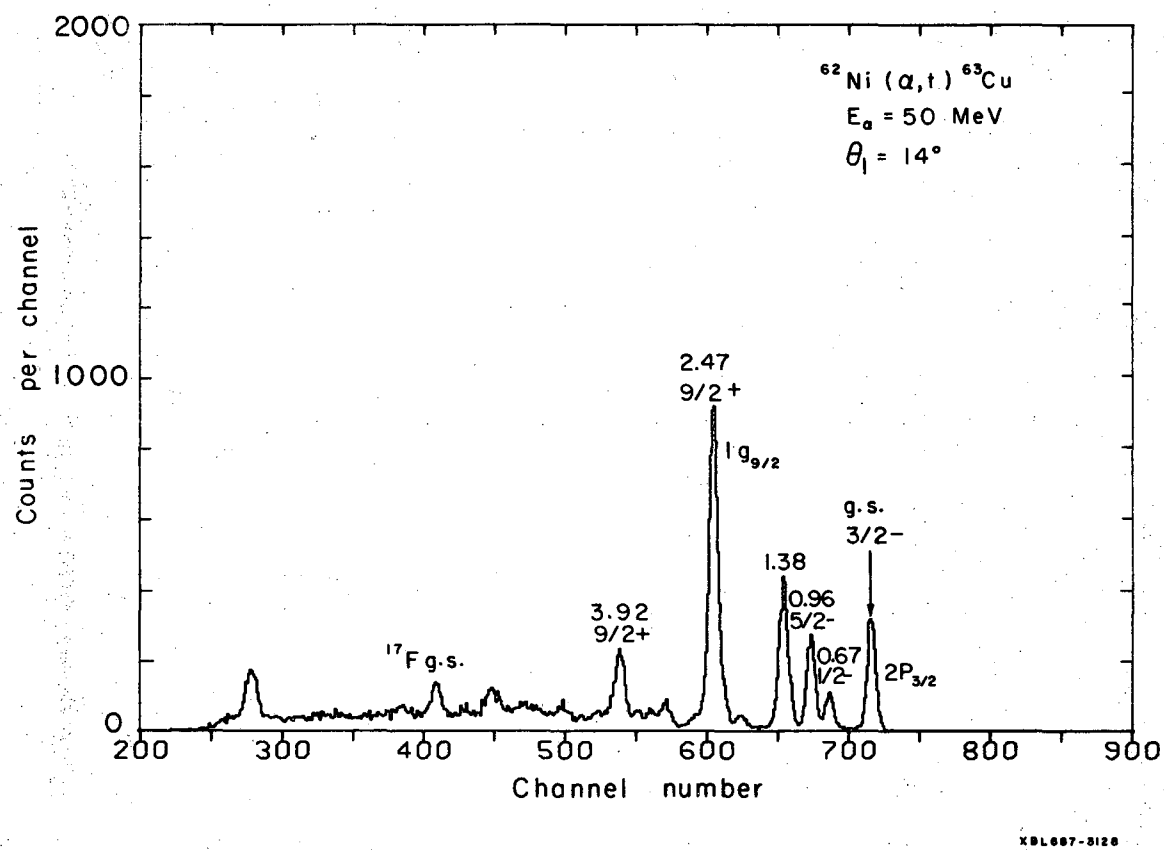

Fig. 40 Triton energy spectrum for the reaction $^{62}Ni(\alpha,t)^{63}Cu$ at θ(lab) = 14 deg with E(α) = 50.0 MeV.

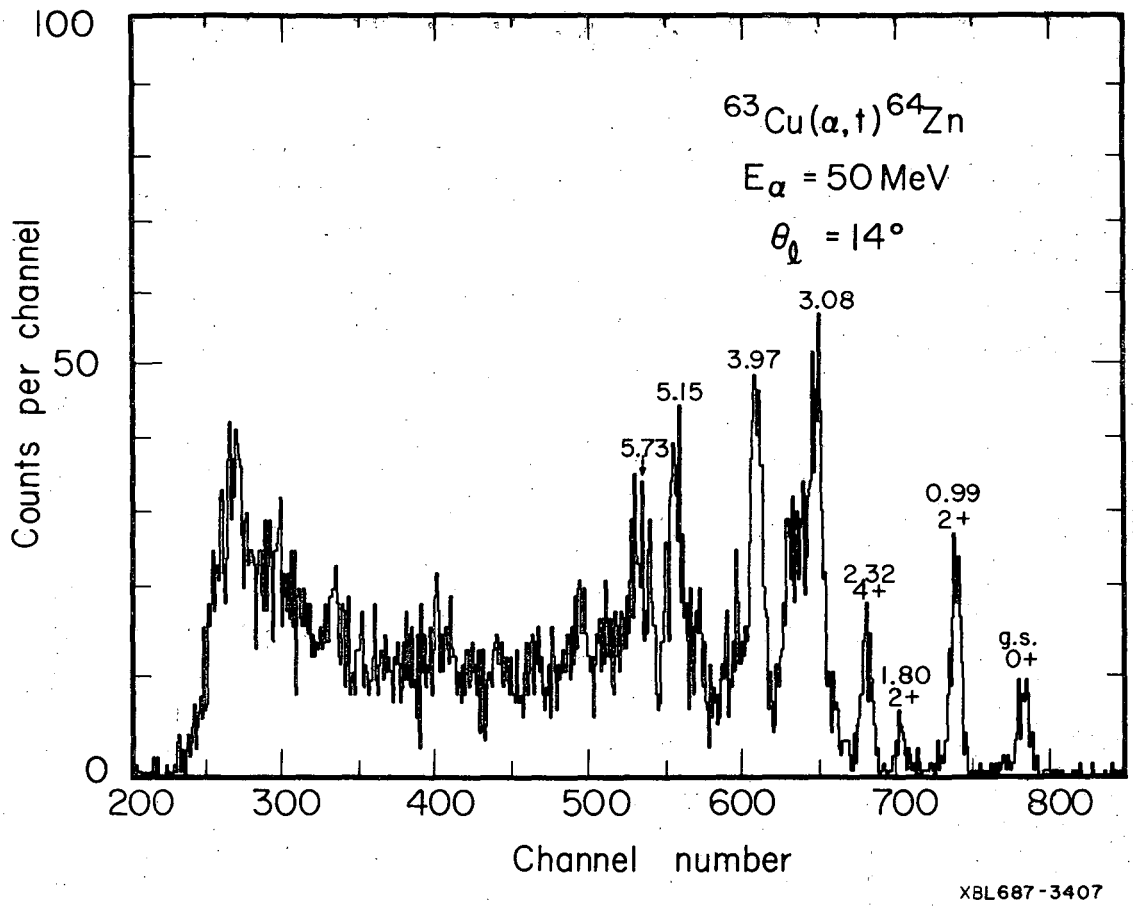

Fig. 41 Triton energy spectrum for the reaction $^{63}Cu(\alpha,t)^{64}Zn$ at θ(lab) = 14 deg with E(α) = 50.0 MeV.

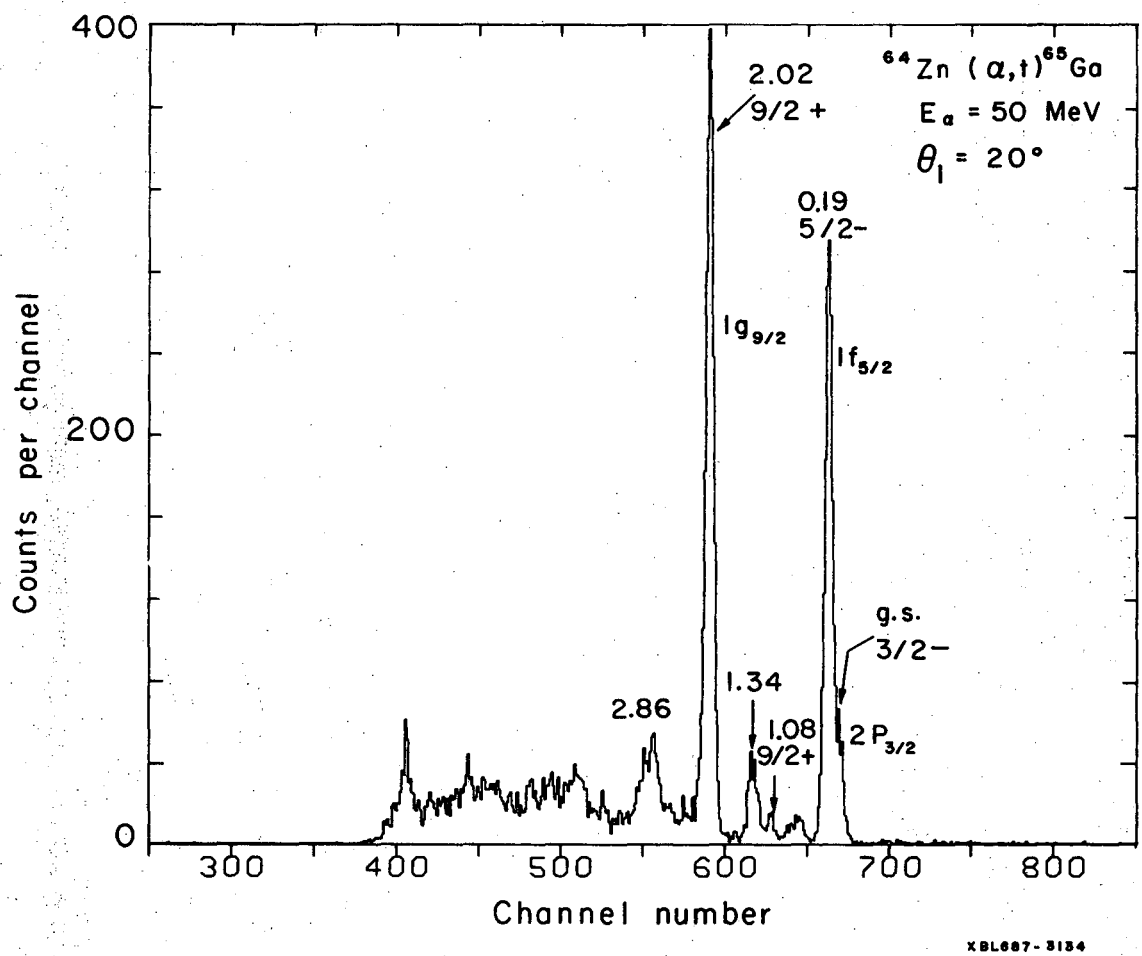

Fig. 42 Triton energy spectrum for the reaction $^{64}Zn(\alpha,t)^{65}Ga$ at θ(lab) = 20 deg with E(α) = 50.0 MeV.

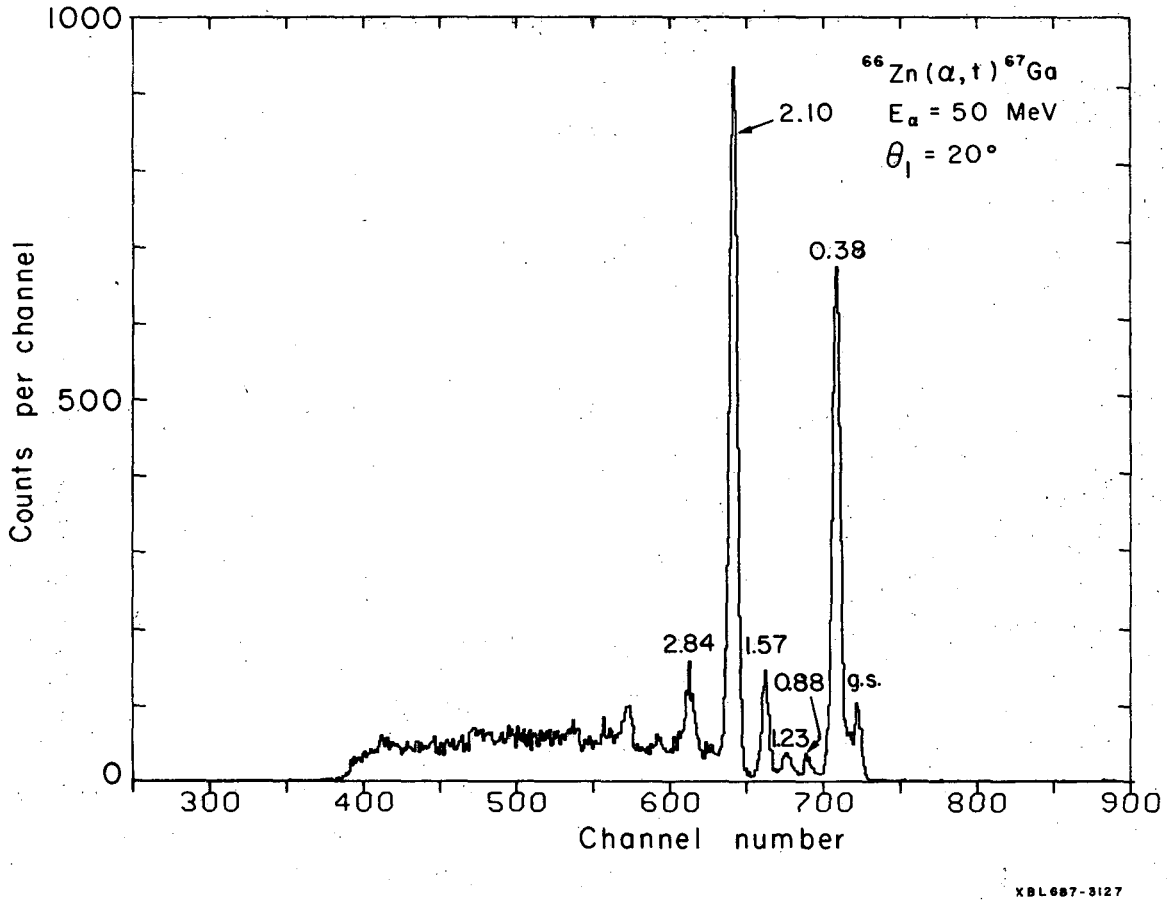

Fig. 43 Triton energy spectrum for the reaction $^{66}Zn(\alpha,t)^{67}Ga$ at θ(lab) = 20 deg with E(α) = 50.0 MeV.

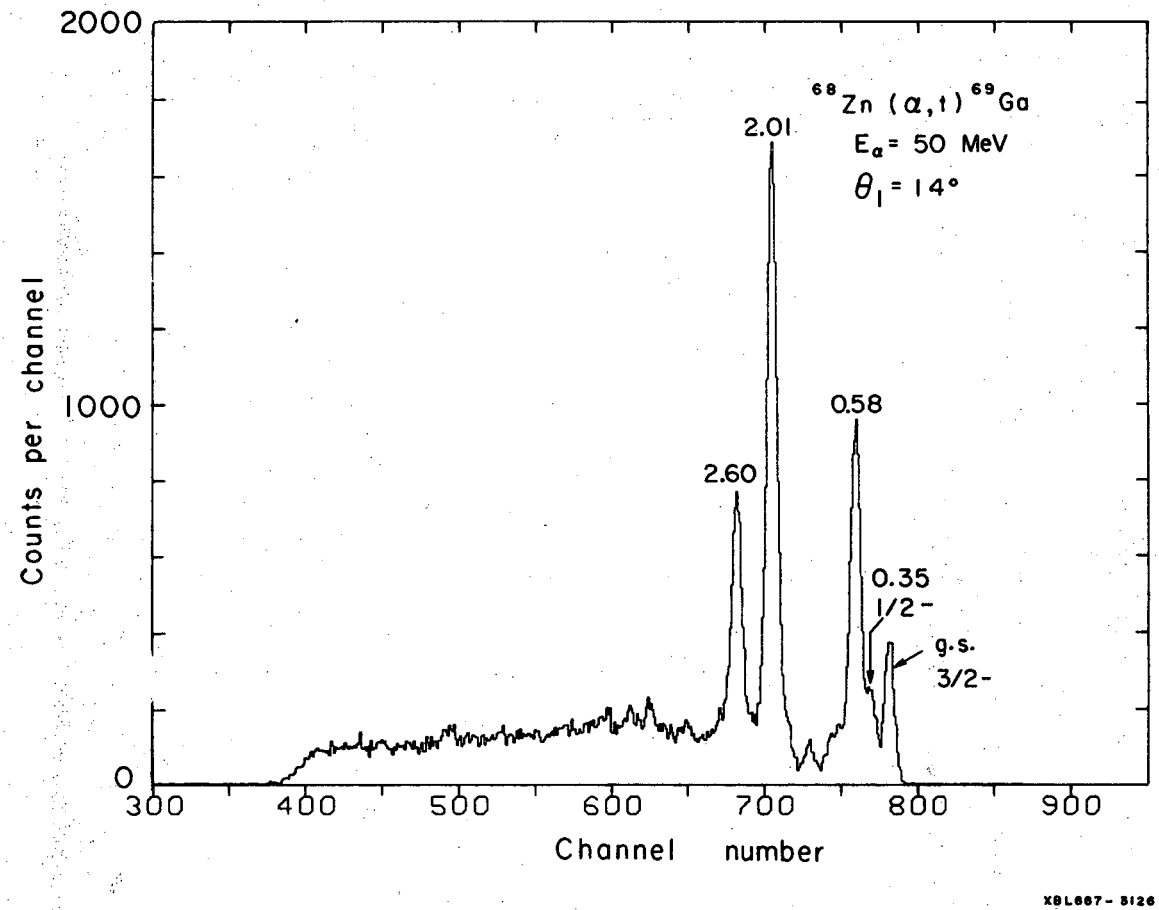

Fig. 44 Triton energy spectrum for the reaction $^{68}Zn(\alpha,t)^{69}Ga$ at θ(lab) = 14 deg with E(α) = 50.0 MeV.

From these results, it is clear that at alpha particle beam energies from 40-50 MeV the (α,t) reaction prefers to populate single particle states where the stripped proton is captured into the $1d_{5/2}$ or $1p_{1/2}$ shell model state in the light nuclides and into the $1f_{7/2}$, $1f_{5/2}$, or $1g_{9/2}$ state in the medium mass nuclides studied.

V. DISCUSSIONS

A. Criteria to Identify the $(1d_{5/2})^2_{5+}$ and $(1g_{9/2})^2_{9+}$ Levels and Rationale for These Criteria

The $(1d_{5/2})^2_{5+}$ levels in light nuclides assigned by the present study and previous work[2,3] are summarized in Table V. If from other work there are more accurately determined excitation energies for these levels, these values are listed. The angular distributions of the $(1d_{5/2})^2_{5+}$ levels obtained by this work are shown in Fig. 45. These angular distributions are similar to those of known 5+ levels of previous (α,d) work. Only one of the latter, that of the 8.963 MeV 5+ level of ^{14}N, is also shown in Fig. 45.

As stated in the introduction, the criteria for identification of these states are that the cross section be large, the angular distributions be similar to each other and that there be a monotonically decreasing $-Q_f$ value with increasing A of the residual nucleus. ($-Q_f$ is the Q-value for formation of the level.)

The large cross sections arise from the following causes:

a) These states have higher spins than other states and hence the cross section is enhanced by a large statistical factor (2J+1) due to the equal probability of populating the magnetic substates.

b) The structure factor G for these states is large.[57] This means roughly that the initial state and the deuteron picked up from the α particle have large overlap with the final state.

c) At 40-50 MeV alpha particle beam energy the momentum transferred to the target ($12 \leq A \leq 24$) by the captured proton-neutron pair at the

Table V. The $(1d_{5/2})^2_{5+}$ levels observed in the (α,d) reaction and their $-Q_f$ values.

Final nucleus	Energy of Excitation (MeV)	$-Q_f$ (MeV)	$J\pi$	T
^{14}N	8.963±0.002[a]	22.54	5+[a]	0
^{15}N	11.95 ±0.02	19.64	(9/2-)	1/2
	13.03 ±0.02	20.72	(11/2-)	1/2
^{16}N	5.75 ±0.02	19.13	(5+)	1
^{16}O	14.33 ±0.10[b]	17.44	(4,5+)[i]	0
	14.74 ±0.10[b]	17.85	(5,4+)[i]	0
	16.16 ±0.10[b]	19.27	(6+)[i,e]	0
^{17}O	7.74 ±0.02	17.54	(11/2-)	1/2
	9.14 ±0.03	18.94	(9/2-)	1/2
^{18}F	1.1310±0.0015[c]	17.45	5+[f]	0
^{22}Na	1.5281±0.0003[d]	14.10	5+[g]	0
^{26}Al	g.s.	12.43	5+[h]	0

[a]Ref. 5; [b]Ref. 3; [c]Ref. 58; [d]Ref. 34; [e]Ref. 59; [f]Ref. 7; [g]Ref. 8; [h]Ref. 60; [i]Assigned by this work.

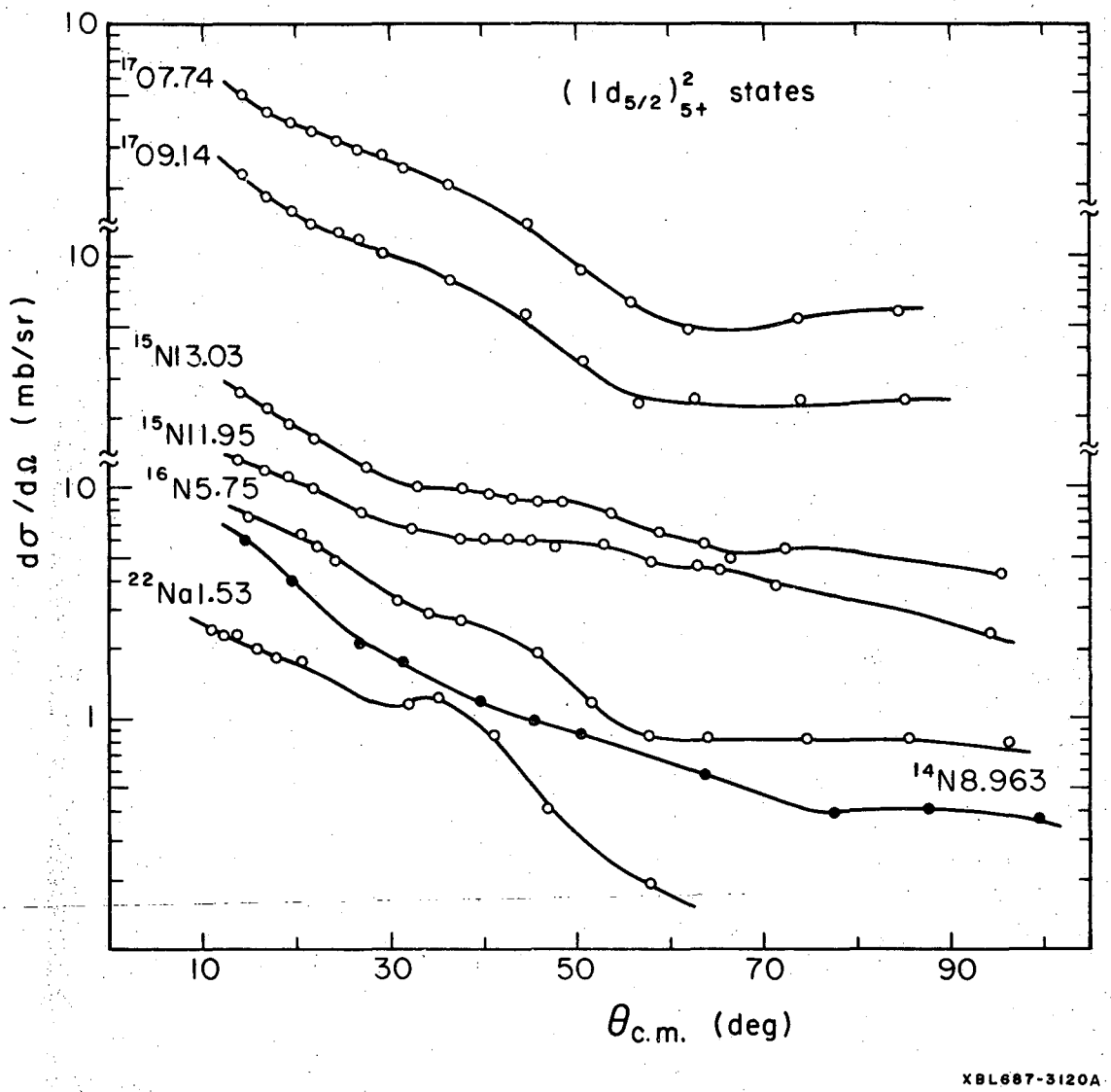

Fig. 45 Deuteron angular distributions from (α,d) reactions for states with $(1d_{5/2})^2_{5+,0}$ configuration.

nuclear surface is about $4\hbar$ which favors capture of the two particles both into $1d_{5/2}$ shell model state and which can give an $L = \ell_n + \ell_p = 2 + 2 = 4$ transfer.[3]

The gross similarity of the angular distributions is caused by the fact that they are all characterized by L = 4 transfer. The monotonically decreasing nature of the $-Q_f$ vs $A_{residual}$ curve can be expected by the following considerations.

The monotonical decreasing of $-Q_f$ value with increasing A of the residual nucleus can be understood by the following consideration. To form the level, one needs energy to break an alpha particle into deuteron, proton and neutron, denoted by $E_{\alpha\text{-}d,p,n}$. When the proton and neutron are captured into the $1d_{5/2}$ shell, one gets back energy equal to the separation energies of the $1d_{5/2}$ proton and neutron from the target core, denoted by S_p and S_n. Further energy is liberated from the residual interaction between proton, neutron in the state $(1d_{5/2})^2_{5+}$, denoted by $-E_{pn}$. Here $-E_{pn}$ is positive. Hence

$$\begin{aligned} -Q_f &= E_{\alpha\text{-}d,p,n} - S_p - S_n + E_{pn} \\ &= E_{\alpha\text{-}d,p,n} - (T_p + V_{p\text{-core}}) - (T_n + V_{n\text{-core}}) + E_{pn} \\ &= E_{\alpha\text{-}d,p,n} - T_p - T_n + E_{pn} - (V_{p\text{-core}} + V_{n\text{-core}}) \\ &= \text{constant} - (V_{p\text{-core}} + V_{n\text{-core}}), \end{aligned} \tag{5-1}$$

where T_p, T_n are the kinetic energies of the proton and neutron respectively in the $1d_{5/2}$ state and $V_{p\text{-core}}$, $V_{n\text{-core}}$ are their interaction energies with

the target core. The convention is adopted where $V_{p\text{-core}}$ and $V_{n\text{-core}}$ usually have negative values. Since the interaction energy between the proton-neutron pair and the target core, i.e. $(V_{p\text{-core}} + V_{n\text{-core}})$, becomes stronger when the core has more $1p_{1/2}$ nucleons (discussed in Section E), $-Q_f$ decreases as A increases. Further discussion in Section E will clarify this point. Figure 46 shows a plot of $-Q_f$ vs A for $(1d_{5/2})^2_{5+}$ levels as well as for previously assigned $(1d_{5/2},1f_{7/2})_{6-}$ and $(1f_{7/2})^2_{7+}$ levels[3] and for the $(1g_{9/2})^2_{9+}$ levels assigned by this work. For each configuration, a monotonically decreasing pattern is followed.

The $(1g_{9/2})^2_{9+}$ levels assigned by this study are listed in Table VI. Since no angular distributions were taken for these states, the assignment of these states was based on the two criteria of a smooth monotonically decreasing curve of the $-Q_f$ vs $A_{residual}$ plot and largest cross section.

The causes for the relatively large cross sections for states with configuration $(1g_{9/2})^2_{9+,0}$ are still the same as discussed in the case for those with $(1d_{5/2})^2_{5+,0}$ configuration. Here, at 40-50 MeV alpha particle beam energy the momentum transferred to the target ($52 \leq A \leq 68$) by the captured proton-neutron pair at the nuclear surface is about $8\hbar$ which favors capture of the two particles both into $1g_{9/2}$ shell model state and which can give an $\mathbf{L} = \ell_n + \ell_p = 4 + 4 = 8$ transfer.

It was found, however, that in ^{54}Mn and ^{56}Co it was necessary to choose the second most strongly populated level in order to obtain a smoothly varying $-Q_f$ vs $A_{residual}$ plot. This is not unreasonable, since the (α,t) spectra show that $1f_{7/2}$ single-particle proton capture predominates

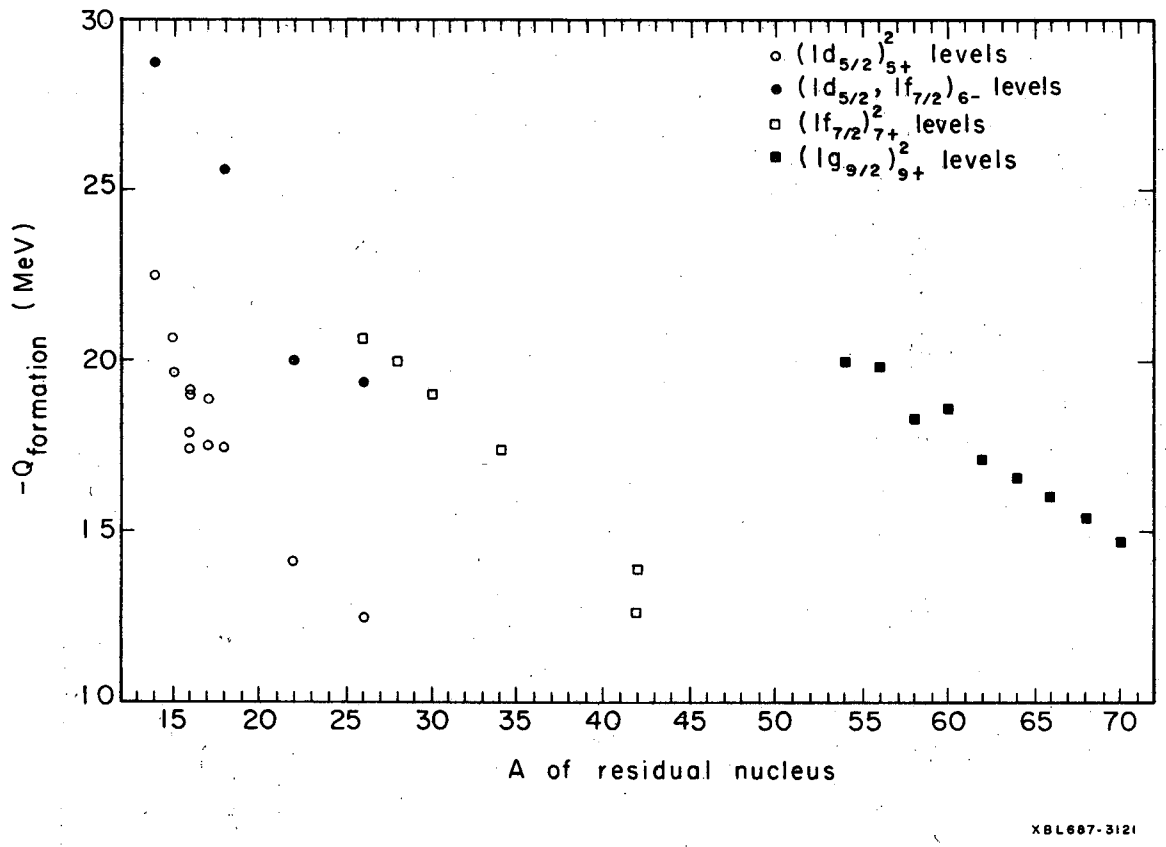

Fig. 46 Relation between the mass number A of product nucleus and the Q-value of formation of the levels with $(1d_{5/2})^2_{5+,0}$, $(1f_{7/2})^2_{7+,0}$, $(1d_{5/2}, 1f_{7/2})_{6-,0}$, and probably $(1g_{9/2})^2_{9+,0}$ configuration strongly populated by the (α,d) reaction.

Table VI. High spin [probably $(1g_{9/2})^2_{9+}$] levels observed in the (α,d) reaction.

Final nucleus	Energy Level (MeV)	$-Q_f$ (MeV)
^{54}Mn	9.47±0.05	20.04
^{56}Co	8.92±0.03	19.85
^{58}Co	6.79±0.03	18.27
^{60}Cu	5.99±0.03	18.58
^{62}Cu	4.75±0.03	17.12
^{64}Cu	4.57±0.03	16.60
^{66}Ga	2.99±0.03	16.00
^{68}Ga	2.88±0.03	15.40
^{70}Ga	2.88±0.03	14.69

over the $1g_{9/2}$ single-particle capture in these nuclides, and thus we might expect large cross sections for levels with a configuration which includes a $1f_{7/2}$ proton to appear in the (α,d) reaction in addition to the $(1g_{9/2})^2_{9+}$ levels. In the higher mass region the (α,t) reaction shows that $1g_{9/2}$ proton capture is predominant, and here we find that the most strongly populated level should be chosen as the $(1g_{9/2})^2_{9+}$ levels.

For the two odd-A targets, ^{59}Co and ^{63}Cu, there are no strongly populated levels in the (α,d) spectra. This is consistent with previous results. For a target with ground state spin $J_i \neq 0$ a multiplet of $(2J_i+1)$ states can be formed from vector coupling J_i to the total angular momentum, 2j, of the captured pair, if $J_i < 2j$. In the present case, the ground state spins are ^{59}Co(J_i = 7/2) and ^{63}Cu(J_i = 3/2) and we expect that the capture strength will be distributed over many states in the multiplet. This has the effect of decreasing the strength of each of the high-spin levels relative to the other states made in the reaction, and a single strongly-excited level is no longer observed.

B. Residual Interaction Energies between Proton and Neutron In the Configuration of $(1d_{5/2})^2_{5+,0}$, or $(1f_{7/2})^2_{7+,0}$ or $(1g_{9/2})^2_{9+}$

In the previous section we have discussed the assignment of proton-neutron two-particle excited states with the configuration $(1d_{5/2})^2_{5+}$. From the excitation energies of these two-particle excited states together with known neighboring single-particle excitation energies, the residual interaction energy E_{pn} between the proton and neutron can be calculated. The method of calculation is outlined below.

For $T_z = 0$ nuclei the calculation is simple. For example in ^{18}F, the 1.131 MeV 5+ level was assigned to have the configuration

$$[(^{16}O \text{ core})\ (1d_{5/2})^2_{5+,0}]_{5+,0}$$

The total separation energy of the proton and neutron in this configuration from the ^{16}O is:

$$S_T = S_{p,n} - E^*$$

where S_{pn} is the separation energy of the last proton and neutron in the ground state of ^{18}F from the ^{16}O core and E^* is the excitation energy of the $(1d_{5/2})^2_{5+}$ state. E^* is equal to 1.131 MeV in this case. Let S_p denote the separation energy of a proton in the $1d_{5/2}$ single particle state of ^{17}F and S_n represent the separation energy of a neutron in the $1d_{5/2}$ single particle state of ^{17}O. Then,

$$S_T = S_p + S_n - E_{pn}$$

where $E_{pn} = E(1d_{5/2})^2_{5+,0}$ is the residual interaction energy for $T_z = 0$ nuclei. The results of these calculations for the nuclides ^{14}N, ^{18}F, ^{22}Na and ^{26}Al are listed in Table VII. The neighboring single particle states used in the calculation are also tabulated. The residual interaction energies stay fairly constant over this mass region from A = 14 to 26 with a value of about -3.9 MeV, (i.e., attractive). Except for the nucleus ^{26}Al, the residual interaction decreases slightly with increasing A.

For $T_z \neq 0$ nuclei the situation is more complicated. As an example, the 11/2-, T = 1/2 state of ^{15}N will be discussed in the following paragraphs

Table VII.* Experimental residual interaction energies for $(1d_{5/2})^2_{5+,0}$ configuration.

Two-particle excited states	Single particle state: Assumed $1d_{5/2}$ neutron states	Single particle state: Assumed $1d_{5/2}$ proton states	$E(1d_{5/2})^2_{5+,0}$ See Note 1
^{14}N: 8.963 5+[a]	^{13}C: 3.85 5/2+[b,n]	^{13}N: 3.56 5/2+[b,n]	-4.05
^{18}F: 1.131 5+[c]	^{17}O: 0.000 5/2+[b,n]	^{17}F: 0.000 5/2+[b,n]	-3.88
^{22}Na: 1.528 5+[d]	^{21}Ne: 0.353 5/2+[p]	^{21}Na: 0.338 5/2+[e]	-3.47
^{26}Al: 0.000 5+[e]	^{25}Mg: 0.000 5/2+[e]	^{25}Al: 0.000 5/2+[e]	-4.04
^{15}N: 13.03 (11/2-)[f]	^{14}C: 6.723 e-,T=1[g,n,ℓ]	^{14}N: 5.83 3-,T=0[h,n]	-3.57+
^{17}O: 7.74 (11/2-)[f]	^{16}N: 0.300 3-,T=1[i,n]	^{16}O: 6.135 3-,T=0[j] 13.26 3-,T=1[j]	-3.69+
^{16}O: 16.16 (6+)[f]	^{15}N: 7.57 7/2+[k]	^{15}O: 7.28 (7/2+)[k] ℓ_n=2	-3.52+
^{16}N: 5.75 (5+)[f]	^{15}C: 0.75 5/2+,T=3/2[ℓ,n]	^{15}N: 5.276 5/2+,T=1/2[k] 12.502 5/2+,T=3/2[m]	-3.82+

*All the energies are in units of MeV.

+Calculated by using the interaction model discussed in the text.

Note 1: Experimental proton-neutron residual interaction energy.

[a]Ref. 5,6; [b]Ref. 22; [c]Ref. 7; [d]Ref. 8; [e]Ref. 60; [f]Ref. 61; [g]Ref. 62; [h]Ref. 22; [i]Ref. 32; [j]Ref. 50; [k]Ref. 28; [ℓ]Ref. 29; [m]Ref. 63; [n]Ref. 26; [p]Ref. 51.

in considerable detail. This state is assumed to have the following configuration:

$$[(^{13}\mathrm{C\ core})_{1/2-,1/2}\ (1d_{5/2})^2_{5+,0}]_{11/2-,1/2}$$

Assume that the ground state of ^{13}C has the pure configuration $[(^{12}\mathrm{C\ core})\ p_{1/2}]$. The interaction energy of two nucleons in $(1d_{5/2})^2_{5+,0}$ with one nucleon in the $1p_{1/2}$ state can be calculated by applying Eq. (3-19). The result is:

$$\langle (d_{5/2})^2_{5+,0}\ p_{1/2}\ J = 11/2,\ T = 1/2 \left| \sum_{i=1}^{2} V_{i3} \right| (d_{5/2})^2_{5+,0}\ p_{1/2}\ J = 11/2,$$

$$T = 1/2\rangle = (1/2)V_{3,T'=0} + (3/2)V_{3,T'=1}$$

where

$$V_{J',T'=0} = \langle d_{5/2}\ P_{1/2} J',T' = 0 \quad |V| d_{5/2}\ P_{1/2}\ J',\ T' = 0\rangle$$

$$V_{J',T'=1} = \langle d_{5/2}\ P_{1/2} J',T' = 1 \quad |V| d_{5/2}\ P_{1/2}\ J',\ T' = 1\rangle$$

Here V_{ij} or V is a charge-independent interaction. A $1d_{5/2}$ neutron interacts with a $1p_{1/2}$ neutron only in the T' = 1 state. This interaction is:

$$\langle d_{5/2}\ P_{1/2}\ J' = 3,T' = 1|V|d_{5/2}\ P_{1/2}\ J' = 3,\ T' = 1\rangle = V_{3,T'=1}$$

Only J' = 3 is possible, for if J' = 2, the $d_{5/2}$ proton (J = 5/2) cannot couple to this value (2) to give a final state with J = 11/2, as is seen in the following diagram.

$$\xrightarrow{P_{1/2}} \xrightarrow{d_{5/2}} \xrightarrow{d_{5/2}}$$

$$\xrightarrow{\qquad\qquad\qquad\qquad}$$

$$J = 11/2$$

However a $d_{5/2}$ proton can interact with a $p_{1/2}$ neutron both in T = 0 or T = 1 state. The present physical picture suggested that the total interaction between the $1p_{1/2}$ neutron and the $(1d_{5/2})^2_{5+}$ nucleons can be represented by two terms, the n-n interaction $V_{3,1}$, and a combination of $V_{3,1}$ and $V_{3,0}$ which equals the n-p interaction V_3. Let the coefficients of the latter be a and b. Then,

$$V_3 = a\, V_{3,0} + b\, V_{3,1}.$$

Here a and b can be interpreted as the probabilities that the $d_{5/2}$ proton will interact with the $p_{1/2}$ neutron to form T = 0, J = 3, and T = 1 J = 3 states, respectively, where the proton is in the $1d_{5/2}$ state specified and the configuration:

$$[p_{1/2-,1/2}\ (d_{5/2})^2_{5+,0}]_{11/2-,1/2} \qquad T_z = 1/2$$

states: ν π and ν

The proof of this statement follows from the discussion of Chapter III, Section B. The quantities a and b can be determined by requiring that the above total interaction energy of $d_{5/2}$ nucleons to the $p_{1/2}$ neutron be equal to the sum of the interaction of the $d_{5/2}$ proton to the $p_{1/2}$ neutron and of the $d_{5/2}$ neutron to the $p_{1/2}$ neutron. That is:

$$(1/2)V_{3,T'=0} + (3/2)V_{3,T'=1} = [a\, V_{3,T'=0} + b\, V_{3,T'=1}] + V_{3,T'=1} \qquad (5\text{-}2)$$

Hence a = 1/2 and b = 1/2. Then the quantities in the bracket represent the neutron-proton interaction and the last term represents the neutron-neutron interaction. Since (a+b) is the total probability of a $d_{5/2}$ proton

interacting with a $p_{1/2}$ neutron, it should be equal to one: the above values of a and b satisfy this requirement.

The interaction between the $1d_{5/2}$ nucleons and the ^{12}C core is neglected in the above discussion. If this interaction is taken into account, then the meaning implied by Eq. (5-2) is as follows:

The total interaction energies of the proton-neutron pair in the $(1d_{5/2})^2_{5+,0}$ configuration to the ^{13}C core can be separated into two parts:

a) The $d_{5/2}$ neutron-to-core interaction which is the same as that in the $(d_{5/2},p_{1/2})_{3-,1}$ state in ^{14}C.

b) The $d_{5/2}$ proton-to-core interaction which half of the time (because a = 1/2) is the same as that in the $(d_{5/2},p_{1/2})_{3-,0}$ state in ^{14}N and half of the time (because b = 1/2) is the same as that of the $(d_{5/2},p_{1/2})_{3-,1}$ state in ^{14}N.

The residual interaction energies can now be calculated following the same procedure as discussed in the $T_z = 0$ case where S_p should be the average separation energy of T = 0 and T = 1 states of ^{14}N weighted by their respective probabilities a and b. It must be noted that in the $(d_{5/2},p_{1/2})_{3-,0}$ or $(d_{5/2},p_{1/2})_{3-,1}$ state of ^{14}N, the proton is in the $d_{5/2}$ state half of the time while the proton in the $[(d_{5/2})^2_{5,0}\ p_{1/2}]_{J,T}$ state of ^{15}N can only be in the $d_{5/2}$ state. Therefore, an additional Coulomb energy difference must be introduced. The Coulomb energy difference between a $d_{5/2}$ proton coupled to the ^{12}C core and a $p_{1/2}$ proton coupled to the ^{12}C core is just

the difference of the excitation energy between the $d_{5/2}$ single particle excited states of ^{13}C and ^{13}N, which are 3.85 MeV and 3.56 MeV, respectively. This difference is equal to 0.29 MeV. The Coulomb energy correction which will be denoted by C in Eq. (5-4) is equal to half of this value, i.e., 0.15 MeV.

For more general cases, where there are n $p_{1/2}$ nucleons in the ground state of target core with J" T", one can write down the following formula:

$$\langle (p_{1/2})^n_{J'',T''}(d_{5/2})^2_{5,0}{}^{J,T} \left| \sum_{i=1}^{2} \sum_{j=3}^{n+2} V_{ij} \right| (p_{1/2})^n_{J'',T''}(d_{5/2})^2_{5,0}{}^{J,T} \rangle$$

$$= \sum_{J'} \Big[a_{J'} \langle (p_{1/2})^n_{J'',T''} d_{5/2}{}^{J',T'=T''-\frac{1}{2}} \left| \sum_{j=2}^{n+1} V_{1j} \right| (p_{1/2})^n_{J'',T''} d_{5/2}{}^{J',T'=T''-1/2} \rangle$$

$$+ (b_{J'}+1) \langle (p_{1/2})^n_{J'',T''} d_{5/2}{}^{J',T'=T''+\frac{1}{2}} \left| \sum_{j=2}^{n+1} V_{1j} \right| (p_{1/2})^n_{J'',T''} d_{5/2}{}^{J',T'=T''+1/2} \rangle \Big]$$

$$= \sum_{J'} \left\{ a_{J'} \begin{bmatrix} J' \\ T'=T''-1/2 \end{bmatrix} + b_{J'} \begin{bmatrix} J' \\ T'=T''+1/2 \end{bmatrix} + \begin{bmatrix} J' \\ T'=T''+1/2 \end{bmatrix} \right\} , \qquad (5\text{-}3)$$

if $T'' \neq 0$. If $T'' = 0$, then T' can only have the value $T'' + 1/2 = 1/2$. Hence $a_{J'} = 0$ and $b_{J'} = 1$. Here, J' must satisfy the following relation:

$$\vec{J}' + \vec{5}/2 = \vec{J},$$

and $\left[\begin{smallmatrix} J' \\ T' \end{smallmatrix}\right]$ represents the following matrix element:

$$\langle (p_{1/2})^n_{J'',T''} d_{5/2}{}^{J',T'} \left| \sum_{j=2}^{n+1} V_{1j} \right| (p_{1/2})^n_{J'',T''} d_{5/2}{}^{J',T'} \rangle .$$

Both the left side of Eq. (5-3) for n+2 nucleons, and the two terms on the right side for n+1 nucleons can be expressed in terms of two body matrix elements by using Eq. (3-19). From such expressions, it would be actually possible to obtain Eq. (5-3) directly for each example in this thesis. The solution of the constants $a_{J'}$, and $b_{J'}$, is obtained by requiring that the coefficients of a two body matrix element occurring in the left side of Eq. (5-3) should be equal to those at the right side. The probability that the $d_{5/2}$ proton (in a configuration $(d_{5/2})^2_{5,0}$) will interact with the target in the (J',T'=T"- 1/2) or (J',T'=T"+ 1/2) configuration is $a_{J'}$ or $b_{J'}$ respectively. The proof of this statement follows from considerations similar to those of Section III.B applied to the configurations on both sides of Eq. (5-3). The $(d_{5/2},p_{1/2})$ interaction energies can be taken from the excited states of the "target plus one" nucleus. The probability that the $d_{5/2}$ neutron (in the configuration $(1d_{5/2})^2_{5,0}$) will interact with the target core in the (J',T'=T"+ 1/2) state is equal to 1. These $(d_{5/2},p_{1/2})$ interaction energies can be taken from the excited states of the "target plus one neutron" nucleus. The residual interaction energies between the $1d_{5/2}$ proton and neutron in the $(1d_{5/2})^2_{5,0}$ configuration can now be calculated by following the same procedure as discussed in the $T_z = 0$ case, provided that $S_p = S_{d_{5/2}p}$ is now the average separation energy of the J'T' states in the "target plus one proton" nucleus weighted by their respective probabilities $a_{J'}$ and $b_{J'}$. The detailed proof is omitted. Coulomb energy correction must be introduced because in the $[(p_{1/2})^n_{J"T"}(d_{5/2})^2_{5,0}]_{J,T}$ configuration, there is always one proton in the $1d_{5/2}$ state, while in the $[(p_{1/2})^n_{J"T"}d_{5/2}]_{J'T'}$ configuration of

the "target plus one proton" nucleus, the probability of a proton in the $1d_{5/2}$ state is not always equal to 1. This probability, denoted by $K_{T'}$, is equal to $(T'',T_z'+1/2,1/2,-1/2|T'T_z')^2$, where T", T' is the T's of the ground state of the target and the states in "target plus one proton" nucleus considered and T_z' is the "T_z'' value [=(N-Z)/2] of the "target plus one proton" nucleus. Now the Coulomb correction can be included in the following way:

$$S'_{d_{5/2}p} = S_{d_{5/2}p} + C$$

$$= S_{d_{5/2}p} + E'_c \left\{(1-K_{T'=T''-1/2})\sum_{J'} a_{J'} + (1-K_{T'=T''+1/2})\sum_{J'} b_{J'}\right\},$$

where E'_c is the Coulomb energy which is equal to:

$$E'_c = [E_c(\pi d_{5/2} - {}^{12}C) - E_c(\pi p_{1/2} - {}^{12}C)] + [E_c[\pi d_{5/2} - (\pi p_{1/2})^m\}$$

$$- E_c\{\pi p_{1/2} - (\pi p_{1/2})^m\}]$$

with $E_c(\ell_j - X)$ represents the Coulomb energy between an ℓ_j proton and a structure X which may consist of many nucleons or just one. Here, m is the number of $p_{1/2}$ protons in the ground state of the target nucleus. $S_{d_{5/2}p}$ is the separation energy weighted by the $a_{J'}$ and $b_{J'}$ and $S'_{d_{5/2}p}$ is the separation energy after correction for the Coulomb energy. The $K_{T'}$ values thus calculated are 1/2 for both T'=0 and 1 with T" = 1/2 (i.e., ^{13}C or ^{15}N target), 1 for T'=1/2 with T"=0 (i.e., ^{14}N target), and 2/3 and 1/3 respectively for T'=1/2 and 3/2 with T"=1 (i.e., ^{14}C as target). The E'_c value used for both ^{15}N and ^{16}N is 0.29 MeV. This is the difference between the excitation energies of the $d_{5/2}$ single particle state of the

^{13}C and ^{13}N nuclei (i.e., 3.85 and 3.56 MeV respectively). The $E_c(\pi p_{1/2} - \pi p_{1/2})$ value is calculated from the binding energies of the ground states of ^{15}N and ^{15}O. The $E_c(\pi p_{1/2} - \pi d_{5/2})$ is equal to 0.40 MeV which is calculated from the analog states of ^{14}C and ^{14}O with configuration $(d_{5/2}p_{1/2})_{3-,1}$. No Coulomb energy correction, C, is needed for the ^{16}O case.

The above method is used to calculate the residual interaction for the ^{15}N 13.023 MeV, ^{17}O 7.743 Mev, ^{16}O 16.16 Mev, and ^{16}N 5.747 MeV levels assuming that these states have spins 11/2, 11/2, 6, and 5 respectively. The values obtained, as well as the level information of neighboring nuclides used, are listed in Table VII. The residual interaction energies again stay fairly constant at about -3.7 MeV. The results of the interaction energy calculation between $d_{5/2}$ and $p_{1/2}$ nucleons obtained by applying Eq. (3-19) are also summarized in Table VIII. ; These results are then used to deduce the constants $a_{J'}$ and $b_{J'}$ needed in breaking the total interaction of $(1d_{5/2})^2_{5+,0}$, to core into proton-to-core and neutron-to-core interactions. Results obtained are given in Table IX. The name "interaction model" is used to signify the present separation of interaction energy.

From (α,d) experiments, a level in each of the four $T_z = 0$ nuclei ^{14}N, ^{18}F, ^{22}Na and ^{26}Al was assigned spin 5+ and the configuration $(1d_{5/2})^2_{5+}$. From independent work, each of these levels is known to have spin 5+. One may therefore safely assume that the main configuration is indeed $(1d_{5/2})^2_{5+}$. Further, the experimental residual interaction energies stay constant at about -3.9 MeV over the mass region A = 14 to 26. As

Table VIII. Interaction energy between $1p_{1/2}$ and $1d_{5/2}$ nucleons expressed in terms of two body interaction energies

Nucleus A	Nucleus A-1		Interaction energy (diagonal matrix elements only)
^{15}N		$\langle (d_{5/2})^2_{5,0}\, p_{1/2}{}^{J=11/2}_{T=1/2} \left\| \sum_{i=1}^{2} V_{i3} \right\| '' \rangle$	$= \frac{1}{2} V_{3,T=0} + \frac{3}{2} V_{3,T=1}$
^{17}O		$\langle (d_{5/2})^2_{5,0} (p_{1/2})^3_{1/2,1/2}{}^{J=11/2}_{T=1/2} \left\| \sum_{i=1}^{2} \sum_{j=3}^{5} V_{ij} \right\| '' \rangle$	$= \frac{13}{12} V_{3,T=0} + \frac{5}{12} V_{2,T=0} + \frac{13}{4} V_{3,T=1} + \frac{5}{4} V_{2,T=1}$
	^{16}O	$\langle d_{5/2}\, (p_{1/2})^3_{1/2,1/2}{}^{J=3}_{T=0} \left\| \sum_{j=2}^{4} V_{1j} \right\| '' \rangle$	$= \frac{2}{3} V_{3,T=0} + \frac{5}{6} V_{2,T=0} + \frac{3}{2} V_{3,T=1}$
	$^{16}N, ^{16}O$	$\langle d_{5/2}\, (p_{1/2})^3_{1/2,1/2}{}^{J=3}_{T=1} \left\| \sum_{j=2}^{4} V_{1j} \right\| '' \rangle$	$= \frac{1}{2} V_{3,T=0} + \frac{5}{6} V_{2,T=1} + \frac{5}{3} V_{3,T=1}$
^{16}O		$\langle (d_{5/2})^2_{5,0}\, (p_{1/2})^2_{1,0}{}^{J=6}_{T=0} \left\| \sum_{i=1}^{2} \sum_{j=3}^{4} V_{ij} \right\| '' \rangle$	$= V_{3,T=0} + 3V_{3,T=1}$
	$^{15}N, ^{15}O$	$\langle d_{5/2}\, (p_{1/2})^2_{1,0}{}^{J=7/2}_{T=1/2} \left\| \sum_{j=2}^{3} V_{1j} \right\| '' \rangle$	$= \frac{1}{2} V_{3,T=0} + \frac{3}{2} V_{3,T=1}$
^{16}N		$\langle (d_{5/2})^2_{5,0} (p_{1/2})^2_{0,1}{}^{J=5}_{T=1} \left\| \sum_{i=1}^{2} \sum_{j=3}^{4} V_{ij} \right\| '' \rangle$	$= \frac{7}{12} V_{3,T=0} + \frac{5}{12} V_{2,T=0} + \frac{7}{4} V_{3,T=1} + \frac{5}{4} V_{2,T=1}$
	^{15}N	$\langle d_{5/2}\, (p_{1/2})^2_{0,1}{}^{J=5/2}_{T=1/2} \left\| \sum_{j=2}^{3} V_{1j} \right\| '' \rangle$	$= \frac{7}{8} V_{3,T=0} + \frac{5}{8} V_{2,T=0} + \frac{7}{24} V_{3,T=1} + \frac{5}{24} V_{2,T=1}$
	$^{15}C, ^{15}N$	$\langle d_{5/2}\, (p_{1/2})^2_{0,1}{}^{J=5/2}_{T=3/2} \left\| \sum_{j=2}^{3} V_{1j} \right\| '' \rangle$	$= \frac{7}{6} V_{3,T=1} + \frac{5}{6} V_{2,T=1}$

Table IX. Interaction model. The Coulomb energy correction, C, is not included.

State	Interaction model		
	Total interaction	Proton-core	Neutron-core
^{15}N 11/2-	$E[(d_{5/2})^2_{5,0} \leftrightarrow (p_{1/2})_{1/2,1/2}]$	$=([^{J'=3}_{T'=0}]+[^{J'=3}_{T'=1}])/2$	$+([^{J'=3}_{T'=1}])$
^{17}O 11/2-	$E[(d_{5/2})^2_{5,0} \leftrightarrow (p_{1/2})^3_{1/2,1/2}]$	$=([^{J'=3}_{T'=0}]+[^{J'=3}_{T'=1}])/2$	$+([^{J'=3}_{T'=1}])$
^{16}O 6+	$E[(d_{5/2})^2_{5,0} \leftrightarrow (p_{1/2})^2_{1,0}]$	$=([^{J'=7/2}_{T'=1/2}])$	$+([^{J'=7/2}_{T'=1/2}])$
^{16}N 5+	$E[(d_{5/2})^2_{5,0} \leftrightarrow (p_{1/2})^2_{0,1}]$	$=(\frac{2}{3}[^{J'=5/2}_{T'=1/2}]+\frac{1}{3}[^{J'=5/2}_{T'=3/2}])$	$+([^{J'=5/2}_{T'=3/2}])$

will be shown in the Section D, this value of the $(1d_{5/2})^2_{5+}$ interaction energy is very reasonable. Thus one may have considerable confidence in the method used for the extraction of the interaction energies for the T = 0 nuclei. Since the calculation of the interaction energy for the $T_z \neq 0$ nuclei gives a result in excellent agreement with that obtained for the $T_z = 0$ nuclei, one may have considerable confidence in the method of calculation as well as in the assignments of spin and parities for the levels of $T_z \neq 0$ nuclei shown in Table VII. Alternatively, an experimental verification of the spin of these states would prove the correctness of the above "interaction model" method approach used for those $T_z \neq 0$ nuclides.

One can expect that the above calculational method, for both $T_z = 0$ or $T_z \neq 0$ nuclides, is quite good on the following two accounts:

a) Because of the high spin value of the state considered, configuration mixing is small.

b) By using experimental energies of neighboring nuclei, some core excitation has already been taken into account. That is to say, the states of neighboring nuclei used in the calculation do not have to have a very pure configuration. As long as the presence of the additional $d_{5/2}$ nucleon of the two particle state does not alter this configuration appreciably, the interaction energy thus calculated may still be accurate even though the true configuration of the target is not purely $[(^{12}C \text{ core})(p_{1/2})^n]$.

Following the same method as discussed above, the residual interaction energies between proton and neutron in $(1f_{7/2})^2_{7+,0}$ configuration are calculated. The results are listed in Table X. The excitation energies of the two-particle excited states used here are from Ref. 3. For ^{28}Al, the value of $a_{J'=7/2}$ and $b_{J'=7/2}$ are 2/3 and 1/3 respectively. The E'_c value of Eq. (5-4) is 0.25 MeV which is the difference of the assumed 7/2 single particle state in ^{25}Mg and ^{25}Al (i.e., 3.97 Mev and 3.72 MeV respectively). The residual interaction energy stays fairly constant but decreases slightly faster with increasing A as compared to the $(1d_{5/2})^2_{5+,0}$ residual interaction energies.

Similarily, the "interaction model" method can be applied to calculate the residual interaction energies between proton and neutron in $(1g_{9/2})^2_{9+,0}$ configuration. These calculations need the value of the excitation energies of the analog states. The single particle $1g_{9/2}$ states in ^{59}Cu and ^{61}Cu analog to ^{59}Ni and ^{61}Ni are known.[54] The Coulomb displacement energy, E_c, of ^{53}Mn, ^{55}Co, ^{63}Cu, Ga (natural mixture of isotopes) analog to the ground state of ^{53}Cr, ^{55}Fe, ^{63}Ni, and Zn is equal to 8.390 MeV, 8.660 MeV, 9.300 MeV, and 9.76 MeV respectively.[69] The $1g_{9/2}$ analog states are assumed to have the same excitation energies above the analog states of the ground states of ^{53}Cr, ^{55}Fe, ^{63}Ni, ^{65}Zn and ^{67}Zn as the excitation energies of the $1g_{9/2}$ single particle states of the latter nuclei. Coulomb energy corrections are not included because there is not enough experimental information to calculate these values. This is justified from the previous calculations for $(1d_{5/2})^2_{5+,0}$ which have shown that these corrections are only about 150-220 keV.

Table X.* Experimental residual interaction energies for $(1f_{7/2})^2_{7+,0}$ configuration.

Two-particle excited states	Single particle states[a] Assumed $1f_{7/2}$ neutron states	Assumed $1f_{7/2}$ proton states	$E(1f_{7/2})^2_{7+,0}$ See note 1.
^{26}Al: 8.27	^{25}Mg: 3.97(5/2,7/2)- (d,p) ℓ_n=3	^{25}Al: 3.72 7/2-[a,b]	-3.44
^{30}P : 7.03	^{29}Si: 3.623 7/2- (d,p) ℓ_n=3	^{29}P : 3.44 7/2-[c,d,b] (^{3}He,d),(d,n) ℓ_p=3	-2.89
^{34}Cl: 5.2	^{33}S : 2.937 7/2- (d,p) ℓ_n=3	^{33}Cl: (2.5)[d]	-(3.11)
^{42}Sc: 0.60	^{41}Ca: 0.000 7/2- (d,p) ℓ_n=3	^{41}Sc: 0.000 7/2- (t,d),(d,n) ℓ_p=3	-2.62
^{28}Al: 9.80	^{27}Mg: 3.575(7/2,5/2)- T=3/2	^{27}Al: 6.48 7/2(5/2)[e,b] T=1/2	
		10.50 7/2-[f] T=3/2	-(2.96)

*All the energies are in the units of MeV.

Note 1: Experimental proton-neutron residual interaction energy.

[a]All the single particle states information are from ref. 60 if not otherwise indicated.

[b]Ref. 64, [c]Ref. 65, [d]Ref. 66, [e]Ref. 67, [f]Ref. 68.

The constants $a_{J'}$ and $b_{J'}$ for each nucleus are determined with the following assumption about the configuration of the ground state of the target core:

^{52}Cr: $(1f_{7/2})^{12}_{0+,2}$

^{54}Fe: $(1f_{7/2})^{14}_{0+,1}$

^{58}Ni: $(2p_{3/2})^{2}_{0+,1}$ or $(1f_{5/2})^{2}_{0+,1}$

^{60}Ni: $(2p_{3/2})^{4}_{0+,2}$ or $(1f_{5/2})^{4}_{0+,2}$

^{62}Ni: $(1f_{5/2})^{6}_{0+,3}$

^{64}Zn: $(1f_{5/2})^{8}_{0+,2}$

^{66}Zn: $(2p_{1/2})^{4}_{0+,0}(2p_{3/2})^{2}_{0+,1}$ or $(2p_{1/2})^{4}_{0+,0}(1f_{5/2})^{2}_{0+,1}$

In all the cases thus calculated, the constants $a_{J'}$ and $b_{J'}$ have the value:

$$a_{J'} = 2T_i/(2T_i + 1) \qquad b_{J'} = 1/(2T_i + 1)$$

where T_i is the isobaric spin quantum number of the target. The results of these calculations are listed in Table XI. For the nuclei ^{58}Co and ^{70}Ga, the target nuclei (i.e., ^{56}Fe and ^{68}Zn) have to occupy two shell model states beyond a closed $1f_{7/2}$ shell. Equation (3-19) is no longer adequate to treat this case. Hence, no calculation has been made for these two nuclides. Although configurations which may be different from the true ones are assumed for the g.s. of ^{62}Ni, ^{64}Zn, and ^{66}Zn, the calculated values may still be good on account of the second reason discussed above.

Table XI.* Experimental residual interaction energies for $(1g_{9/2})^2_{9+,0}$ configuration.

Two-Particle excited states	Single particle states: Assumed $1g_{9/2}$ neutron states	Single particle states: Assumed $1g_{9/2}$ proton states[k]	$E(1g_{9/2})^2_{9+,0}$ See note 1
^{54}Mn: 9.47	^{53}Cr: 3.70 9/2+[a]	^{53}Mn: (6.4)[e] (10.72)[f]	-(2.49)
^{56}Co: 8.92	^{55}Fe: 3.80 9/2+[b]	^{55}Co: 6.01 9/2+[e,g,h] (8.56)[f]	-(2.54)
^{60}Cu: 5.99	^{59}Ni: 3.07 9/2+[c]	^{59}Cu: 2.99 9/2+[e,i] 6.86 (9/2+)[f]	-2.42
^{62}Cu: 4.75	^{61}Ni: 2.13 9/2+[c]	^{61}Cu: 2.71 9/2+[e,i] 8.56 (9/2+)[f]	-2.34
^{64}Cu: 4.57	^{63}Ni: 1.7[b] (centroid)	^{63}Cu: 2.51 9/2+[j] (10.46)[f]	-(1.93)
^{66}Ga: 2.99	^{65}Zn: 1.04 9/2+[d]	^{65}Ga: 2.03 9/2+[k,e] (7.10)[f]	-(2.22)
^{68}Ga: 2.88	^{67}Zn: 0.64[d] (centroid)	^{67}Ga: 2.10[e] (8.98)[f]	-(2.07)

*All the energies are in units of MeV.

Note 1: Experimental proton-neutron residual interaction energy.

[a]Ref. 70, [b]Ref. 71, [c]Ref. 39, [d]Ref. 43,44, [e]Ref. 72, [f]Ref. 73, [g]Ref. 52, [h]Ref. 53, [i]Ref. 54, [j]Ref. 55.

[k]Of the two excitation energies listed for each nucleus, the lower one is the analog $g_{9/2}$ state to the neutron $g_{9/2}$ state.

The $(1g_{9/2})^2_{9+,0}$ interaction energies stay fairly constant and vary from -2.54 to -2.07 MeV as A increases from 54 to 68. This gradual decreasing of interaction energy with increasing A is expected from shell model calculations. This point will be further discussed in Section D.

C. Calculation of Excitation Energies of States With the Configuration $(1d_{5/2})^2_{5+,0}$

One could also use the following method to calculate the excitation energies of the $(1d_{5/2})^2_{5+,0}$ states for the nuclei - ^{15}N, ^{16}N, ^{16}O and ^{17}O. It is assumed that the residual interaction energy of $(1d_{5/2})^2_{5+,0}$ stays constant over this mass region and has a value of 3.90 MeV. Then one uses Talmi's method with the change that the $(d_{5/2}\ p_{1/2})$ interaction energies (i.e., $V_{3,0}$, $V_{2,0}$, $V_{3,1}$, and $V_{2,1}$) are expressed in terms of excitation energies of certain states of neighboring nuclei that can also be expressed in terms of $(d_{5/2}\ p_{1/2})$ interaction energies. Let $B(^AZ)_{J,T}$ denote the binding energy relative to ^{12}C, $\epsilon_{\pi j}$ denote the separation energy of a j proton from ^{13}N, and $\epsilon_{\nu j}$ denote the separation energy of a j neutron from ^{13}C. As an example, in order to calculate the excitation energy of the state in ^{15}N with the configuration $[p_{1/2}(d_{5/2})^2_{5,0}]_{11/2-,1/2}$, one can write down the following expressions:

$$B[^{15}N,\ p_{1/2}(d_{5/2})^2_{5,0}]_{11/2,1/2} = V_{5,0} + \tfrac{1}{2}V_{3,0} + \tfrac{3}{2}V_{3,1} + \epsilon_{\pi 5/2} + \epsilon_{\nu 5/2} + B(^{13}C)$$

$$B(^{14}N)_{3,0} = V_{3,0} + \tfrac{1}{2}(\epsilon_{\pi 5/2} + \epsilon_{\nu 5/2}) + \tfrac{1}{2}\,[B(^{13}C) + B(^{13}N)]$$

$$B(^{14}N)_{3,1} = V_{3,1} + \frac{1}{2}(\epsilon_{\pi 5/2} + \epsilon_{\nu 5/2}) + \frac{1}{2}\,[B(^{13}C) + B(^{13}N)]$$

$$B(^{14}C)_{3,1} = V_{3,1} + \epsilon_{\nu 5/2} + B(^{13}C)$$

$$\therefore\ B(^{15}N)_{11/2,1/2} = V_{5,0} + \frac{1}{2}[B(^{14}N)_{3,0} + B(^{14}N)_{3,1}] + B(^{14}C)_{3,1}$$

$$+ \frac{1}{2}(\epsilon_{\pi 5/2} - \epsilon_{\nu 5/2}) - \frac{1}{2}[B(^{13}C) + B(^{13}N)]$$

$$= 10.608 \text{ MeV.} \qquad (5\text{-}5)$$

Here, $V_{5,0}$ is $\langle d^2_{5/2}\ J=5,\ T=0|V|d^2_{5/2}\ J=5,\ T=0\rangle$ and is assumed to have a value 3.90 MeV. The 5.832 MeV 3-,0; 5.104 MeV 2-,0; 8.906 MeV 3-,1; and 9.508 MeV 2-,1 levels of ^{14}N and the 6.723 MeV 3-,1 level of ^{14}C are assumed to have the configuration $(d_{5/2}\ p_{1/2})_{J,T}$ with J=3 or 2 and T=0 or 1. The binding energies of these levels are calculated from these excitation energies and the ground state binding energy of ^{14}N. Since

$$B(^{15}N,\ g.s.)_{1/2,1/2} = 23.331 \text{ MeV},$$

it follows that the excitation energy E_x is given by:

$$E_x[^{15}N,\ p_{1/2}(d_{5/2})^2_{5,0}]_{11/2-,1/2} = 23.331 - 10.608 = 12.723 \text{ MeV}.$$

This method is just another form of the "interaction model" method mentioned previously. The direct connection can be seen by the following considerations. The proton separation energies for the ^{14}N states with configuration $(p_{1/2}\ d_{5/2})_{3-,0}$ or $(p_{1/2}\ d_{5/2})_{3-,1}$ are:

$$S_p(^{14}N)_{3,0} = B(^{14}N)_{3,0} - B(^{13}C)$$

$$S_p(^{14}N)_{3,1} = B(^{14}N)_{3,1} - B(^{13}C),$$

respectively. The neutron separation energy for the ^{14}C state with configuration $(p_{1/2}\ d_{5/2})_{3-,1}$ is:

$$S_n(^{14}C)_{3,1} = B(^{14}C)_{3,1} - B(^{13}C).$$

The total separation energy of a neutron and a proton for the ^{15}N state with configuration $[p_{1/2}(d_{5/2})^2_{5,0}]_{11/2-,1/2}$ is:

$$S_{pn} = B(^{15}N)_{11/2,1/2} - B(^{13}C).$$

From these definitions of separation energies and Eqs. (5-5), it follows that:

$$S_{pn} = V_{5,0} + \{\tfrac{1}{2}[S_p(^{14}N)_{3,0} + S_p(^{14}N)_{3,1}] + S_n(^{14}C)_{3,1}\}$$

$$+ \{\tfrac{1}{2}[B(^{13}C) - B(^{13}N)] + \tfrac{1}{2}[\epsilon_{\pi 5/2} - \epsilon_{\nu 5/2}]\}.$$

$$S_{pn} = V_{5,0} + \{\tfrac{1}{2}[S_p(^{14}N)_{3,0} + S_p(^{14}N)_{3,1}] + S_n(^{14}C)_{3,1}\}$$

$$+ \{\tfrac{1}{2}[E_c(p_{1/2} - {}^{12}C) - E_c(d_{5/2} - {}^{12}C)]\}$$

where $E_c(p_{1/2} - {}^{12}C)$ or $[E_c(d_{5/2} - {}^{12}C)]$ denotes the Coulomb energy between a $p_{1/2}$ proton [or a $d_{5/2}$ proton] and the ^{12}C core. The quantity in the last bracket {} of the last equation is exactly the additional Coulomb energy difference needed in the previous method and denoted C previously. The two methods are identical.

In the calculations for ^{16}N, the 0.75 MeV 5/2+,3/2 level of ^{15}C and the 5.276 MeV 5/2+,1/2; 12.502 MeV 5/2+,3/2 level of ^{15}N are assumed to be the J,T states of the configuration $[(p_{1/2})^2_{0,1}\ d_{5/2}]_{J,T}$, where J = 5/2 and T = 1/2 or 3/2. For ^{16}O, the 7.563 MeV 7/2+,1/2 and 7.154 MeV 5/2+, 1/2 levels of ^{15}N and the 7.28 MeV 7/2(+), 1/2 and 6.86 MeV 5/2+,1/2 levels of ^{15}O are assumed to be the J,T states of the configuration $[(p_{1/2})^2_{1,0}\ d_{5/2}]_{J,T}$ with J = 7/2 or 5/2 and T = 1/2. For ^{17}O, the 6.13 MeV 3-,0; 8.88 MeV 2-,0; 13.26 MeV 3-,1; and 12.97 MeV 2-,1 levels of ^{16}O and the 0.300 MeV 3-,1 level of ^{16}N are assumed to be the J,T states of the configuration $(p^{-1}_{1/2}\ d_{5/2})_{J,T}$ with J = 3 or 2 and T = 0 or 1. The results are presented in Fig. 47.

D. Shell Model Calculations

In this section the results of the calculations using two kinds of shell model calculation methods, the conventional method and Talmi's method, will be discussed and compared with the results obtained in the last two sections. The method of conventional shell model calculation has been discussed in Chapter III, Section A. This method as well as a computer program written by Dr. W. W. True are used to calculate the residual interaction energies between the proton and neutron in the configuration $(1d_{5/2})^2_{5+,0}$, $(1f_{7/2})^2_{7+,0}$, and $(1g_{9/2})^2_{9+,0}$. Tables XII, XIII, and XIV list the results of these calculations for the above mentioned three configurations respectively.

In these calculations, only V_{TE} is needed. For the $(1d_{5/2})^2_{5+,0}$ configuration, two sets of Harmonic Oscillator parameter, ν's are used. The first set corresponds to selecting the ν for ^{18}F as follows:

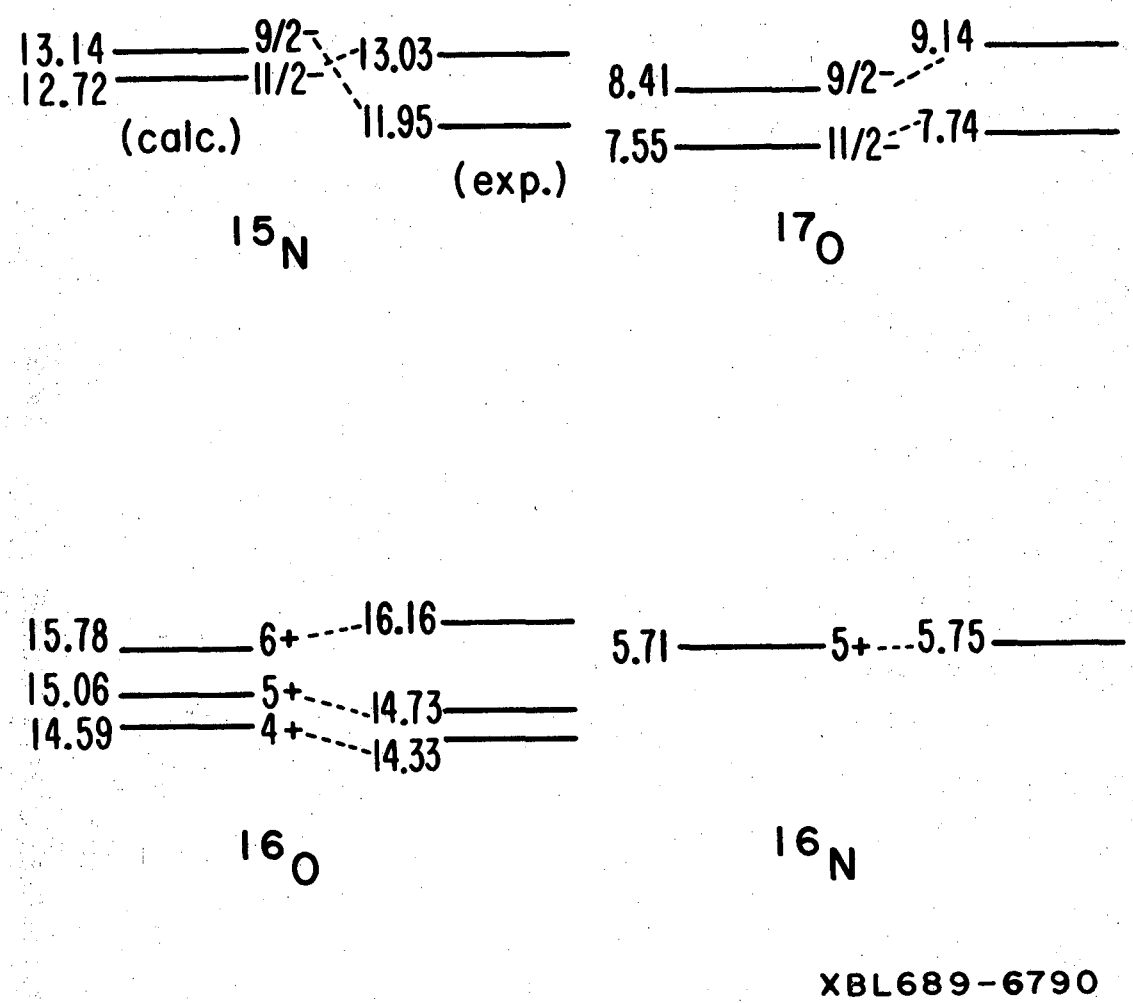

Fig. 47 Comparison between the experimental excitation energies of the $(1d_{5/2})^2_{5+,0}$ levels and the theoretical values using the interaction model method.

Table XII. Comparison between theoretical and experimental proton-neutron residual interaction energies of $(1d_{5/2})^2_{5+}$ configuration.

Nucleus	Shell model calculation[a]				Experimental[b]
	ν_1(in F^{-2})	E_1	ν_2(in F^{-2})	E_2	$E(1d_{5/2})^2_{5+,0}$
^{14}N	0.326	-4.601	0.306	-4.291	-4.05
^{15}N	0.318	-4.481	0.299	-4.177	-3.57
^{16}N	0.311	-4.365	0.292	-4.068	-3.82
^{16}O	0.311	-4.365	0.292	-4.068	-3.52
^{17}O	0.304	-4.258	0.285	-3.968	-3.69
^{18}F	0.298	-4.165	0.280	-3.880	-3.88
^{22}Na	0.278	-3.847	0.261	-3.582	-3.47
^{26}Al	0.262	-3.601	0.246	-3.349	-4.04

[a]The choices of two sets of ν's are discussed in the text.

All the energies are in units of MeV.

[b]From Table VII.

Table XIII. Comparison between theoretical and experimental proton-neutron residual interaction energies of $(1f_{7/2})^2_{7+,0}$ configuration.

Nucleus	Shell model calculation[a]		Experimental[b]
	ν(in F^{-2})	E	$E(1f_{7/2})^2_{7+,0}$
^{26}Al	0.276	-3.150	-3.44
^{28}Al	0.269	-3.064	-(2.96)
^{30}P	0.262	-2.980	-2.89
^{34}Cl	0.251	-2.836	-(3.11)
^{42}Sc	0.234	-2.614	-2.62

[a]The choice of ν's is discussed in the text. All the energies are in the units of MeV.

[b]From Table X.

Table XIV. Comparison between theoretical and experimental proton-neutron residual interaction energies of $(1g_{9/2})^2_{9+,0}$ configuration.

Nucleus	Shell model calculation[a]				Experimental[b]
	ν_1(in F^{-2})	E_1	ν_2(in F^{-2})	E_2	$E(1g_{9/2})^2_{9+,0}$
^{54}Mn	0.226	-2.198	0.244	-2.400	-(2.49)
^{56}Co	0.224	-2.167	0.241	-2.366	-(2.54)
^{60}Cu	0.219	-2.111	0.236	-2.303	-2.42
^{62}Cu	0.216	-2.083	0.233	-2.275	-2.32
^{64}Cu	0.214	-2.059	0.231	-2.247	-(1.93)
^{66}Ga	0.212	-2.033	0.228	-2.221	-(2.22)
^{68}Ga	0.209	-2.008	0.226	-2.195	-(2.07)

[a]The choice of two sets of ν's are discussed in the text. All the energies are in the units of MeV.

[b]From Table XI.

$$\nu(^{18}F) = (2n + \ell + 3/2)/R^2 = 3.5/3.428^2 = 0.2978$$

where R (which is equal to $3.428 = 1.333 \times 17^{1/3}$F) is the equivalent uniradius of A = 17 nuclei obtained from the Coulomb energy difference of mirror nuclei.[74] From this relation $\nu \propto A^{-2/3}$. However, empirically, from the present results $\nu \propto A^{-1/3}$ gives a better fit, and will be used. The other ν's are obtained by assuming an inverse dependence on $A^{1/3}$. For example:

$$\nu(A = 16) = \nu(^{18}F) \cdot (17/15)^{1/3}$$

The second set is chosen such that the ν of ^{18}F will give the same residual interaction energy as the experimental value. The other ν's are again obtained from the value for ^{18}F by taking inverse proportionality to $A^{1/3}$. For $(1f_{7/2})^2_{7+,0}$ the same approach as for the first set of ν's of $(1d_{5/2})^2_{5+,0}$ configuration is used. The radius of A = 41 nuclei which is equal to 4.388 F is used to fix the ν for ^{42}Sc first. Two sets of ν's are also used for $(1g_{9/2})^2_{9+,0}$ configuration. The first set of ν's is obtained by calculating the radius of ^{73}Ge first. From the table and Eq. (1) of Ref. 69:

$$\Delta E_c = 10.2 \text{ MeV} \quad \text{for Ge experimental data}$$

$$\Delta E_c(z + 1,z) = [0.6(28 + 1) - 0.613\, z^{1/3} - (-1)^z 0.3]\frac{e^2}{r_o A^{1/3}}$$

Hence

$$R(^{73}Ge) = r_o\, 73^{1/3} = 5.20 \text{ fm} \quad r_o = 1.244$$

The ν for ^{73}Ge is then calculated and the other ν's are obtained by using the inverse proportionality to $A^{1/3}$. The second set of ν's is obtained by requiring that the ν of ^{66}Ga will give an interaction energy equivalent

to the experimental values and the other ν's are obtained by applying the inverse proportionality to $A^{1/3}$. The ν values which are calculated from the often used formula $\hbar\omega = 41\ A^{-1/3}$ give too strong interaction energies and are not used here.

Comparison of the theoretical results thus obtained for the residual interaction energy with the experimentally extracted values allows the conclusion that the agreement is in general satisfactory. A reasonable slight adjustment of ν's (the second set) for $(1d_{5/2})^2_{5+,0}$ and $(1g_{9/2})^2_{9+,0}$ configuration gives excellent agreement while no adjustment is needed for the ν's of the $(1f_{7/2})^2_{7+,0}$ configuration. Kuo and Brown have calculated the residual interaction energy between proton and neutron in the $(1d_{5/2})^2_{5+,0}$ configuration from the free nucleon-nucleon scattering potential (i.e., Hamada-Johnston potential).[75] The result, -3.67 MeV, is in agreement with the experimentally extracted values as well as with the value obtained from simple shell model calculations. These results indicate that the assignments of states with configuration $(1d_{5/2})^2_{5+,0}$, $(1f_{7/2})^2_{7+,0}$, and $(1g_{9/2})^2_{9+,0}$ made in the last section and previous work[3] are correct.

One can also follow Talmi's method[26] to predict the excitation energy of states which have $(1d_{5/2})^2_{5+,0}$ configuration by assuming that the residual interaction matrix element of $(1d_{5/2})^2_{5+,0}$ configuration remains constant and has a magnitude 3.90 MeV. The following parameters are taken from Ref. 26, with the convention that if an energy represents attraction, it has positive sign.

$V_2 = 1.750 \pm 0.041$ MeV $\qquad V_2' = -0.486 \pm 0.048$ MeV

$V_3 = 1.604 \pm 0.035$ MeV $\qquad V_3' = 0.067 \pm 0.039$ MeV

$C_d = 0.979 \pm 0.044$ MeV $\qquad C_d' = -1.639 \pm 0.057$ MeV

where they are defined by:

$$V_J = \frac{1}{2}\,[\langle d_{5/2}p_{1/2}J,T = 0|V|d_{5/2}p_{1/2}\ J,T = 0\rangle$$

$$+\ \langle d_{5/2}p_{1/2}J,T = 1|V|d_{5/2}p_{1/2}\ J,T = 1\rangle]$$

$$V_J' = \frac{1}{2}\ \langle d_{5/2}p_{1/2}J,T = 1|V|d_{5/2}p_{1/2}\ J,T = 1\rangle]$$

and C_d', C_d are the sum of the interaction to the ^{12}C core and the kinetic energy of a $d_{5/2}$ proton or of a $d_{5/2}$ neutron respectively. Here, V_J is the matrix element of the interaction between a neutron and a proton, and V_J' is that between two like nucleons.

$E_T(^{13}C) = 4.95$ MeV $\qquad E_T(^{14}C) = 13.12$ MeV

$E_T(^{14}N) = 12.49$ MeV $\qquad E_T(^{15}N) = 23.33$ MeV

$E_T(^{16}N) = 25.99$ MeV $\qquad E_T(^{16}O) = 35.44$ MeV

$E_T(^{17}O) = 39.59$ MeV

where E_T is the total experimental binding energy beyond ^{12}C. The Coulomb energy between a $d_{5/2}$ proton and a $p_{1/2}$ proton is 0.40 MeV. This is estimated from the excitation energies of the analog states of ^{14}C and ^{14}O. Equation (3-19) is also used to calculate the interaction energies for configurations with $d_{5/2}$ and $p_{1/2}$ nucleons. The calculation results are listed in Table XV and are also plotted in Fig. 48.

Table XV.* Calculated excitation energies of $[(d_{5/2})^2_{5+,0}(p_{1/2})^n]$ configurations using Talmi and Unna's parameters of V_J, V'_J, C_d and C'_d and experimental ground state binding energies.

Nucleus		Configuration	Total energy[a]		E'[b]
^{15}N	11/2-	$(d_{5/2})^2_5 p_{1/2}$	$E_T(^{13}C\ g.s.)+C_d+C'_d+V_3+V'_3+V_5$	= 9.85 MeV	13.48
	9/2-	"	" $+C_d+C'_d+\frac{1}{12}(V_3+V'_3)+\frac{11}{12}(V_2+V'_2)+V_5$	= 9.48	13.85
^{16}N	5+	$(d_{5/2})^2_5(p_{1/2})^2_0$	$E_T(^{14}C\ g.s.)+C_d+C'_d+\frac{7}{6}(V_3+V'_3)+\frac{5}{6}(V_2+V'_2)+V_5$	=19.36	6.63
^{16}O	6+	$(d_{5/2})^2_5(p_{1/2})^2_1$	$E_T(^{14}N\ g.s.)+C_d+C'_d+2(V_3+V'_3)+V_5+E_c$	=18.67	16.77
	5+	"	" $+V_3+V'_3+V_2+V'_2+V_5+E_c$	=18.27	17.17
	4+	"	" $+\frac{1}{6}(V_3+V'_3)+\frac{11}{6}(V_2+V'_2)+V_5+E_c$	=17.93	17.51
^{17}O	11/2-	$(d_{5/2})^2_5(p_{1/2})^3_{1/2}$	$E_T(^{15}N\ g.s.)+C_d+C'_d+\frac{13}{6}(V_3+V'_3)+\frac{5}{6}(V_2+V'_2)+V_5+E_c$	=30.84	8.75
	9/2-	"	" $+\frac{5}{4}(V_3+V'_3)+\frac{7}{4}(V_2+V'_2)+V_5+E_c$	=30.47	9.12
^{18}F	5+	$(d_{5/2})^2_5(p_{1/2})^4_0$	$E_T(^{16}O\ g.s.)+C_d+C'_d+\frac{7}{3}(V_3+V'_3)+\frac{5}{3}(V_2+V'_2)+V_5+2E_c$	=43.89	1.32

*All the energies are in units of MeV.

[a]Binding energy of ^{12}C was subtracted. E_c is the Coulomb energy between $d_{5/2}$ proton and $p_{1/2}$ proton and is equal to -0.40 MeV.

[b]Calculated excitation energy.

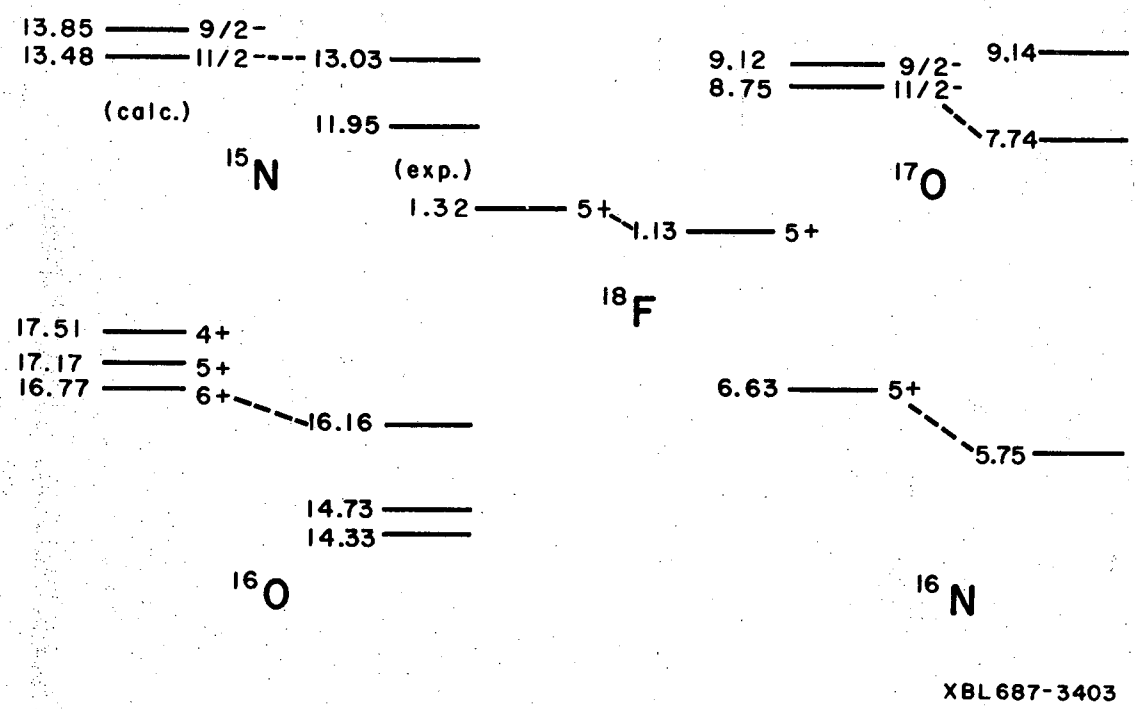

Fig. 48 Comparison between the experimental excitation energies of the $(1d_{5/2})^2_{5+,0}$ levels and the theoretical values using Talmi's method of shell model calculation.

For the 9/2-state of ^{15}N and ^{17}O and 4+ and 5+ state of ^{16}O, other configurations such as $[(d_{5/2}\ d_{3/2})_{4+,0}(p_{1/2})^n]$ may mix with the $[(d_{5/2})^2_{5+,0}(p_{1/2})^n]$ configuration. Hence, for such states one does not expect good agreement between the experimental excitation energies and the above theoretically calculated values which are based on the assumption of only one single configuration. For the 5+ state of ^{16}N, the configuration $[(d_{5/2}\ d_{3/2})_{4+,1}(p_{1/2})^2_{1+,0}]$ may mix with the configuration $[(d_{5/2})^2_{5+,0}(p_{1/2})^2_{0+,1}]$. However for the 11/2-states of ^{15}N and ^{17}O, and the 6+ state of ^{16}O, no configuration of simple structure can be mixed in, so that good agreement is expected. For these states the association of the calculated level to the experimental levels for ^{15}N, ^{16}O is obvious and is indicated by the dashed lines in Fig. 48. For ^{17}O, the calculated 11/2-state at 8.62 MeV can be equally well associated with either the 9.14 MeV or the 7.74 MeV level. However, in the "interaction model" calculation in the last section (see Fig. 47), the choice of 7.74 MeV level as 11/2- gives a better agreement with the theoretical calculations. Because the interaction model method uses the excitation energies of neighboring nuclides which may contain some core excitation (i.e., of ^{15}N in this case), this method will give better agreement to the experimental value if the target core has a core excitation component. Recent analysis of core polarization effects in ^{15}N-^{15}O by Brown and Shukla suggest that there may be 10% of 2p-3h components in the ground state wave function of ^{15}N or ^{15}O.[76]

The position of the 2p-2h 6+ state in ^{16}O is very perplexing. From the systematics of (α,d) work, the 2p-2h 6+ state must be one of

the triplet of levels-14.33, 14.74, 16.16 MeV, strongly populated by the (α,d) reaction. If the cross sections for the formation of the members of the triplet are proportional to (2J+1), the spin-parity assignment would be 4+, 6+, 5+ for the 14.33, 14.74, 16.16 MeV states respectively.[3] (This (2J+1) rule is not followed for both the doublet level of ^{15}N and ^{17}O populated through (α,d) reaction. The cross sections after dividing by (2J+1) are 0.40 mb and 0.32 mb for the 13.03 MeV and 11.95 MeV level of ^{15}N assuming that the former state has spin 11/2 and the latter has spin 9/2. Those for the 7.74 MeV (11/2-) and 9.14 MeV (9/2) level of ^{17}O are 0.55 mb and 0.27 mb respectively. Hence determination of spin by this (2J+1) rule may not be too reliable.) Carter et al.[77] have shown the 16.2 MeV level to have spin 6+ from a $^{12}C(\alpha,\alpha')^{12}C$ study. This state was considered as one of the members of the 4p-4h rotational band. The downward bending of this band was explained by Celenza et al.[78] by introducing 2p-2h mixture to the 4p-4h component. The dominant 4p-4h 6+ state was predicted to lie at 15.83 MeV and 2p-2h 6+ state at 12.17 MeV. Kelson predicted the 4p-4h 6+ state at about 14 MeV.[50] Recent shell model calculations by Zaker et al.[79] predicted a 4p-4h state at 17.4 MeV and a 2p-2h state at around 15 MeV with a 6+ state at about 14.5 MeV. However, the calculations in the last sections (see Fig. 47) indicate that the 16.16 MeV level is a 2p-2h state with spin and parity 6+. Since it is unlikely that two levels with the same spin and parity will have energy very close to each other, the 16.16 MeV level of ^{16}O strongly populated by the $^{14}N(\alpha,d)^{16}O$ reaction may be the same state as observed by Carter et al. at 16.2 MeV. A spin parity determination for the 14.33, 14.73 and 16.16 MeV level of ^{16}O is needed in order to clarify this confusion.

E. $-Q_f$ vs $A_{residual}$ Plot for States with Configuration $(1d_{5/2})^2_{5+,0}$

In Section A it is stated that one expects a monotonically decreasing $-Q_f$ value (i.e., Q-value for formation of the level) with increasing A or residual nucleus for states with configuration $(1d_{5/2})^2_{5+,0}$. The reason for this expection can be understood clearly by the following considerations.

The interaction energy between $d_{5/2}$ and $p_{1/2}$ nucleons in the configuration $[(d_{5/2})^2_{5+,0}(p_{1/2})^n_{J',T'}]_{J,T}$ where n ranges from 1 to 4, was obtained in the above calculation by first applying Eq. (3-19) and then substituting values of V_3, V_2, V_3', and V_2' determined by Talmi and Unna (listed in the last section). These values are plotted against n, the number of $1p_{1/2}$ nucleons, or the mass number A of the residual nucleus as shown in Fig. 49. For cases where the mentioned configuration gives two or three allowed J values, the centroid position of each of this multiplet is calculated by the following center-of-mass theorem:

$$\bar{V}(jj') = \sum_J (2J+1)\, V(jj'J) / \sum_J (2J+1) \qquad |j-j'| \leq J \leq |j+j|$$

where $\bar{V}(jj')$ is the average interaction energy (i.e., the interaction energy of the centroid). The positions of these centroids are designated in Fig. 49 by a triangle. These points form a straight line with a slope:

$$\frac{dE}{dn} = -\frac{7}{12}(V_3 + V_3') - \frac{5}{12}(V_2 + V_2') = -1.502 \text{ MeV}$$

This is the additional $p_{1/2}$-$d_{5/2}$ interaction energy gained by adding one more nucleon to the $p_{1/2}$ shell. From Eq. (5-3), $-Q_f$ is the sum of a constant and the interaction energy of $d_{5/2}$ nucleons (with configuration

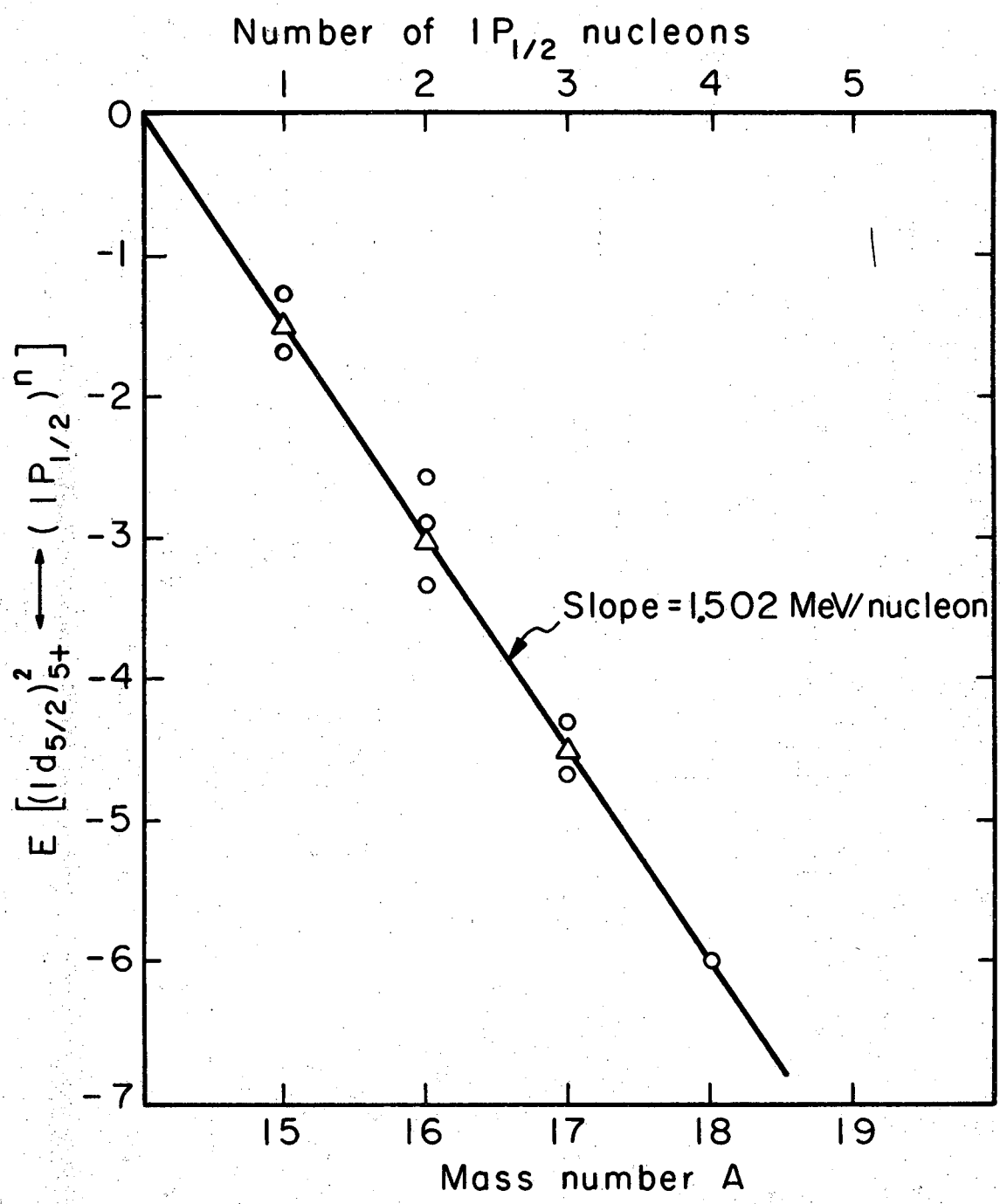

XBL687-3117

Fig. 49 Interaction energies between $d_{5/2}$ and $p_{1/2}$ nucleons in the configuration $[(1d_{5/2})^2_{5+,0}(1p_{1/2})^n_{J',T'}]_{J,T}$ as a function of n, the number of nucleons in $1p_{1/2}$ shell.

$(d_{5/2})^2_{5+,0}$) to the target core. The interaction of the $d_{5/2}$ nucleon to the target core can be separated into the sum of the interaction of $d_{5/2}$ proton and neutron to the ^{12}C core, a constant, and the interaction of $d_{5/2}$ proton and neutron to the $p_{1/2}$ nucleons. Thus, in a $-Q_f$ vs A plot one can expect a general smooth, monotonical decrease of $-Q_f$ value (increasing $p_{1/2}$-$d_{5/2}$ interaction) with increasing A (increasing number of $p_{1/2}$ nucleons). The experimental results can be shown to be in agreement with this expectation by the following consideration. Since the highest spin state in each multiplet usually has less configuration mixing, one can first assume that one of the experimentally determined multiplet states is this state. Then, the position of the multiplet centroid relative to this state is taken from Fig. 49. After correcting for the $p_{1/2}$-$d_{5/2}$ Coulomb energy difference, a line giving the best fit to these estimated centroid positions has a slope equal to -1.55 MeV/nucleon with the choice that the 13.03 MeV state of ^{15}N and the 7.75 MeV of ^{17}O are the 11/2-states, and that the 16.16 MeV state of ^{16}O is the 6+ state. These choices are the same as those made in Section C. The centroid position for ^{17}O is off the line. Figure 50 is a different representation (graphical) of the results obtained by applying Talmi's method. This graph is plotted in order to see more clearly why one expects a general monotonic decrease of $-Q_f$ values with increasing A.

F. Other Possible Two-Nucleon Excited States

Speculations concerning two-nucleon excited states with configuration other than $(1d_{5/2})^2_{5+,0}$ in the light nuclides are made in this section with the hope that this may arouse interest in the further study of these

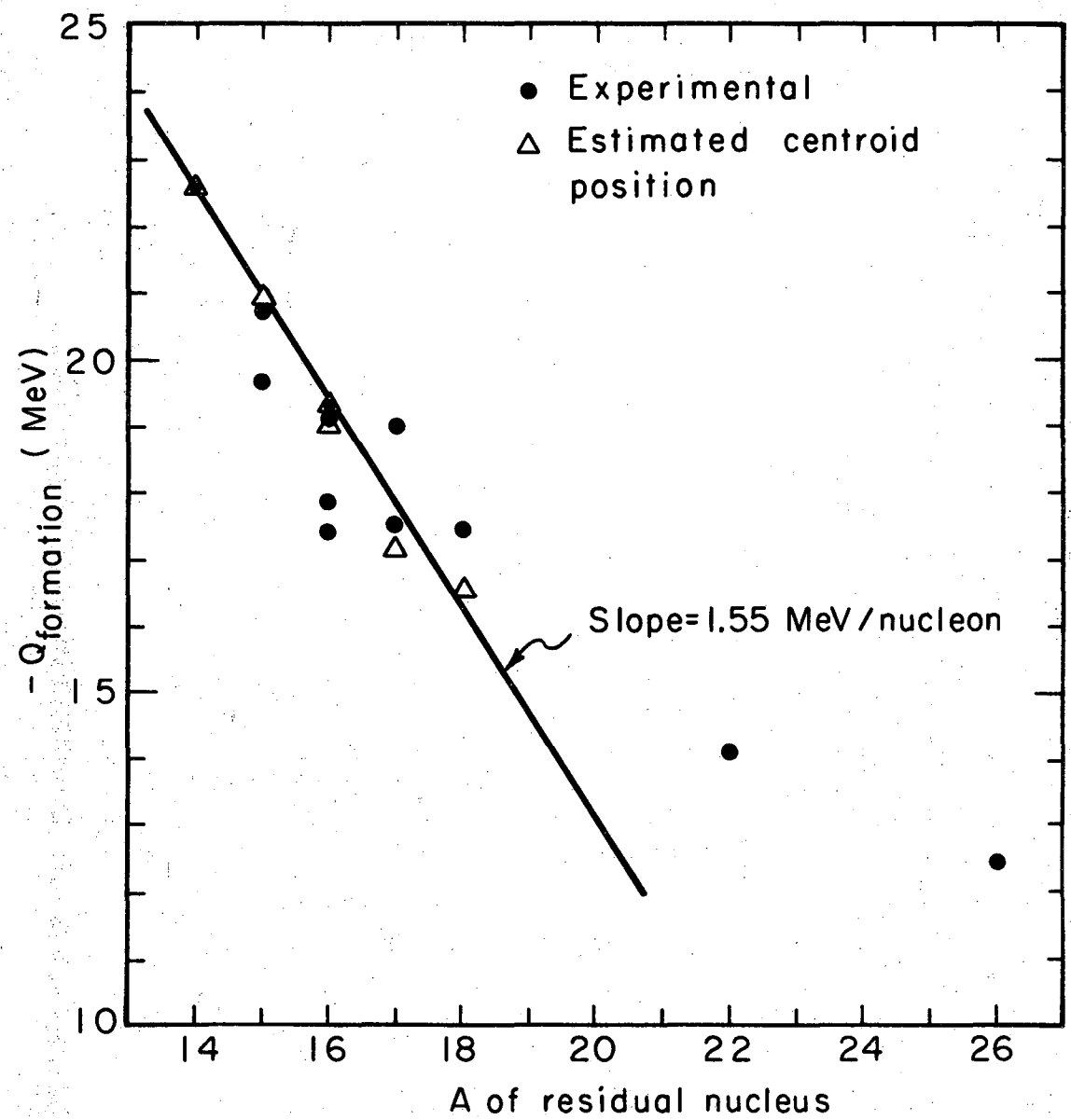

XBL687-3119

Fig. 50 Relation between A and Q_f of estimated centroid position of $(1d_{5/2})^2_{5+,0}$ configuration.

states. These speculations are highly tentative and need further evidence to confirm their correctness.

In the previously studied $^{12}C(\alpha,d)^{14}N$ reaction,[80] the magnitudes of the cross sections for populating states of different configurations have the following order:

$$\sigma[(d_{5/2})^2_{5+,0}] > \sigma[(p_{1/2}d_{5/2})_{3+,0} \text{ or } 2+,0] \approx \sigma[(s_{1/2}d_{5/2})_{3+,0}] > \sigma[(p_{1/2}s_{1/2})_{1-,0} \text{ or } 0-,0] \text{ or } [(s_{1/2})^2_{1+,0}]$$

This would imply that a medium size peak in a deuteron spectrum of light nuclides from (α,d) reaction may result from a $(s_{1/2}\ d_{5/2})_{5+,0}$ capture of the proton-neutron pair. Thus the 9.808 MeV state of ^{15}N may have the dominant configuration:

$$[(s_{1/2}d_{5/2})_{3+,0}p_{1/2}]_{7/2-,0}$$

The possible association of 9.808 MeV level with the known 9.832 MeV 7/2 state makes this assignment appear to be very plausible. The 5.690 MeV level of ^{17}O may have the cominant configuration:

$$[(s_{1/2}d_{5/2})_{3+,0}\ p^{-1}_{1/2}]_{7/2-,0}$$

Since the known 5.697 MeV level has spin-parity 7/2-, this assignment appears to be very probable. The 3.961 MeV level of ^{16}N determined by the present work is presumably the same as the previously known 3.957 MeV level. This level was populated by the (t,p) reaction on ^{14}N target[32] with an angular momentum transfer L equal to 2 (determined by plane wave analysis of the angular distribution). A possible spin-parity of (1,2,3)+

was assigned. Combining this result with the expectation from the results of the (α,d) reaction, it appears that this state may have a dominant configuration:

$$a[(s_{1/2}d_{5/2})_{3+,0}(p_{1/2})^2_{0+,1}]_{3+,1} + b[(s_{1/2}d_{5/2})_{3+,1}(p_{1/2})^2_{1+,0}]_{3+,1}$$

where a and b are the amplitude of each configuration. The g.s. of ^{22}Na is a 3+ state. It may have some component of the $(s_{1/2}d_{5/2})_{3+,0}$ configuration. The 0.9371 MeV 3+,0 state of ^{18}F is known to have dominant configuration $(s,d)^2$ and was populated by the (α,d) reaction with medium cross section.[4] The 11.09 MeV level of ^{16}O populated by the (α,d) reaction[3] may have the configuration:

$$[(s_{1/2}\ d_{5/2})_{3+,0}\ (p_{1/2})^2_{1+,0}]_{4+,0}$$
$$\text{or } 3+,0$$
$$\text{or } 2+,0$$

with $J\pi$, T = 4+,0 most likely. This assignment is supported by the existence of a previously known 4+ level at 11.094 MeV and a 3+ level at 11.080 MeV.[81]

The 7.46 MeV state of ^{22}Na was assigned a configuration $(d_{5/2}f_{7/2})_{6-,0}$ (ref. 3). However, the ^{21}Ne(p,γ)^{22}Na study of Arnell et al.[35] showed that the 7.48 MeV level decays 90% to the g.s. 3+,0 state, 8% to the 1.95 MeV (2+), T = 1 or 1.94 MeV 1+ state, and 2% to the 3.07 MeV (2) state. The 7.89 MeV state decays 60% to the 1.53 MeV, 5+,0 state and 40% to the 0.89 MeV 4+,0 state. A 6- assignment to the 7.48 MeV level would require an E3 transition to the g.s. and M4 or E5 transition to the (2+)

or 1+ state respectively. It is unlikely that one would observe a prompt M4 or E5 transition. However if the 7.89 MeV level is assigned as 6-, the transition to the 1.53 MeV 5+,0 level is an E1 transition and the transition to the 0.89 MeV 4+,0 level is an M2 transition. Although E1 transitions between two T = 0 states (i.e., $\Delta T = 0$) in self conjugate nuclides (i.e., $T_z = 0$ nuclides) are T-forbidden with a retardation factor which is often approximately 10, there are other cases where T-forbidden E1 transitions have the same transition strengths as those of the average normal E1 transitions.[82] The occurrence of E1, $\Delta T = 0$ transitions in ^{22}Na cannot be ruled out. If the 7.48 MeV level of ^{22}Na is assigned to have a configuration $(d_{5/2}\ d_{3/2})_{4+,0}$, the transition to the g.s. 3+,0 level would be M1 and the transitions to the 1.95 MeV (2+), 1.94 MeV 1+ levels would be E2 and M3 respectively. As discussed in Chapter IV, Section B, it is very likely that the 5.106 MeV state, strongly populated in the ^{20}Ne(α,t) ^{21}Na reaction, may have a dominant configuration [(^{20}Ne core)$d_{3/2}$]. Hence, in the (α,d) reaction, the state with configuration $(d_{5/2}\ d_{3/2})_{4+,0}$ may be strongly populated. Since in the (α,d) reaction the cross sections for population of the 7.46 and 7.87 MeV levels are not much different, a shift in assignment does not contradict severly to the criteria used in establishing this assignment.[3] The assignment of dominant configuration of $(d_{5/2}\ d_{3/2})_{4+,0}$ and $(d_{5/2}\ f_{7/2})_{6-,0}$ to the 7.46 and 7.87 MeV levels respectively seems in more reasonable agreement with the results of (p,γ) work.

VI. CONCLUSIONS

From the evidence presented in the previous Chapter of discussion, it can be concluded that:

a) The systematic trend of (α,d) reactions at alpha particle energy 40-50 MeV to populate strongly the states with a $(j)^2_{2j+,0}$ configuration still persists in the medium mass region nuclides studied.

b) States with configuration $[(\text{target core})(1g_{9/2})^2_{9+,0}]$ are located.

c) States with configuration $[(\text{target core})(1d_{5/2})^2_{5+,0})]$ of ^{15}N, ^{16}N, ^{17}O and ^{20}Ne are located.

d) The residual interaction energies between proton and neutron in the configurations $(1d_{5/2})^2_{5+,0}$, $(1f_{7/2})^2_{7+,0}$, and $(1g_{9/2})^2_{9+,0}$ are about -3.9, -3.0, -2.2 MeV respectively. There is a slight decrease of these residual interaction energies with increasing A for all these three configurations. The magnitudes of these residual interaction energies and their variation with A are reproduced excellently by conventional shell model calculations.

e) The "interaction model" method used to extract from the experimental results the residual interaction energies for $T_z \neq 0$ nuclides is believed to be correct, because it generates residual interaction energies which are in agreement with those obtained for $T_z = 0$ nuclides, as well as in agreement with the results obtained by the conventional shell model calculations. This method which uses the excitation energy information of nuclei with mass number A to calculate the residual interaction energies or excitation energies of levels in nucleus with mass

number A+1 is believed to be more accurate than the method which tries to get a set of matrix elements from fitting the excitation energies of nuclides with a wider range of A.

f) The 16.16 MeV level of ^{16}O has a dominant 2p-2h configuration, $[(1d_{5/2})^2_{5+,0}(1p_{1/2})^2_{1+,0}]$, and may have a spin-parity 6+.

The identification of the configuration of those states which are populated with medium cross sections in the (α,d) reaction by establishing systematic trends, spin and parity determination, and shell model calculation will be very interesting.

ACKNOWLEDGMENTS

I would like to express my sincere appreciation to:

Dr. Bernard G. Harvey, my research adviser, whose encouragement, guidance, teaching and consideration are always there whenever needed. Without his support, the completion of this work would not have been possible. His suggestion of this experiment and a shell model theoretical analysis of the experimental results are appreciated:

Professor Joseph Cerny III to whom I am most indebted for his firm support enabling me to pursue this study;

Dr. Martin G. Redlich for reading and correcting the manuscript of this thesis and for numerous precious discussions and fruitful suggestions which greatly enhances its completeness.

I would also like to thank:

Dr. William W. True for his teaching and stimulating discussions and also for allowing me to use his shell model matrix element calculation program;

Dr. David L. Hendrie and Dr. John R. Meriwether for their guidance in the operation of equipment;

Dr. Nolan F. Mangelson for his invaluable assistance in setting up electronic equipment, help in collecting data, and many helpful explanations and discussions;

Dr. Richard H. Pehl and Dr. Ernest J-M. Rivet for their interest in this work and enlightening discussions;

Miss Jeannette Mahoney for using her PDP-5 data collecting and analyzing programs and help in collecting data;

Mr. Frederick S. Goulding and Mr. Donald Landis for providing the electronic equipment;

Mr. Creve Maples for his generosity in allowing me to use several computer programs;

Dr. Arthur Springer for discussions of electronic equipment and nuclear physics;

Dr. Gordon C. Ball for many helpful discussions;

Dr. Mary F. Reed, Mr. Michael S. Zisman, Mr. Joel M. Moss and Mr. Heinz Brunader for assistance in collecting data;

Dr. Gilbert W. Butler and Dr. Donald G. Fleming for several relevant discussions;

Mr. Claude Ellsworth and Mrs. Ruth-Mary Larimer for preparing targets;

All the people associated with the 88-inch cyclotron for providing excellent quality of beam and other support;

My parents and fiancee for their constant encouragement;

My friends David D. S. King, Mr. and Mrs. F. S. Tao, and Mr. and Mrs. Oliver Yu for their considerable help.

This work was performed under the auspices of the United States Atomic Energy Commission.

REFERENCES

1. J. Cerny, Two-Nucleon Transfer Reactions in the Light Elements (Ph.D. Thesis), UCRL-9714, May 1961.
2. E. J.-M. Rivet, Investigation of Highly Populated Levels of the $(d_{5/2})^2_5$ and $(f_{7/2})^2_7$ Configurations by the (α,d) Reaction (Ph.D. Thesis), UCRL-11341, March 1964.
3. E. Rivet, R. H. Pehl, J. Cerny, and B. G. Harvey, Phys. Rev. 141, 1021 (1966).
4. N. F. Mangelson, The $(^3He,p)$ and (α,d) Two-Nucleon Stripping Reactions on ^{12}C and ^{16}O: Mechanism and Nuclear Spectroscopy (Ph.D. Thesis), UCRL-17732, August 1967.
5. R. W. Detenbeck, J. C. Armstrong, A. S. Figuera, and J. B. Marion, Nucl. Phys. 72, 552 (1965).
6. A. Gallmann, F. Haas, and B. Heusch, Phys. Rev. 164, 1257 (1967).
7. E. K. Warburton, Phys. Rev. 163, 1032 (1967).
8. A. R. Poletti, E. K. Warburton, and J. W. Olness, Phys. Rev. 164, 1479 (1967).
9. C. Williamson and J. P. Boujot, Table of Range and Rate of Energy Loss of Charged Particles of Energy 0.5 to 150 MeV, Rapport CEA 2189, 1962.
10. F. S. Goulding, D. A. Landis, J. Cerny, and R. H. Pehl, IEE Trans. Nucl. Sci. 13, [3] 514 (1966).
11. F. S. Goulding and D. Landis, National Research Council Publication 1184, 1964, p. 124; F. S. Goulding, D. A. Landis, J. Cerny, and R. H. Pehl, Nucl. Instr. and Methods 31, 1 (1964).

12. L. B. Robinson and F. S. Goulding, An On-Line Computer Installation At Lawrence Radiation Laboratory, Berkeley, UCRL-11458, July 1967.

13. Hamilton Watch Co., Lancaster, Pennsylvania.

14. Obtained from Mosanto Research Corporation, Mound Laboratory, Miamisburg, Ohio.

15. Obtained from Isomat Corporation, Palisades Park, New Jersey.

16. Obtained from Mound Research Corporation.

17. A detergent manufactured by Shell Oil Co., Berkeley, California.

18. Union Carbide Nuclear Company, Oak Ridge National Laboratory, Oak Ridge, Tennessee.

19. The ^{14}C target was kindly loaned to us by Brookhaven National Laboratory.

20. This program was written by C. Maples, Lawrence Radiation Laboratory, Berkeley.

21. T. Brody and M. Moshinsky, Tables of Transformation Brackets for Nuclear Shell-Model Calculations, Monografias del Institute de Fisica, Mexico (1960).

22. W. W. True, Phys. Rev. 130, 1530 (1963).

23. M. G. Redlich, Phys. Rev. 138, B544 (1965).

24. M. G. Redlich, Phys. Rev. 99, 1427 (1955).

25. A. de-Shalit and I. Talmi, Nuclear Shell Theory (Academic Press, New York, 1963), p. 480.

26. I. Talmi and I. Unna, Ann. Rev. Nucl. Sci. 10, 353 (1960).

27. G. W. Phillips, F. C. Young, and J. B. Marion, Phys. Rev. 159, 891 (1967).

28. E. K. Warburton and J. W. Olness, Phys. Rev. 147, 698 (1966); E. K. Warburton, J. W. Olness, and D. E. Alburger, Phys. Rev. 140, B1202 (1965).

29. F. Ajzenberg-Selove and T. Lauritsen, Nucl. Phys. 11, 1 (1959).

30. E. C. Halbert and J. B. French, Phys. Rev. 105, 1563 (1957).

31. E. K. Warburton, P. D. Parker, and P. F. Donovan, Phys. Letters 19, 397 (1965).

32. P. V. Hewka, C. H. Holbrow, and R. Middleton, Nucl. Phys. 88, 561 (1966).

33. C. H. Johnson and J. L. Fowler, Phys. Rev. 162, 890 (1967).

34. E. K. Warburton, J. W. Olness, and A. R. Poletti, Phys. Rev. 160, 938 (1967); A. R. Poletti, E. K. Warburton, J. W. Olness, and S. Hechtl, Phys. Rev. 162, 1040 (1967).

35. S. E. Arnell and E. Wernbom-Selin, Arkiv Fysik 27, 1 (1964).

36. S. A. Hjorth, Arkiv Fysik 33, 147 (1966).

37. T. A. Belote, W. E. Dorenbusch, and J. Rapaport, Nucl. Phys. A109, 666 (1968).

38. M. Croissaux, E. Dally, H. Distelzwey, and C. Gehringer, J. de Phys. 25, 906 (1964).

39. J. B. Ball and R. F. Sweet, Phys. Rev. 140, B904 (1965).

40. R. H. Fulmer, A. L. McCarthy, B. L. Cohen, and R. Middleton, Phys. Rev. 133, B955 (1964).

41. R. G. Miller and R. W. Kavanagh, Nucl. Phys. A94, 261 (1967).

42. S. A. Hjorth and L. H. Allen, Arkiv Fysik 33, 207 (1967); W. W. Daehnick and Y. S. Park, Bull. Am. Phys. Soc. 12, 1189 (1967).

43. E. K. Lin and B. L. Cohen, Phys. Rev. 132, 2632 (1963).

44. D. von Ehrenstein and J. P. Schiffer, Phys. Rev. 164, 1374 (1967).

45. Nuclear Data Sheets.

46. W. Menti, Helv. Phys. Acta 40, 981 (1967).

47. D. H. Rester, F. E. Durhma, and C. M. Class, Nucl. Phys. 80, 1 (1966).

48. D. D. Armstrong, A. G. Blair, and H. C. Thomas, Phys. Rev. 155, 1254 (1967).

49. M. Matoba, I. Kumaba, H. Ogata, Y. Okuma, and T. H. Kim, International Conference on Nuclear Structure, Tokyo, Japan (1967), contribution paper 8.74.

50. I. Kelson, Phys. Letters 16, 143 (1965).

51. A. J. Howard, J. P. Allen, and D. A. Bromley, Phys. Rev. 139, B1135 (1965).

52. B. J. O'Brien, W. E. Dorenbusch, T. A. Belote, and J.Rapaport,Nucl. Phys. A104, 609 (1967); D. D. Armstrong and A. G. Blair, Phys. Rev. 140, B1226 (1965); P. H. Vuister, Nucl. Phys. A91, 521 (1967).

53. B. Rosner and C. H. Holbrow, Phys. Rev. 154, 1080 (1967).

54. A. G. Blair and D. D. Armstrong, Phys. Letters 16, 57 (1965); A. G. Blair, Los Alamos Scientific Laboratory Report LADC-6370, 1964 (unpublished).

55. A. G. Blair, Phys. Rev. 140, B648 (1965).

56. M. G. Betigeri, H. H. Duhm, R. Santo, R. Stock, and R. Bock, Nucl. Phys. A100, 416 (1967).

57. N. K. Glendenning, Phys. Rev. 137, B102 (1965).

58. T. K. Alexander, K. W. Allen, and D. C. Hearly, Phys. Letters 20, 402 (1966).

59. This spin assignment which is different from those in ref. 3, will be discussed in Sections C and D.

60. P. M. Endt and C. van der Leun, Nucl. Phys. A105, 1 (1967).

61. Assigned by this work.

62. R. K. Gupta, and P. C. Sood, Phys. Rev. 152, 917 (1966).

63. P. Loncke and J. Pradal, Nuovo Cim. (10), 48B, 457 (1967).

64. My analysis of the (α,t) reaction data collected by R. Pehl, E. Rivet, J. Cerny, and B. G. Harvey showed: g.s. 5/2+ and 3.72 MeV 7/2-states of ^{25}Al, 1.38 MeV 3/2+ and 3.44 MeV 7/2-states of ^{29}P, and g.s. 5/2+, 2.98 MeV 3/2+, and 6.48 MeV states of ^{27}Al were strongly populated.

65. H. Ejiri, T. Ishimatsu, K. Yagi, G. Breuer, Y. Nakajima, H. Ohmura, T. Tohei, and T. Nakagawa, J. Phys. Soc. (Japan) 21, 2110 (1966).

66. The only known level that could be the analog state of ^{33}S 2.937 MeV 7/2-state are 2.5 MeV and 2.979 MeV state. The former is more likely because systematic trend indicates that the odd proton states usually have excitation energy less than the analog odd neutron states.

67. C. van der Leun, D. M. Sheppard, and P. M. Endt, Nucl. Phys. A100, 316 (1967); D. M. Sheppard, and C. van der Leun, Nucl. Phys. A100, 333 (1967).

68. Average value of the two 7/2-,T=3/2 states at 10.51,10.48 MeV in ref. 67 were used.

69. R. Sherr, Phys. Letters 24B, 321 (1967); J. D. Anderson, C. Wong, and J. W. McClure, Phys. Rev. 138, B615 (1965).

70. A. A. Rollefsen, R. C. Bearse, J. C. Legg, G. C. Phillips, and G. Roy, Nucl. Phys. 63, 561 (1965).

71. R. H. Fulmer and A. L. McCarthy, Phys. Rev. 131, 2133 (1963).

72. (α,t) data in this thesis.

73. Analog states. See discussion in the text.

74. L. R. B. Elton, Nuclear Sizes (Oxford University Press, Oxford, England, 1961), p. 56.

75. T. T. S. Kuo and G. E. Brown, Nucl. Phys. 85, 40 (1966).

76. G. E. Brown and A. P. Shukla, Princeton University Report PUC-937-268 (1967).

77. E. B. Carter, G. E. Mitchell, and R. H. Davis, Phys. Rev. 133, B1421 (1964); E. B. Carter, Phys. Letters 27B, 202 (1968).

78. L. S. Celenza, R. M. Dreizler, A. Klein, and G. J. Dreiss, Phys. Letters 23, 241 (1966).

79. A. P. Zaker, B. Buck, and J. B. McGrory, Phys. Rev. Letters 21, 39 (1968).

80. R. H. Pehl, E. Rivet, J. Cerny, and B. G. Harvey, Phys. Rev. 137, B114 (1965).

81. J. D. Larson and T. A. Tombrello, Phys. Rev. 147, 760 (1966).

82. S. J. Skorka, J. Hertel, and T. W. Retz-Schmidt, Nuclear Data 2 347 (1966).

This report was prepared as an account of Government sponsored work. Neither the United States, nor the Commission, nor any person acting on behalf of the Commission:

A. Makes any warranty or representation, expressed or implied, with respect to the accuracy, completeness, or usefulness of the information contained in this report, or that the use of any information, apparatus, method, or process disclosed in this report may not infringe privately owned rights; or

B. Assumes any liabilities with respect to the use of, or for damages resulting from the use of any information, apparatus, method, or process disclosed in this report.

As used in the above, "person acting on behalf of the Commission" includes any employee or contractor of the Commission, or employee of such contractor, to the extent that such employee or contractor of the Commission, or employee of such contractor prepares, disseminates, or provides access to, any information pursuant to his employment or contract with the Commission, or his employment with such contractor.